Università degli Studi di Palermo

AREA RICERCA E TRASFERIMENTO TECNOLOGICO
SETTORE DOTTORATI E CONTRATTI PER LA RICERCA
U. O. DOTTORATI DI RICERCA

Tecnologie e Scienze per la Salute dell'Uomo
Dipartimento di Scienze e Tecnologie Biologiche Chimiche e FarmaceuticheSTEBICEF
BIO/10

CX3CL1 modulator in the inflammatory processes of Alzheimer's disease

IL DOTTORE
MATILDA IEMMOLO

IL COORDINATORE
BRUNO GIUSEPPE PIGNATARO

IL TUTOR
GIULIO GHERSI

CO TUTOR
GIULIA BIVONA

CICLO XXXVI
2024

INDEX

1. Introduction

1.1 Alzheimer's disease

Alzheimer's disease (AD) is the most common form of dementia affecting nearly 45 million people worldwide. It is a leading cause of dementia cases globally. In the United States alone, approximately 5.3 million Americans have AD, of whom 5.1 million are age 65 or older, and 200,000 have younger-onset AD [1]. The discovery of AD is attributed to Alois Alzheimer, a German neurologist who examined a 51-year-old woman named Auguste Deter, who suffered from memory loss, speech, disorientation, and hallucinations. Her autopsy revealed plaques and tangles in her cerebral cortex, which convinced him this was beyond typical dementia. His discovery was followed by further research revealing the presence of amyloid β (Aβ) neuritic plaques in dementia patients [2]. The most characteristic manifestations of AD are amnesiac, individuals with very mild or mild AD dementia exhibit different changes in multiple cognitive, functional, and behavioral domains. Many of the symptoms of the disease manifest themselves years before receiving a clinical diagnosis of dementia, including changes in mood, anxiety, and sleep patterns. Characteristics of the early or preclinical stages of AD are heightened anxiety, depressive symptoms, apathy, and withdrawal. Progression to advanced stage symptoms, such as impaired judgment, disorientation, and confusion; major behavioral changes, such as aggression and agitation; and neuropsychiatric symptoms, such as delusions and hallucinations, may go unrecognized and untreated until diagnosed [3]The strongest risk factors for Alzheimer's disease are older age (over 65, although this is not a fixed definition) and possession of at least one APOE ε4 allele. Additionally, women are more likely to develop Alzheimer's disease than men, especially after age 80. Women are also more likely to have a higher tau burden, despite having a similar amyloid-β burden. Additionally, cardiovascular risk factors and an unhealthy lifestyle have been associated with an increased risk of dementia [4]. Most AD patients have sporadic disease onset, while a small percentage (<0.5%) have a rare familial form of AD (FAD) caused by mutations in three genes: amyloid precursor protein (APP), presenilin 1 (PSEN1) and presenilin 2 (PSEN2) [5]. In FAD, symptoms develop earlier than in sporadic AD, typically between 30 and 50 years of age. Late-onset AD is likely to be caused by both genetic factors and environmental factors that influence each other. In reality, 70% of the risk of AD is mainly attributable to genetic factors. The APOE gene, which has three variants, ε2, ε3, and ε4, is the greatest risk for sporadic AD: Compared to non-ε4 carriers, ε4 heterozygotes have an odds ratio (OR) for AD of approximately 3, rising to about 12 in homozygotes [6] [7] Next-generation sequencing techniques have shown rare protein-damaging variants in the SORL1 [8], ABCA7 [9], and TREM2 [10] (figure 1) genes. These findings suggest that the intact protein products of these genes are essential for maintaining brain health [4].

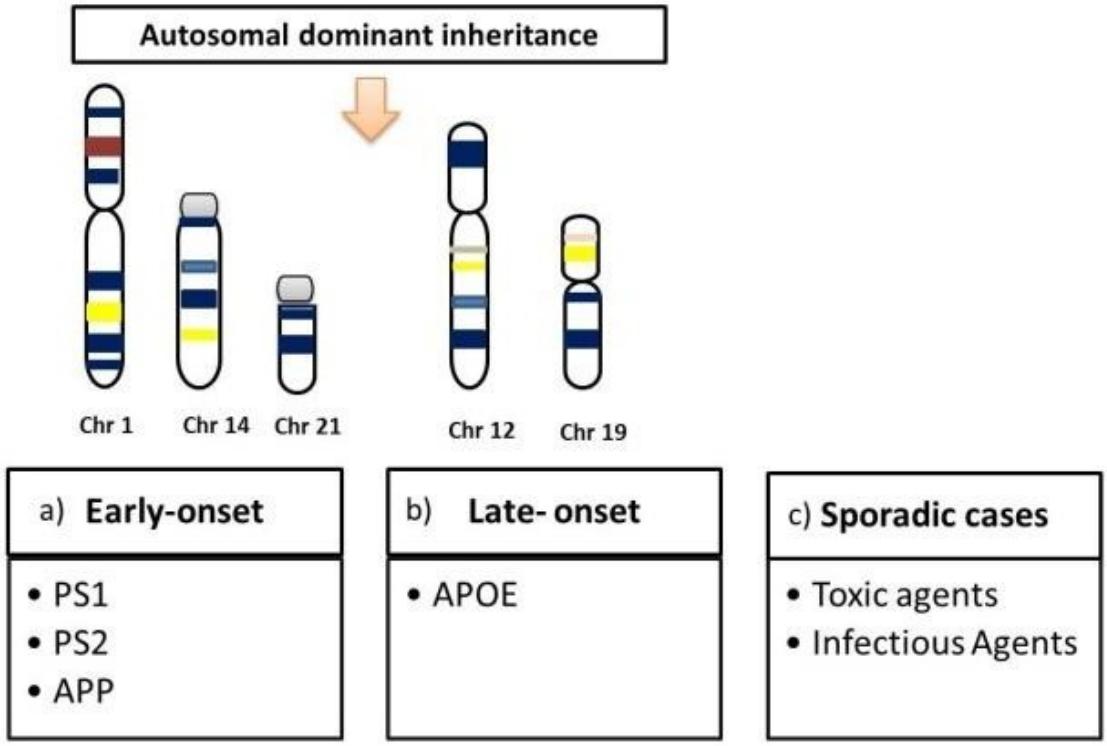

Figure 1: Genetic aspect of Alzheimer's disease [11].

1.2 Molecular characteristic of Alzheimer disease

The main neuropathological features of AD are the accumulations of β-amyloid plaques, tau tangles, neuroinflammation, and synaptic and neuronal loss, the latter being the most vital correlating factor with memory and cognitive impairment. In older individuals there is also the presence of Lewy bodies and vascular diseases even in cases of FAD, Lewy body pathology often coexists, the mechanism of which remains uncertain. Many of these pathological signs influence each other during the onset and progression of the disease. Recent genetic evidence suggests the possibility of a causal link between impaired immune pathways and synaptic dysfunction in AD. Emerging studies also suggest that immune-mediated synaptic pruning could initiate the early-stage pathogenesis of AD [12]. Aβ plaquesinitially develop in the basal, temporal, and orbitofrontal neocortex regions of the brain and later stages progress through the neocortex, hippocampus, amygdala, diencephalon, and basal ganglia. In critical cases, Aβ is also found throughout the midbrain, lower brainstem, and cerebellar cortex [2]. Amyloid plaques are formed by Aβ peptides obtained from amyloid precursor protein (APP) by enzymatic cleavage by α, β, and γ-secretase [13]. The process of amyloid plaque formation originates from the cleavage of amyloid precursor protein (APP) by β-secretase to

produce a c-terminal fragment attached with fragments of 89 or 99 amino acids (figure 2). This β-secretase includes BACE 1 (APP β-site cleavage enzyme), which is also called Asp2 or memapsin2. APP is cleaved at the Asp1 and Glu11 β sites by BACE 1. The C-terminal membrane-bound fragment of 99 amino acid residues is further cleaved by γ-secretase to produce the Aβ1-40 and Aβ1-42 isoforms. γ-secretase mainly includes presenilin 1 (PS1) or presenilin 2 (PS2). Aβ1-40 is the non-toxic soluble isoform, while the Aβ1-42 form is the form that easily aggregates and forms plaques due to two additional amino acidsisoleucine and alanine [14]. The change in cleavage mode occurs due to mutations in the APP gene, the presenilin 1, and presenilin 2 genes, or the apolipoprotein E (APOE4) gene [15].

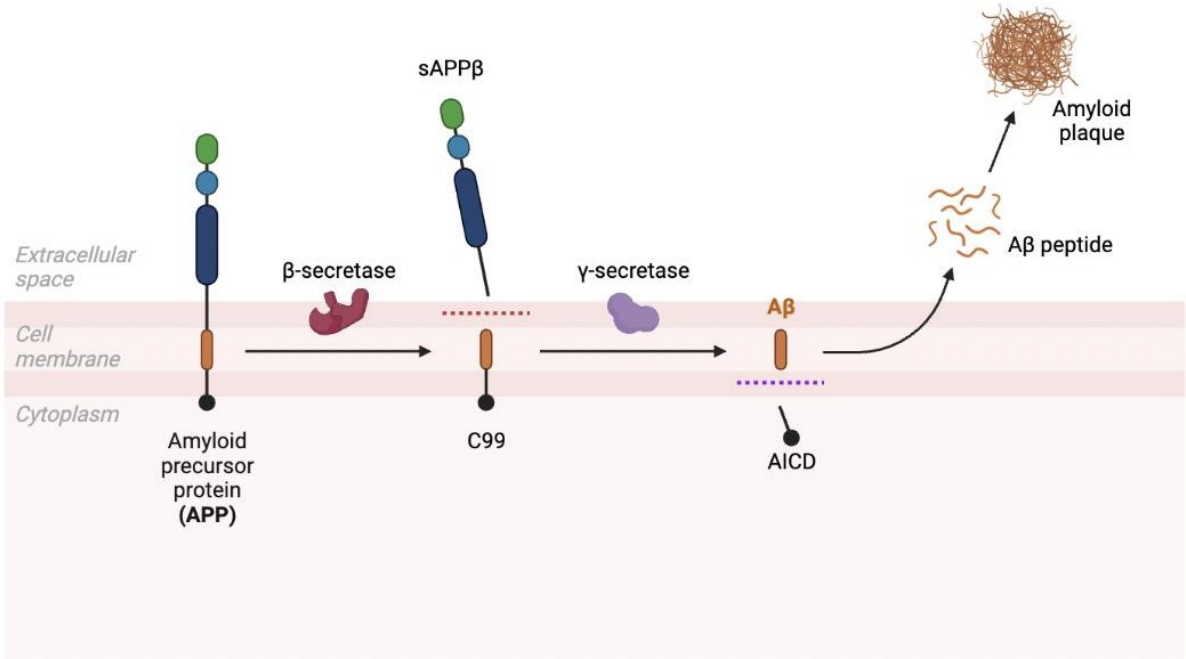

Figure 2: Amyloidogenic Pathway in Alzheimer's disease.

The neurofibrillary tangles characteristic of AD are composed primarily of paired helical strands made up of hyperphosphorylated tau. Tau pathology begins in the medial temporal lobe allocortex (entorhinal cortex and hippocampus) before spreading to the association isocortex [12]. Tau proteins are neuronal proteins that have a microtubule-binding domain, which is involved in the polymerization and stabilization of microtubule assembly to maintain the integrity of the cytoskeleton. This binding is regulated by the phosphorylation of serine/threonine residues by a variety of kinases such as Fyn Kinase, glycogen synthase kinase-3β (GSK3β), and cyclin-dependent

kinase-5 (CDK5) [16]. Hyperphosphorylation by these kinases causes a decrease in the affinity of tau proteins for microtubules. Hyperphosphorylated tau forms NFT and is deposited in the cytosol and can no longer perform the function of maintaining the structure of the cell [17]. Furthermore this deposition affects normal cell functions such as synaptic transmission, axonal transport, and signal transduction, and the cell gradually undergoes degeneration [15].

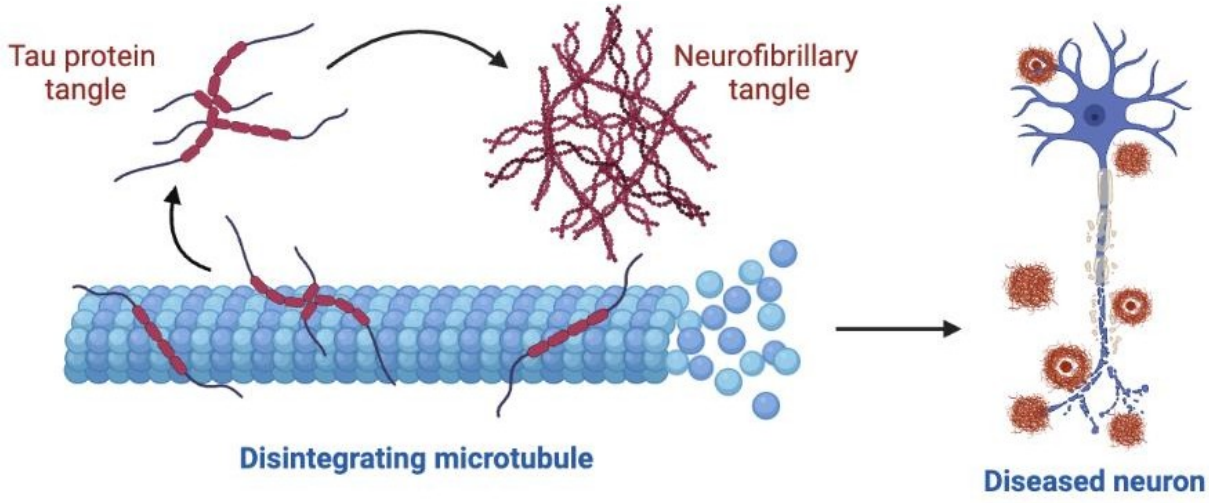

Figure 3: Formation of the tangle of tau in Alzheimer's disease.

Mitochondrial dysfunction and oxidative stress have also long been implicated in the pathogenesis of AD from the earliest stages of the disease [18]. Mitochondrial dysfunction is caused by the decreased level of cytochrome c-oxidase. Furthermore, hyper excitation of glycogen synthase kinase (GSK-3) due to oxidative stress (OS) can alter the permeability of mitochondria. This could lead to an overproduction of ROS, thus mitochondrial dysfunction and oxidative stress are closely related to each other [19]. The production of ROS determines an oxidative change in the Aβ peptide itself making its removal difficult and also causing lipid and protein oxidation of the cell membrane making it permeable and therefore susceptible to degeneration. Aβ proteins can directly activate nicotinamide adenine dinucleotide hydrogen phosphate (NADPH) oxidase to initiate free radical synthesis [15].

AD is also referred to as type 3 diabetes, as *in vitro* and animal studies have indicated that insulin resistance may contribute to the pathogenesis of AD through multiple different pathways [20]. According to Farris et al., insulin-degrading enzyme (IDE) regulates the levels of insulin, Aβ protein,

and the intracellular domain of amyloid precursor protein (APP) in non-AD subjects. Thus, there is a regulatory relationship between insulin, IDE, and Aβ. In the case of AD patients, however, the state of cerebral insulin resistance means that insulin probably fails to stimulate the clearance of Aβ and thus allows its accumulation within neurons causing neurodegeneration or neuronal loss [21]. The insulin-resistant state could lead to impaired neuronal function and cognitive ability, accompanied by an extreme increase in insulin and relatively reduced insulin activity [22] [23]. Consequently, this leads to the development of neuritic plaques, hippocampal atrophy, cognitive performance, and lower cerebrocortical glucose metabolism which may be closely related to memory impairment [24]. Neuronal insulin protects against neuroinflammation and redox stress, so any impaired insulin function in the brain hampers neuronal function [25], [26]. Interestingly, insulin can directly modulate synaptic plasticity, learning, and memory, and disturbances in insulin signaling pathways in the periphery and brain have recently been implicated in AD and brain aging. Insulin also negatively regulates the metabolism of Aβ and tau proteins which are key building blocks of amyloid plaques and neurofibrillary tangles and are well-documented neuropathological hallmarks of AD (figure 3). These negative insulin regulations lead to more devastating neurological functions. Conversely, insulin injected into the brain intracerebroventricularly can improve the performance of memory tasks in animals [27]. Furthermore, intranasally administered insulin increased the performance of attention-related tasks in humans [28], [29]. A recent study reported that insulin receptor levels are downregulated in the brain of AD patients [29]. Insulin receptors were found to be internalized in neurons and both insulin receptor (IR)-1 and IRS-2 were reduced which taken together leads to reduced insulin signaling activity. It is becoming increasingly evident that the alteration of signaling molecules that are known to be involved in insulin signal transduction may play a role in the pathogenesis of AD [30]. Although the actions of brain insulin are not fully understood, binding of insulin to its receptor initiates autophosphorylation of the β-subunit of the receptor, leading to tyrosine binding and phosphorylation of multiple insulin receptor substrates including IRS- 1 and IRS-2, which play a role in synaptic plasticity and memory formation [31] [26] (figure 4).

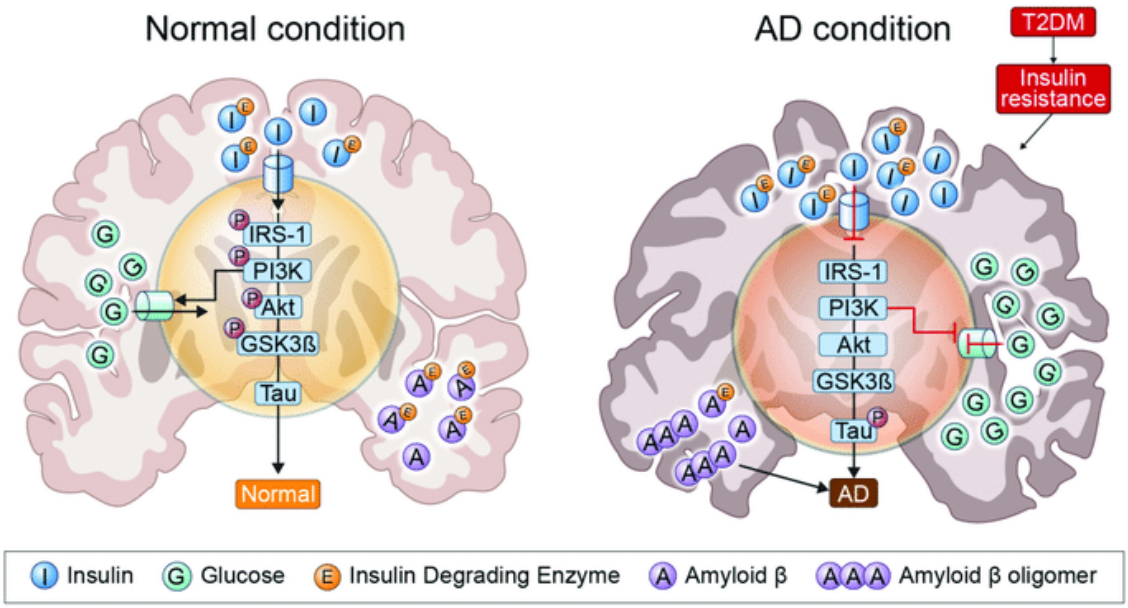

Figure 4: Insulin resistance brain state in Alzheimer's disease compared to insulin signaling in the normal condition brain [32].

1.3 Diagnosis of Alzheimer's disease

As far as the diagnosis of Alzheimer's disease is concerned, this depends mainly on imaging techniques and the analysis of cerebrospinal fluid (CSF) proteins. Imaging techniques include magnetic resonance imaging (MRI) (figure 5) which is used for both structural and functional evaluation [33],[34], fluorodeoxyglucose (FDG), and PET for the evaluation of amyloid and brain metabolism. MRI also allows you to rule out other neurodegenerative disorders and evaluate the presence and extent of cerebrovascular disease (eg, white matter hyperintensity and lacunar infarcts) that may mimic or coexist with AD. The imaging techniques are based on three biomarkers for Alzheimer's disease: medial temporal lobe atrophy on MRI, posterior cingulate and temporoparietal hypometabolism using18FDG PET as measures of neurodegeneration, cortical amyloid deposition-β on PET-amyloid imaging [35]. The diagnostic accuracy of AD with a specialized PET scan has 100% specificity and 96% sensitivity in AD even in patients with a milder condition. Florbetapir, florbetaben, and flutemetamolare used as PET ligands for diagnosis but are not widely used due to their high cost [15], [4][36],[37].

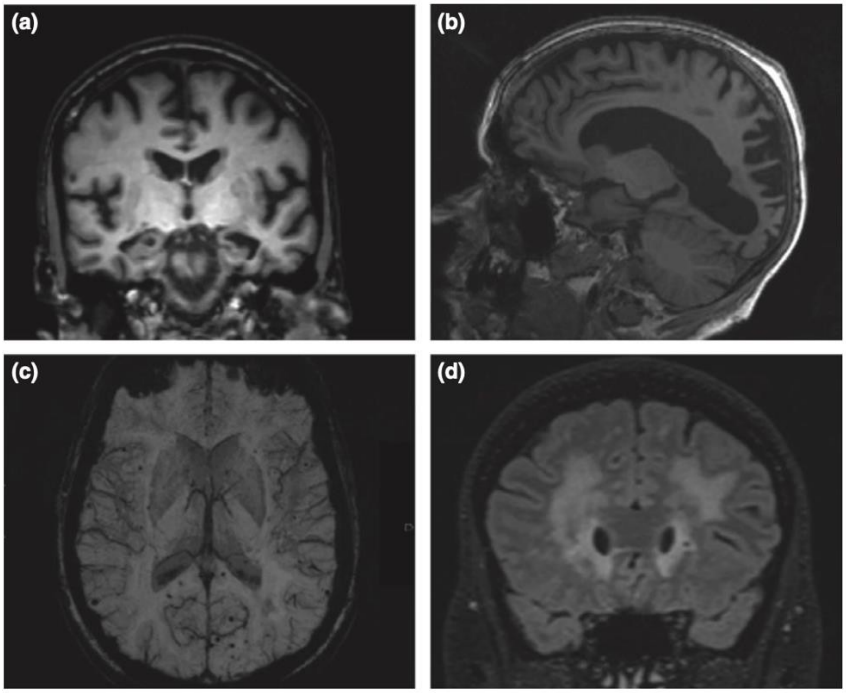

Figure 5: MRI images showing (a) characteristic hippocampal atrophy in a typical Alzheimer's disease case best visualized in the coronal plane on T1; (b) parieto-occipital atrophy in a posterior cortical atrophy case, here demonstrated in the sagittal plane on T1; (c) microbleeds which are best visualized on SWI (the posterior distribution seen on this axial image is characteristic of cerebral amyloid angiopathy); (d) extensive periventricular and subcortical white matter hyperintensities best visual- ized on FLAIR, seen here on a coronal image [6].

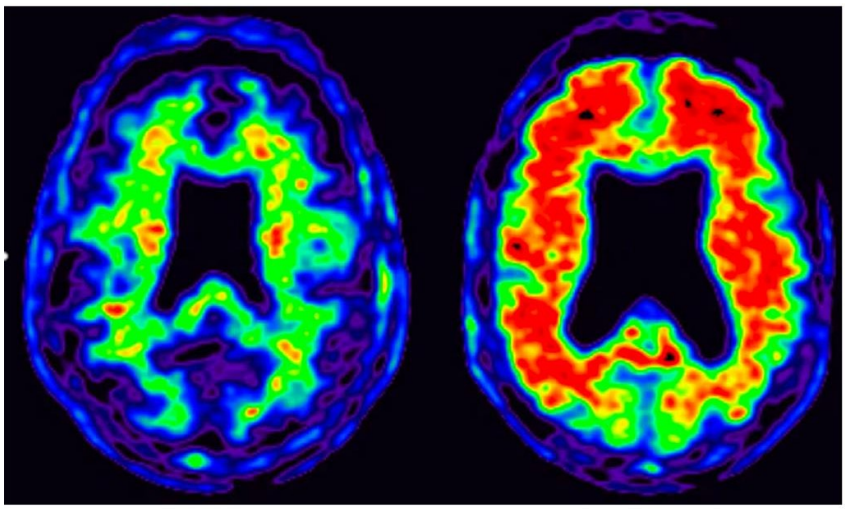

Figure 6: Florbetapir amyloid positron-emission tomography scan in healthy control (left) and an Alzheimer's disease patient (right). Warm colors indicate high amyloid accumulation. For clinical

purposes, florbetapir scans are read on a grey scale [6]

Instead, as regards the diagnosis by analysis of the cerebrospinal fluid (CSF), Jack et al grouped the biomarkers in A (amyloid), T (phosphorylated tau), and N (neurodegeneration measured in total tau): the ATN picture. In this context, the diagnosis of Alzheimer's disease is defined by the presence of amyloid β and phosphorylated tau [38]. The subjects to be considered as Alzheimer's subjects must have a concentration of amyloid fibers 1-42 less than 650 pg/ml, the ratio of amyloid fibers 1-42/1-40 must be less than 0,069 pg/ml, t-tau and p-tau must have a value greater than 416 pg/ml and 61 pg/ml, respectively. This method has 85-90% accuracy in diagnosing AD. Brain imaging and cerebrospinal fluid analysis revealed that the pathological changes begin two decades before the onset of symptoms. Thus, diagnosing AD at symptom onset is not very helpful as pathological changes and cognitive impairment are already accelerated to higher stages. Consequently, it would be useful to find new biomarkers, which can help in an early diagnosis of AD when the clinical and behavioral manifestations are not yet evident. Possible markers for AD pathology could be those reflecting axonal damage and synaptic dysfunction considering the presence of synaptic pathology early in the disease course and its relationship to functional outcomes and cognitive decline. Some of these biomarkers are for example neurogranin, SNAP25, synaptotagamins, and the neuronal calcium-sensing protein VLP1 [39] [40] [41] [42]. Even if Aβ and NFT are considered the main actors of the disease the neuroinflammatory process potentially represents one of the cornerstones of AD pathogenesis, it would therefore be useful to look for new markers for AD precisely in the inflammatory pathway. Indeed, amyloid plaques are recognized as foreign material by the brain that initiates an inflammatory and immune response by activating microglia that co-localize with amyloid plaques and the release of cytokines, which ultimately lead to cell death and neurodegeneration. The question of whether or when neuroinflammation is protective, harmful, or perhaps both may depend on the disease stage and genotypes and remains to be fully elucidated. Neuroinflammation plays a fundamental role in the development and progression of neurodegeneration. It could therefore be said that neuroinflammation in neurodegenerative pathologies is not a consequence but a cause of them and could represent a therapeutic target of neuronal degeneration.

1.4 Neuroinflammation in Alzheimer's disease

Even if Aβ and NFT are considered the main actors of the disease, the neuroinflammatory process potentially represents one of the cornerstones of the pathogenesis of AD [43], [44], [45]. Activated astrocytes and microglia are typically found around neurons and plaques. Indeed, amyloid plaques are recognized as foreign material by the brain that initiates an inflammatory and immune response

by activating microglia that co-localize with amyloid plaques and the release of cytokines, which ultimately lead to cell death and neurodegeneration [46]. The question of whether or when neuroinflammation is protective, harmful, or perhaps both may depend on disease stage and genotypes and remains to be fully elucidated. Neuroinflammation plays a fundamental role in the development and progression of neurodegeneration. It could therefore be said that neuroinflammation in neurodegenerative pathologies is not a consequence but a cause of them and could represent a therapeutic target of neuronal degeneration. Microglia are the resident immune cells of the central nervous system. In AD, microglia interact with Aβ oligomers and fibrils with scavenger receptors (SCARA-1, MARCO, SCARB-1, CD36 and RAGE), G protein-coupled receptors (FPR2 and CMKLR1) [47], Toll-like receptors (TLR2, TLR4 , TLR6 and TLR9), CD47, integrin α6β1 and TERM2 [48] . After initial recognition, microglia are activated through the NF-κB pathway. The presence of Aβ fibrils causes an overactivated and chronic form of microglia that produce proinflammatory mediators, which lead to a reduced capacity for phagocytosis and prolong neuroinflammation. Astrocytes are also involved in the neuroinflammatory pathway in AD. Astrocytes are multifunctional glial cells involved in neuron nutritional supplementation, waste elimination, and maintenance of the blood-brain barrier. In AD, astrogliosis and astrocyte atrophy occur early in the disease course, even before amyloid plaque formation. Furthermore, the formation of Aβ fibrils subsequently activates astrocytes even more, possibly through the NF-κB pathway. Activated astrocytes degrade Aβ itself and increase microglial phagocytosis through ApoE lipidation. However, activated astrocytes also produce inflammatory mediators, contributing to the process of neuroinflammation [49], [50] Oligodendrocytes are the source of myelin in the central nervous system. The role of oligodendrocytes in AD neuroinflammation is stilllargely unknown. In an *in vitro* study, oligodendrocytes can synthesize complement and therefore could contribute to the neuroinflammation process [50]. Central to the inflammatory process of AD is cytokine activity. For example, TNF-α increases the generation of Aβ from APP via β- and γ- secretase [51]. IL-1 intervenes both in the formation of Aβ by increasing the synthesis and secretion of APP and in the formation of tau tangles by increasing the phosphorylation of tau protein through the p38-MAPK pathway [52]. IL-6 increases the expression of APP [53] and increases the phosphorylation of tau protein via the cdk5/p35 pathway [54] [55]. One of the pivotal cytokines involved in the inflammatory pathway of AD pathology is CX3CL1 also called Fraktalina (FKN). This cytokine appears on the one hand to prevent the neurodegeneration of AD on the other hand to contribute to the pathogenesis.

1.5 CX3CL1 and its double form

CX3CL1 is a chemotactic cytokine present throughout the body and involved in inflammatory processes. This cytokine exists in two forms: a membrane-bound transmembrane form that acts as an adhesion molecule, and a soluble form that could take on several functions. The transmembrane form (mCX3CL1) at the brain level is expressed on the surface of astrocytes and neurons and interacts with its unique receptor CX3CR1 present on microglia [56]. mCX3CL1 is composed of 373 total amino acids consisting of an extracellular N-terminal domain (residues 1–76), a mucin-like stalk (residues 77–317), a transmembrane α helix (residues 318–336), and a short cytoplasmic tail (residues 337–373) [57]. The soluble form of CX3CL1, however, can be generated by various types of proteolytic processes and is supposed to have a signaling role. Among the various processes of proteolytic cleavage we find that by the metalloprotease ADAM10 which generates various soluble forms of CX3CL1 [58] [59] that of inflammatory agents, such as lipopolysaccharide (LPS), interleukin (IL)-1b or phorbol esters, enhance CX3CL1 cleavage through tumor necrosis factor (TNF)-α converting enzyme (ADAM17) [60], [61] . Fraktalin is synthesized as a 50-75 kDa precursor that undergoes rapid maturation, produced by glycosylation, to produce mature 100 kDa FKN. These data suggest that FKN is initially synthesized as an intracellular precursor that undergoes glycosylation and transport to the cell surfaceas a 100-kDa glycoprotein. The 100 kDa FKN can then be released from the cell surface producing an 85 kDa soluble fragment that likely contains the majority of the glycosylated ectodomain and a transmembrane cytoplasmic tail fragment of ≥ 20 kDa [60] (figure 7).

Cleavage of CX3CL1 is mediated by different members of the ADAM family depending on whether the cleavage is constitutive or induced. The ADAM10 protease has been shown to be involved in the constitutive cleavage of CX3CL1 through inhibition studies with natural inhibitors of metalloproteinases such as TIMP-1. TIMP-1 in fact inhibited the constitutive cleavage of CX3CL1 by blocking the activity of ADAM10. This hypothesis was also confirmed by the overexpression of this protease which led to an increase in constitutive cleavage of CX3CL1 and by the deletion of the Adam10 gene which abolished a major part of the constitutive loss of CX3CL1 ([58]. The cleavage of CX3CL1 in response to stimuli instead appears to be mediated by another protease of the ADAM family, namely ADAM17. *In vivo* the increase in expression of ADAM17 occurs in response to inflammatory stimuli, this suggests ADAM 17 is activated during inflammatory responses by mediating the cleavage of various proteins including circulating TNF-α and the cytokine CX3CL1 itself [62]; [63]. The action of ADAM17 on CX3CL1 was demonstrated by induction with PMA (phorbol-12-myristate-13-acetate) which stimulated cleavage of CX3CL1 by ADAM17 but not ADAM10, this was confirmed by the fact that inhibition of TACE but not inhibition of ADAM10

blocked CX3CL1 cleavage [60]. Furthermore, cell adhesion assays were performed to understand the consequences of CX3CL1 cleavage and the membrane form of fraktalin was found to be critical for maintaining cell adhesion. The mixed ADAM17/ADAM10 inhibitor was shown to block adhesion death with the same potency as the selective ADAM10 inhibitor, suggesting that ADAM10 rather than ADAM17 is relevant in promoting cell adhesion death [58].

It has been demonstrated that secretases, particularly beta and gamma secretases, are also involved in the cleavage of CX3CL1. Overexpression of beta secretase has been shown to generate two low-m.p. C-terminal fragments. (12 kDa and 10 kDa) and three fragments at p.m. higher than CX3CL1. Confirmation that these two C-terminal fragments were generated by BACE1 activity was confirmed by treatment with a potent BACE inhibitor (BACE1 inhibitor IV) which reduced the levels of these two fragments [64]. The cleavage activity of gamma secretase instead appears to act on the intracellular domain of CX3CL1, this was demonstrated using two different inhibitors for the gamma-secretase complex and PSEN 1 and 2 deficient embryonic fibroblasts. The activity of gamma-secretase generates both membrane fragments and intracellular fragments. The generated membrane fragments appear to be degraded by proteasomal activity, as these fragments became detectable upon inhibition of proteasomal degradation but were absent when gamma secretase activity was blocked. This may play a mechanism to clear the cell membrane of C-terminal fragments of transmembrane chemokines that would otherwise accumulate in the cell membrane [65]. Intracellular fragments of CX3CL1 generated by the gamma-secretase complex may instead be involved in intracellular signaling [66]. Fan et al. demonstrated that the intracellular domain of CX3CL1 following cleavage from the gamma-secretase complex undergoes nuclear translocation, altering gene expression, particularly controlling TGFβ/Smad signaling pathways. The C-terminal intracellular domain of CX3CL1 induces the expression of many genes directly or indirectly through TGFβ superfamily effects. One of these molecules is Pax6, involved in neuronal differentiation [67]. Furthermore, this domain controls the Smad pathway and Smad2-mediated transcription is critical for the development, function and/or maintenance of neuronal cells in the brain [68]. Therefore, the C-terminal intracellular domain of CX3CL1 generated by cleavage of the gamma-secretase complex can be said to promote neurogenesis. Unfortunately, however, the dual role, perhaps even with completely opposite effects, that the membrane form of CX3CL1 and its soluble form plays is not yet completely clear. To try to clarify this aspect, the action of mCX3CL1 and sCX3XL1 was evaluated in CX3CL1 - / - mice [69]The knockout mice showed deficits in motor performance, long-term memory, and spatial learning. These deficits clearly also affected hippocampal neurogenesis and long-term potentiation (LTP). Regarding neurogenesis and long-term potentiation (LTP) only sCX3CL1 seems to have a positive effect. Treatment with sCX3CL1 restored the expression of both Ki67 and DCX in the

subgranular zone (SGZ), indicative of enhanced neurogenesis, and restored LTP. Also, regarding motor performance, only sCX3CL1 has been shown to restore neural pathwaysassociated with motor function. Regarding deficits in long-term memory and spatial learning, treatment of CX3CL1 - / - mice with both sCX3CL1 and mCX3XL1 improved memory and spatial learning deficits. [70].

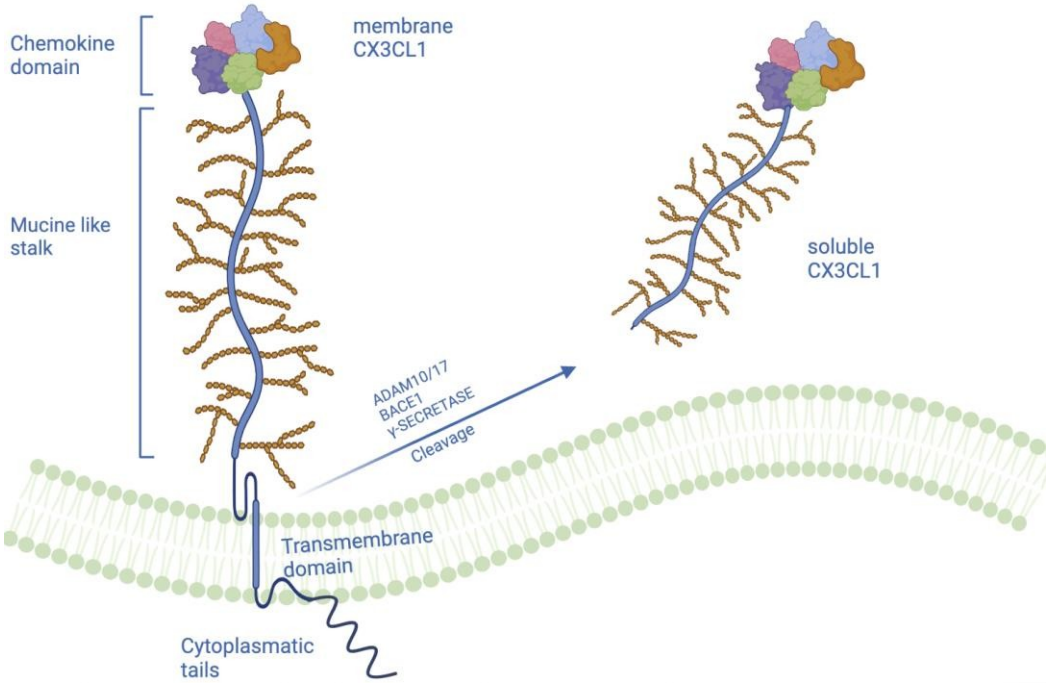

Figure 7: Representation of the structure of CX3CL1 composed by chemokine domain, mucine-like stalk, transmembrane domain and cytoplasmatic tails. The cleavage of CX3CL1 by metalloproteases and disintegrins ADAM10, ADAM 17, BACE1, and γ-secretase generates the soluble form of CX3CL1 composed only of the chemokine domain and mucine-like stalk [71].

CX3CL1 in neuroinflammation CX3CL1 is primarily expressed by epithelial cells in the lung, kidney, and intestine and is creased in endothelial cells at sites of local inflammation, but CX3CL1 expression is higher in the brain than in most other organs[72] [73]. CX3CL1 is also mainly expressed in the brain. As previously mentioned at the brain level, CX3CL1 is widely expressed by neurons of the hippocampus and cortex and interacts with its exclusive receptor CX3CR1 on microglia. CX3CL1/CX3CR1 binding therefore mediates the interaction between neurons and microglia by maintaining microglia in a resting state (quiescent or inactivated) thus inhibiting the release of proinflammatory cytokines (figure 8) [74]. Furthermore, it enhances phagocytosis of presynaptic elements. ..Microglial responses to CX3CL1/CX3CR1 signaling involve transient calcium mobilization, chemotaxis, production of matrix metalloproteinases 2 and 9, and a cascade

of protein phosphorylation and enzyme activation [75]. Several studies have demonstrated that binding of fraktaline to CX3CR1 induces MAP kinase activation [76]. Exposure to ultraviolet radiation, heat shock or inflammatory cytokines activates the JNK/SAPK pathway. The p38 pathway is activated in response to inflammatory cytokines, endotoxins, and osmotic stress. While binding of extracellular growth factors to tyrosine kinase-related receptors activates the ERK pathway. In turn, the ERK signaling pathway recruits transcription factors such as NF-κB and cyclic adenosine monophosphate response element binding protein (CREB) [77]. The CX3CL1-CX3CR1 pathway therefore plays a fundamental role in neuroinflammation. Binding of CX3CL1 to its microglial receptor has also been shown to reduce microglial toxicity and protect neurons from apoptosis in inflammatory conditions; in fact, the increase in microglial activity due to an interruption of CX3CL1/CX3CR1 signaling is accompanied by an increase in neuronal death. Furthermore, because microglia react rapidly to protect normal neurons and eliminate damaged neurons in the brain, microglia can act as a sentinel for neurons [78]. Therefore, these findings suggest that CX3CL1 activity may result from direct activation of signaling pathways in microglia. CX3CL1 can prevent activated microglia from producing proinflammatory cytokines and reactive oxygen species, release neuroprotective adenosine to stimulate astrocytes to upregulate glutamate transporter expression, andmodulate the entry of hematogenous leukocytes into the brain [79].

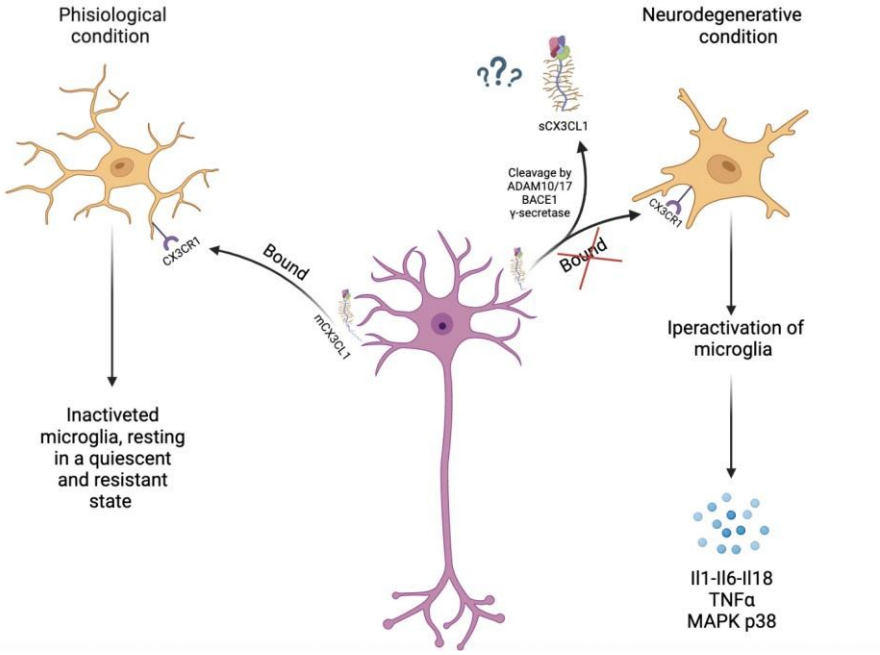

Figure 8: Signaling CX3CL1-CX3CR1. Physiologically mCX3CL1 bound its only receptor present on the microglia resulting in inactivation of microglia maintaining it in a resistant and quiescent state. In neurodegenerative disease there is interrupt of signaling CX3CL1-CX3CR1 resulting in overactivation of microglia and production of inflammation factors. Moreover, in inflammation

conditions there is a cleavage of mCX3CL1 resulting in formation of the soluble form of CX3CL1 [71].

1.6 CX3CL1 and Alzheimer disease

The CX3CL1/CX3CR1 interaction plays a vital role in maintaining a healthy and anti-inflammatory condition in the brain. In Alzheimer's disease, CX3CL1/CX3CR1 signaling initially attempts to control the progression of the disease by inhibiting inflammation and tau phosphorylation, thereby causing an increase in the deposition of β-amyloid fragments. Subsequently, intra-neuronal accumulation of β-amyloid triggers CX3CL1/CX3CR1 signaling, resulting in increased phagocytosis of Aβ and hyperphosphorylation of tau. The decrease in CX3CL1/CX3CR1 signaling also causes hyperactivation of microglia and hyperproduction of inflammatory elements [80]. However, CX3CL1-mediated neuron-glia crosstalk in the context of AD has reported conflicting results [81]; [82]. There is a close correlation between the CX3CL1/CX3CR1 pathway and some transcription factors (P38, β-catenin, NF-kB) and associated molecules (AKT and GSK3-β) in AD pathology. In AD, the fact that CX3CL1 no longer binds to its receptor causes hyperactivation of microglia resulting in rapid activation of p38 MAPK which in turn upregulates the production of proinflammatory cytokines, such as IL-1 and TNF-α. Furthermore, IL-1 activates p38 MAPK in astrocytes and neurons, causing excessive inflammation and tau phosphorylation [83]. Amyloid beta fragments have also been reported to stimulate microglia to express high levels of IL-1, IL-6, and IL-18. The production of proinflammatory cytokines induces astrocyte activation, followed by microgliosis [84]. CX3CL1 is also involved in the activation of the NF-kB pathway [85]. NF-kB plays a vital role in inflammation, signaling, and AD progression. Activation of NF-kB contributes to increasing β-secretase in neuronal cells *in vitro* and *in vivo*. AD brains reduce increased levels of BACE1 and NF-kB p65, and NF-kB p65 leads to increased BACE1 promoter activity and BACE1 transcription, while deletion of NF-kB p65 reduces the BACE1 gene expression in cells [86]. In addition to having binding sites in the promoter region of genes involved in amyloidogenesis, NF-κB also has binding sites in the promoter region of genes involved in inflammation [87]. NF-kB regulates the expression of proinflammatory cytokines such as IL-6, IL-1β, and TNF-α which are elevated in the brains of AD patients. These cytokines (IL-6 and IL-1β) not only increase inflammation but also induce brain cell death by apoptosis. In the brains of AD patients, activated NF-κB was found predominantly in neurons and glial cells in the areas surrounding Aβ plaques [86]. Another AD-related pathway is the activation of Wnt/β-catenin signaling, which inhibits the production of amyloid peptides and the hyperphosphorylation of brain tau protein. An increase in the Wnt antagonist DKK1 causes a rapid decrease in the levels of essential signaling proteins, including β-catenin, cyclin D1, c-myc, Wnt7a,

and PSD95. Another important hallmark of AD is the presence of intracellular tangles composed of hyperphosphorylated forms of the microtubule-associated protein tau in neurons. GSK3 is an important kinase associated with the hyperphosphorylation of the tau protein at the phosphorylation sites relevant for AD. Activation of Wnt/β-catenin signaling results in inhibition of GSK3 activity and subsequent suppression of tau phosphorylation. Furthermore, activation of Wnt/β-catenin signaling can inhibit tau hyperphosphorylation and neuronal death. Apolipoprotein E4 (ApoE4) can inhibit Wnt/β-catenin signaling [88].

The correlation between CX3CL1/CX3CR1 signaling and these fundamental transcriptional factors in the progression of AD pathology highlights the importance of this inflammatory cytokine in the process and neuroinflammation of AD. Indeed, it has been demonstrated that in Alzheimer's patients there is a significant increase in the concentrations of sCX3CL1 in the cerebrospinal fluid and blood, probably due to the role it plays as a mediator of inflammation. Furthermore, it was observed that the difference in sCX3CL1 concentration in CSF and blood is influenced by the stage of the disease. The concentration of sCX3CL1 is increased in the early stages of AD and then gradually decreases during the development and progression of the disease. Therefore, the hypothesis is that neuroinflammation causes an increase in the activity of proteases that cleave CX3CL1, releasing its soluble form into the cerebrospinal fluid and blood, resulting in increased levels of sCX3CL1 in the early stages of the disease as a protective mechanism [89]. Furthermore, the soluble form of CX3CL1 has been shown to influence the deposition of beta-amyloid fragments. In fact, it has been seen that the increase in expression of sCX3CL1 reduces the deposition of beta-amyloids in large regions of the brain since they have a whole structure of total levels of APP determines-C99 and C83, products of APP long cleaved by BACE1 and α-secretase. The reduction of both C-li fragments of APP would be correlated with the cessation of amyloid deposition [27]. Furthermore, sCX3CL1 also influences tau pathology in AD. It has been shown that sCX3CL1 does not have an effect on total tau but specifically reduces the levels of phosphorylated tau and forms a protective effect against neuronal loss [64]. Furthermore, a reduction in the active form of GSK3-beta, responsible for tau phosphorylation, was also observed [56]. The membrane form of CX3CL1 also influences tau pathology in AD. It has been seen that the tau protein and CX3CL1 compete for their binding to the same receptor, namely CX3CR1. It was observed that the binding of Tau to CX3CR1 is weaker in the presence of CX3CL1. We also assessed whether competition between Tau and CX3CL1 affected internalization of Tau by microglia. The results showed that in the presence of CX3CL1 Tau internalization is reduced [81]. Therefore, fractalin plays different roles depending on its soluble or membrane form, influencing beta amyloid deposition and tau pathology in AD. Therefore, it could certainly represent a fundamental element for the progression of Alzheimer's disease and a potential

target for therapeutic intervention (figure 9).

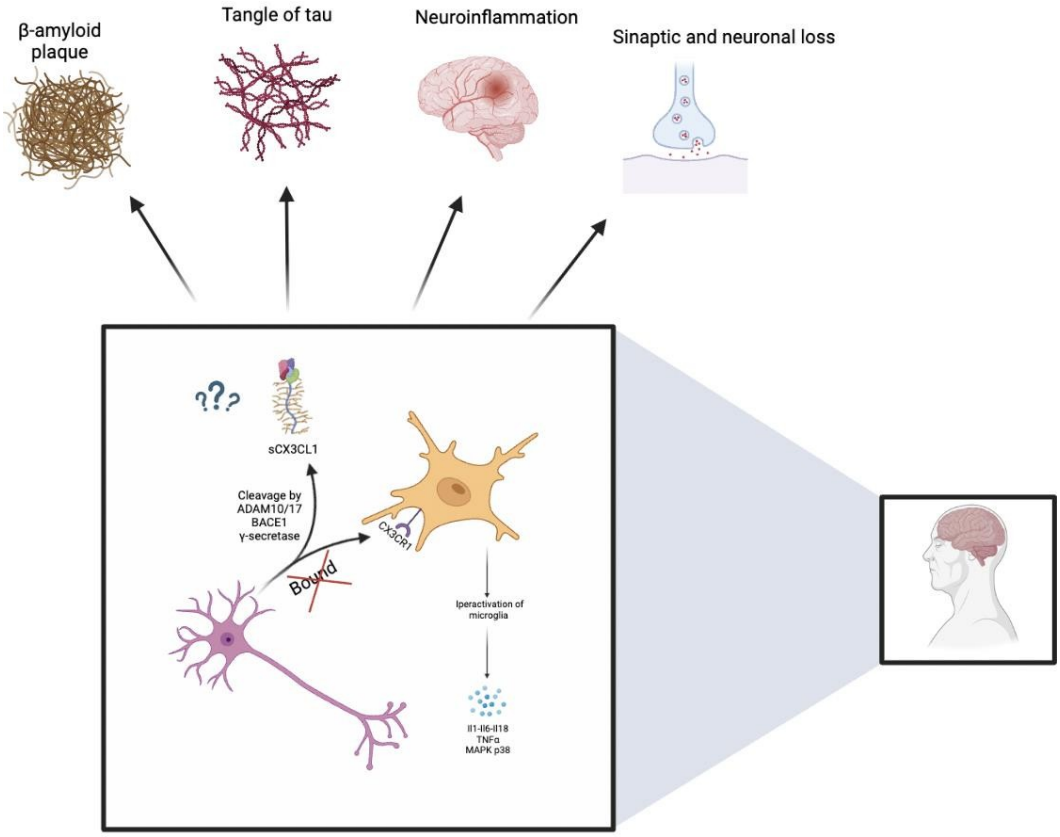

Figure 9: Schematic representation of the role and the influence of CX3CL1 in Alzheimer's disease.

2. AIM OF THE RESEARCH

My research activity is carried out at the Biochemistry laboratory directed by Professor Giulio Ghersi at the STEBICEF department and with the support of Professor Giulia Bivona of the department of Biomedicine, Neuroscience and Advanced Diagnostic. The research project aims to determine from a molecular/cellular point of view the role that CX3CL1 and its receptor CX3CR1 have / can have in the onset of Alzheimer's disease, to identify elements that may be up in the metabolic pathways. - and down-regulated in the early stages of the disease when the clinical and behavioral manifestations of the affected subjects are not yet manifest.

To achieve this goal, the study is developed on two contextual levels *in vivo* and *in vitro*, and will allow analyzing, on the one hand, the proteolytic cascades generated by the interaction between CX3CL1 and CX3CR1 and the role played by the mediators Aβ and/or total and hyperphosphorylated tau in the activation of specific enzymatic cascades, and on the other the expression of some transcription factors and their metabolic "pathways" related to the progression of AD to be used as early markers of the disease.

3. MATERIALS AND METHODS

3.1 Patients and groups selections

For this study we selected 28 patients affected by AD and a control group of 18 subjects affected by cognitive decline not related to AD. AD patients were diagnosed according to current criteria (Albert, 2011; MacKahnn, 2011). All patients were recruited from the Clinic for Cognitive Decline, Dementia and Parkinsonism of the University Hospital Paolo Giaccone Palermo, Italy and underwent a general and neurological examination, cognitive evaluation, brain MRI and FDG-PET as well as a lumbar puncture during the diagnostic work-up. Then, all patients were classified according to the AT(N) biomarkers classification (Clifford R. Jack, Jr ,2018). Group A (mean age 70 ±8; F/M=0.75) consisted of patients categorized as "Alzheimer's Continuum" being only A+T± (N+) patients; Group B (n: 18; Mean Age 66.7 ± 10; F/M=0.83) consisted of 18 A-T-(N+) patients (i.e. "non-AD pathological changes"). Inclusion criteria for Group A were diagnosis of mild cognitive impairment due to AD [42] or probable AD dementia with evidence of AD pathophysiological process [49] as well as being part of "Alzheimer's continuum " according to AT(N) classification. Exclusion criteria for groups A were: any other medical condition explaining cognitive decline, including other degenerative diseases, cerebrospinal disease, metabolic disease, and substance abuse.

3.2 CSF Samples

A lumbar puncture (LP) was performed to collect cerebrospinal fluid (CSF). The CSF was collected as a routine procedure in two different tubes: one for standard physical and chemical analysis and a second, in polypropylene, for neurochemical analysis. All CSF samples were centrifuged, aliquoted, and stored at -80 °C. A chemical-physical examination of the cerebrospinal fluid (cell count, protein, and glucose concentration) was performed to exclude an inflammatory/infectious disease in the brain that could cause CD. Finally, specific levels of CSF biomarkers for AD (A42; t-tau and p-tau) were determined according to clinical biochemistry. This CFS samples obtained from AD and not AD patients were analyzed for the presence of the soluble form of CX3CL1, together with the canonical markers A42, A40, ratio A40/A42, t-tau, and p-tau by ELISA and CLEIA test. Therefore, 3 groups were generated and defined as A', A'' and B. The group A' consist of 16 patients characterized by a high expression of both totals and phosphorylated Tau, and Group A'' includes 12 patients characterized by amyloidosis, where the amyloid fibers are well represented; however, the group A", in which both total Tau and phosphorylated-Tau (p-Tau) are around of normal values, they represent together A' group by clinical evaluation the AD subjects, sick. The third group, Group B, includes 18 subjects defined by us as «non-AD», about characteristics; since all markers are in a range of non-Alzheimer condition, although clinically subject to different neuropathology. The results obtained highlighted the presence of CX3CL1 for a quantity greater than 40% in subjects with AD compared

to non-AD subjects. This suggests that CX3CL1 could be considered a possible new marker for Alzheimer's in the disease.

3.3 Aβ 1-40, Aβ 1-4, Tau-total and Tau-phosphorylated evaluation by Chemiluminescence enzyme immunoassay (CLEIA) in selection groups

CSF CLEIA evaluation of all the patients under examination for the concentration of amyloid fibers, Aβ 1-40 and Aβ 1-42, and the Tau protein in the hyperphosphorylated form (Tau-phosphorylated) and as total Tau (Tau-total) was performed. In particular, we have been used as markers in identification of different molecules, the following: Lumipulse G β-amyloid 1-40, Lumipulse G β-amyloid 1-42, Lumipulse G Total Tau and Lumipulse Gp Tau 181 (in hyperphosphorylated Tau identification), from Fujirebio Inc. Erope, Gent, Belgium) on fully automated platform (Lumipulse G1200 analyzer Fujirebio Inc. Erope, Gent, Belgium) according manufacture's instructions.

3.4 CX3CL1 evaluation by Enzyme Linked Immunosorbent Assay (ELISA) in CSF patients

To evaluate amount of human Fractalkine (Chemiokine CX3CL1, soluble form) in CSF on analyzed patients a sandwich enzyme-linked immune-sorbent assay technology was applied. In particular the Wuhan Fibe Biotech Co., Ltd (Wuhan, Cine) was used, according manufacture's instructions. Briefly, the CSF obtained from patients (previously described in "*Patients and groups selections"*) were resumed in liquid form by cold thawing and then brought back to r.t. and mixed 1:1 in dilution buffer f.v. 100 ml. Samples together standards and background controls were incubated 90' at 37 °C, washed and incubated with Biotin-labeled Antibody 60' at 37 °C; washed, again, and incubated with 3,3',5,5'-tetramethylbenzidine (TMB) 10'-20' at 37 °C; colorimetric reactions were stopped by adding Stop Solution and analyzed by spectrophotometric analysis [microplate reader DU-730 Life Science spectrophotometer] at O.D. 450.

3.5 Statistical Analyses

The data obtained were evaluated for their normality by applying the Shapiro-Wilk test. While the variance found between the different samples, as a function of the analyzed variables, was determined according to one-way ANOVA (p* value). Given the limited number of subjects analyzed (a canonical Student T-test not applicable) for the presence in the CSF of the different molecules, for the statistical analysis of the data, we applied Mann Whitney R - test (non-parametric test). In particular, the evaluation was made on the ratio of the mean of the medians between non-AD and AD subjects. For p-value < 0.05, the null hypothesis (H0 - equality of the values of the two groups) is rejected.

3.6 NAM co-cultures

Neurons were purified from the cerebral cortex of rat fetuses at day 16 of gestation and co-cultured with astrocytes and microglia (5x $10^4/cm^2$) in a serum-free Maat medium [16-17-18].
The cerebral hemispheres of 16-day-old rat fetuses were removed by aseptic surgical procedure, placed in a falcon containing 20 ml of Hams F12 + 20% NCS (newborn calf serum), and cleaned of their meningeal covers under a dissecting microscope. The tissue was fragmented by a series of passes through a Pasteur pipette and then dissociated by filtration through a nylon sieve (50 µm) by gently applying pressure using a rubber "scraper". To remove aggregates and cerebral vessels, the cell suspension was again filtered through another nylon sieve (25 µm). After centrifugation at 250 g for 5 minutes, the cell pellets were resuspended in F12, washed twice, and, finally, resuspended in 5-10 ml of Maat Medium and plated at 2,5 x $10^5/cm^2$. Neurons cells were co-cultured with astrocytes and microglia (5x $10^4/cm^2$), at a density of 2,5 x $10^5/cm^2$ cells per well, in a 24-multiwell. The NAM co-cultures were treated for 24h and 48h with cerebrospinal samples of AD patients and non AD patients. Partly of the NAM co-cultures were treated with only complete sterile PBS and using as a control.

3.7 Immunofluorescence (IF) assays of NAM co-cultures

Neurons cells were co-cultured with astrocytes and microglia (5x $10^4/cm^2$), at a density of 2,5 x $10^5/cm^2$ cells per well, in a 24-multiwell slides containing sterile covers lip in Maat Medium. After 24 h of growth at 37 °C, cell lines on the slides were fixed with 3.7% formaldehyde for 10 min and rinsed with PBS for three times. The cells were labeled with the following primary antibodies diluted in PBS over night at 37 °C: CX3CL1 antibody (1:80), CX3CR1 antibody (1:50), p38 antibody (1:100), β-catenin antibody (1:500), PECAM antibody (1:100), anti-glial fibrillary (1:80) antibody and anti CD11b antibody (1:80). Following 3 washes in PBS, the cell were labeled with the following secondary antibodies diluted in PBS for 2 hours at 37 °C: Mouse Texas Red (1:250), Mouse FITC (1:250), Rabbit Texas Red (1:250), Rabbit FITCH (1:250). In part of the cells the actin cytoskeleton was labeled with phalloidin^{FITC} (1:100 in PBS) for 5 min at room temperature. After 3 washes with PBS, cells were stained with DAPI (1:20000 in PBS) for 10 min, at room temperature for marking the nuclei in blue. Finally, the NAM slides were mounted and observed by epifluorescence microscope (Leica, Wetzlar, Germany), while the Hela slided with confocal microscopy (CLSM, Olympus IX70 laser system with MellesGriot, Shinjuku, Tokyo, Japan).

3.8 Extraction of Soluble Proteins and Zymography assay of NAM co-cultures

Neurons cells were co-cultured with astrocytes and microglia (5x $10^4/cm^2$), at a density of 2,5 x $10^5/cm^2$ cells per well, in a 24-multiwell slides containing sterile covers lip in Maat Medium at 37 °C in a humidified atmosphere of 5% CO_2. After the appropriate treatment, the conditioned medium was taken and the co-cultures were washed with PBS without Ca^{2+} and Mg^{2+}, detached by Trypsin-EDTA 1× in PBS and collected by centrifugation at 1000 rpm for 5 min. The pellets were re-suspended in an appropriate volume (depending of the pellet size) of RIPA Buffer 1× (50 mM Tris-HCl pH 7.5; 0.5% sodium deoxycholate; 150 mM NaCl; 1% Triton X-100) supplemented of proteases inhibitors (1 mM of phenylmethylsulfonyl fluoride (PMSF); 1 µM of Pepstatin A; 100 µM Leupeptin; 10 mM Ethylenediaminetetraacetic acid (EDTA). Therefore, samples were incubated in ice for 15 min and constantly subject to micro vortex mixer treatments and then centrifuged at 10,000 rpm for 20 min. The amount of proteins extracted presented into the supernatant were calculated by the Bradford assay (Bradford Reagent, Sigma Aldrich), using different concentrations of bovine serum albumin (BSA) as Standard Assay. 10µl of each conditioned medium of NAM co-cultures and 1/25 of 2 micrograms of proteins extract separately were mixed with sample buffer 1× (62.5 mM Tris-HCl pH 6.8; 2.5% SDS; 0.002% Bromophenol Blue; 10% glycerol) and immediately situated in ice. The proteins were separate by 7.5% sodium dodecyl sulfate Polyacrylamide gel electrophoresis (SDS-PAGE) gelatine supplemented. After electrophoresis, gelatine zymographies were incubated over night at 37 ◦C in two developing buffers: activator buffer containing 2 mmol/L CaCl2, Tris-HCl buffer (50 mmol/L; pH 7.4) containing 1.5% Triton X-100 and 0.02% Na Azide, to activate gelatinases; and inhibitor buffer Tris-HCl buffer (50 mmol/L; pH 7.4), containing 1.5% Triton X-100 and 0.02% Na Azide plus 2 mmol/L EDTA, to inhibit gelatinase activities. After incubation, gels were stained using Coomassie Brilliant Blue R-250 (Sigma).

3.9 RNA Isolation and cDNA Synthesis of NAM co-cultures

Total RNA was extracted from NAM co-cultures using Trizol reagent (Invitrogen, CA, USA). RNA concentrations and quality were verified by spectrophotometry (optical density (OD) at 260 nm), whereas the RNA integrity was checked using a 1.5 % agarose gel. The RNA was stored at −80 °C for future use. The extracted RNA (500 ng) was treated with RNA qualified 1 (RQ1) RNase-Free DNase (Promega, Madison, WI, USA) to remove any residual genomic DNA contamination, and the DNase was inactivated by adding 25 mM EDTA. First-strand cDNA was synthesized from 250 ng DNase-treated total RNA samples using random primers and High Capacity cDNA Reverse Transcription Kit (Life Technologies Corporation, Carlsbad, CA, USA), following the manufacturer's instructions. The cDNA mixture was stored at −20 °C.

3.10 RT-qPCR of NAM co-cultures

RT-qPCR was performed using the BIO-RAD CFX96 System with Power Sybr Green as the chemical detection method (Applied Biosystems, Forster City, CA, USA). Real-time PCRs were carried out in 96-well plates in a 20 µL mixture containing 1 µL of a 1:20 dilution of the cDNA preparations, using the following PCR parameters: 95 °C for 10 min, followed by 40 cycles of 95 °C for 10 s, and 60 °C for 60 s. The sequences of the specific primer pairs used for qPCR are shown in table 1. Samples were run in duplicate. The GAPDH was chosen as reference gene. A normalization factor was calculated based on geometric averaging of the expression level of these reference genes and was used to quantify the expression levels of the target genes.

Gene	Forward	Reverse
Bace1	CCGAGACCTCCGAAAGTCTG	GTGATGGCAGCAATGTTGG
Bace2	CGAACCACAGAGCCTCAACTG	GAGTCCCCCTGAAGATTGTCC
Psen1	AGCGTCCGTAGCCAGAATG	CGTCTTCCTCCTCATCTTGC
Psen2	CGGAGGAGGAGGAGGAAAG	GCAGGAGGGTGAGACACAAG
App	GCTGATGGCGGTGAAGAC	GTGGCAATGCTGGTTGTTC
Lrp1	ACGAGTGCAGCACCACCTTC	CTTTGCAGCTGTGGGGGTCA
A2m	TCAGCAGCAGAAGGACAATG	GCGGACAACAGGATGAGTG
Apbb1	TCACCAAGAAGGCTTTGAGG	GCTGAGAAGGGCAATGTCC
Apbb2	GGGGTTGGAGAGGAGAAAGC	CTGGACTGGGGTTTGTTTGG
Abca1	TTGGGAACGAAAGTTGGATG	TGCCTGGTTGGTCTCATTG
Apoe	GAACCGCTTCTGGGATTACCTG	GCCTTTACTTCCGTCATAGTGTC
Il1b	CAGCAATGGTCGGGACATAG	TGACTTGGCAGAGGACAAAGG
Il1a	GGAGAAGACAAGCCTGTGTTG	GCTGCGGATGTGAAGTAGTTC
Cdk5	GCAGGGCGACCTCTCTTC	TGGGCACGACATTCACC
Gsk3b	TCCTCACGCTCGGATTCAG	GGCTACTTGGGGCTGTTCAG
Aph1a	TGCTGATTGTGGCTCACTTC	GGAAAGGAGGGGTGCTAATG
Aplp2	CGTCGGCTGATGACAATG	CCTTGGGGAGGTTCTTGG
Gnao1	TAATCTTCGCCGCTGGAATC	CTCAAAGGGGAGAAAATCACG
Gnaz	GGACAACGCCGCTTACTACC	TCCCACATCCACCATCTTG
Prkca	GGAAGCAGCCATCTAACAACC	TGTCAGCAAGCATCACCTTTC
TNF	GGTTCCGTCCCTCTCATACAC	CCTCTGCCAGTTCCACATCTC
NFKB	GCCTTGGTGGGGATGAGATC	GGGAGTTCGGAACACAATGG
il6	AGTTGCCTTCTTGGGACTGATG	CTGGTCTGTTGTGGGTGGTATC
il10	GCAGGACTTTAAGGGTTACTTGG	GCTGTATCCAGAGGGTCTTCAG
tgfb1	CTGCTGACCCCCACTGATAC	AAGCGAAAGCCCTGTATTCC
fmrp	GCCACCAAGTTCCCTACCTTC	GCGATGCTGTCTTTTGTTCC
hnRNPC	CCTCCTCCTCCCATTGCTC	CCCCGTTGTCCACTCTTTG
p38	TCGGTGTGTGCTGCTTTTG	TCCCTGTAGGTCCTTTTGGC
akt	GCCCAACACCTTCATCATCC	TCCTCCTGCCGTTTGAGTC
bcatenina	CTGGCAGCAGCAATCTTACC	CGTGAAGGACTGGGAAAAGC
cx3cl1	GTGTCTCCTGGCTTTGCTG	TGGTGGTGATGGCTCTGTAC
mmp2	AAGGATGGAGGCACGATTG	CGGGGAACTTGATGATGG
mmp9	CACCACCGCCAACTATGAC	AGGGGAAGACGCACATCTC
mmp3	CCTTGGGCTGAAGATGACAG	CATTTGGGTGAACCTGGAAAG
mmp10	TGACCCCACTCACATTCTCC	TGTCCCACTCCATCAAAAGG
mmp11	GGTCCCTGGTCCTGCTAGTAG	CCTGCTCCCTTACAAGTTGC
mmp8	CCGACTCTGGTGATTTCTTGC	AGTGAAGGTCAGGGTTGATGG
mmp7	GCTTCGCAAGGGGAGATC	CCTCACCATCCGTCCAGTAC

Table 1: Oligonucleotide primers used in this study

3.11 Fabrication of Organ-on-chip (oC)

Fabrication of the microfluidic device The microfluidic device was designed with AUTOCAD software (AUTODESK, USA) and the design was printed as an acetate mask. Master molds were obtained in 100 mm diameter silicon wafers using standard photolithography techniques in a clean

room environment. Then, the 100 mm silicon wafers were activated in the plasma chamber at high mode (10.5 W) for 1 min and two layers of SU8-2100 photoresist were spun to a total height of 120µm. Then, the photoresist was soft baked for 25 min and exposed using an I-line mask aligner to transfer the design from the acetate mask. After that, the wafers were post-baked, developed for 20 min and then hard baked for 30 min at 95°C and 10 min at 65°C. Finally, the wafers were silanized for 1 h with trifluorosilane. The PDMS replicas were obtained using the well-established method of soft lithography [90]. PDMS was mixed in a ratio 10:1 (base:crosslinking agent), poured into the mold and cured for 2 h at 65°C. Every single device was cut and bonded with a glass slide through irreversible plasma treatment for 30 s at high mode (10.5 W). Finally, the microdevices were left in the oven at 85°C overnight [91].

3.12 Cell seeding of the Organ-on chip

All steps, including cell culture, were performed in a sterile laminar flow hood, and only sterile materials, solutions and techniques were used. Human ECs were cultured in T75 culture flasks coated with collagen Type I from rat tail solution (25 µg/mL in PBS 1x) and supplied with endoGRO™ medium with 1 ng/mL of bFGF. Human pericytes and astrocytes were cultured in T75 culture flasks coated with poly-Llysine (2 µg/cm2 in sterile water) in the corresponding pericyte and astrocyte media. All cells were kept in a humidified incubator at 37°C and 5% pCO2 and the cell media were changed every two days. Cells were detached using 0.25% trypsin/EDTA for EC and 0.05% trypsin/EDTA for pericytes and astrocytes. For further experiments, cells were used until passage 5 for astrocytes and until passage 7 for pericytes and EC. To mimic the brain neuronal-vasculature network on the chip we adapted a procedure described by Campisi and collaborators [92]. As depicted inScheme 1, pericytes and astrocytes embedded in a hydrogel were injected into the central chamber ofthe chip and after two days, ECs were introduced in one of the lateral channels. For this purpose, human pericytes and astrocytes were trypsinized and 40.000 of each cell type were mixed. This mixture was centrifuged at 1000 g for 5 min, and the pellet was maintained at 4°C while the fibrin hydrogel was prepared. For this purpose, 50 µL of filtered fibrinogen 3 mg/mL in PBS and 1 µL of thrombin 100 U in PBS were mixed with the cell pellet and injected into the central chamber. The microdevice was incubated for 15 min at 37°C and 5% pCO2 to allow the hydrogel polymerization and then, both channels were supplied with a mixture of endothelial and astrocytes medium in a 1:1 ratio (EM:AM medium). After two days, one of the lateral channels was coated with collagen (25 µg/mL in PBS 1x) for 50 min at 37°C and 5% pCO2 while 100.000 EC cells were detached and centrifuged at 1000 g for 5 minutes and resuspended in EM:AM medium. Then, the cells were injected in the collagen-coated channel and the chip was flipped for 1,5 h at 37°C and 5%

pCO2 to allow the attachment of the cells to the hydrogel wall. Lastly, EM:AM medium was supplied on both channelsand the microdevices were maintained in the incubator for 5 days before conducting any experiment.Cell culture medium was changed daily.

3.13 Characterization of assembled Blood-brain barrier (BBB)

Bright-field microscopy images on day 7 of culture, optical images of the BBB-oC microdevice were taken using an inverted optical microscope (Olympus IX71) with an integrated CCD Hamamatsu camera. All the images were further analyzed and processed by ImageJ/Fiji ® software (NIH, USA).

3.14 Treatment of Organ-on chip

On day 7 of culture, the cells in the BBB-oC were treated with the purify protein sCX3CL1, with sample of AD liquor and sample of non-AD liquor for 24h.

3.15 Characterization of Organ-on chip with Immunofluorescence

The cells in the BBB-oC on day 7 were washed with PBS 1x and fixed with commercial formalin solution (4% w/v formaldehyde) for 15 min at room temperature (RT). Fixed cells were rinsed three times with 1.5 mg/mL of glycine in PBS 1x (PBS-G) and later permeabilized with 0.1% TritonX-100 in PBS-G for 10 min at RT. After fixation and permeabilization cells were washed three times with PBS-T and blocked with 3% BSA in PBS-T for 1 h at RT. The cells were incubated with antibodies against TJs proteins such as ZO-1 (1:100), VE-cadherin (1:100), CX3CL1 (1:100), p38 (1:100) and GFP (1:1000) in 3% BSA in PBS-T overnight at 4°C. After that, cells were washed three times with PBS 1x and incubated with the corresponding fluorophore-conjugated secondary antibody anti-rabbit Alexa 568 (1:1000), antimouse Alexa 488 (1:1000) and antichicken Alexa (1:1000) in 1% BSA in PBS-T for 2 h at RT. Then, the chip was washed with PBS-T and incubated with Hoechst 33342 (1:1000) for 15 min at RT. Finally, the cells were washed three times with PBS 1x and the microdevices were inspected by confocal microscopy at 63x (Leica TCS SP5 Multiphoton system). Fiji/ImageJ® software was then employed to treat the acquired images. To determine if GNR-PEG-Ang2/D1 incubation has any influence over the endothelium, immunofluorescence of ZO-1 and VE-cadherin was performed. At day 7, the device was washed with PBS 1x and incubated with GNR-PEG-Ang2/D1 0,4 nM for 24 h at 37°C and 5% pCO2. Controls were conducted using GNR-CTAB 0,1 nM or with the equivalent quantity of the peptides Ang2 (175,6 nM) or D1 (69,2 nM) covering the surface of the GNR. After 24 h, ZO-1 and VE-cadherin were immunostained and imaged.

3.16 Protein extraction from the cells in the BBB-oC

The hydrogel of the BBB-oC was digested using trypsin 0.05% + 5% hyalluronidase in incubation for 2 h at 37°C. The samples were centrifugated for 5 minute at 1000 rpm to obtained the cells pellet. The cells pellet was resuspended in an appropriate volume of RIPA Buffer 1× (50 mM Tris-HCl pH 7.5; 0.5% sodium deoxycholate; 150 mM NaCl; 1% Triton X-100) supplemented of proteases inhibitors (1 mM of phenylmethylsulfonyl fluoride (PMSF); 1 µM of Pepstatin A; 100 µM Leupeptin; 10 mM Ethylenediaminetetraacetic acid (EDTA). Therefore, samples were incubated in ice for 15 min and constantly subject to micro vortex mixer treatments and then centrifuged at 10,000 rpm for 20 min. The amount of proteins extracted presented into the supernatant were calculated by the Bradford assay (Bradford Reagent, Sigma Aldrich), using different concentrations of bovine serum albumin (BSA) as Standard Assay.

3.17 RNA Isolation and cDNA Synthesis of cells in the BBB-oC

The cells in the BBB-oc were lised by RLT Plus buffer lysis (Qiagen) and incubates for 15 minute pippeting every 5 minutes to improve the digestion of the hidrogel presents in the chip. After the simples are recollected and was added the sample volume of ethanol 70%. For the extraction of the RNA was used the RNeasy Mini kit Qiagen following the manufacturer's instructions. RNA concentrations and quality were verified by spectrophotometry (optical density (OD) at 260 nm). First-strand cDNA was synthesized from 250 ng DNase-treated total RNA samples using random primers and High Capacity cDNA Reverse Transcription Kit (Life Technologies Corporation, Carlsbad, CA, USA), following the manufacturer's instructions. The cDNA mixture was stored at −20 °C.

3.18 RT-qPCR of cells in the BBB-oC

RT-qPCR was performed using the BIO-RAD CFX96 System with Power Sybr Green as the chemical detection method (Applied Biosystems, Forster City, CA, USA). Real-time PCRs were carried out in 96-well plates in a 20 µL mixture containing 1 µL of a 1:20 dilution of the cDNA preparations, using the following PCR parameters: 95 °C for 10 min, followed by 40 cycles of 95 °C for 10 s, and 60 °C for 60 s. The sequences of the specific primer pairs used for qPCR are shown in table 2. Samples were run in triplicate. The β-actine was chosen as reference gene. A normalization factor was calculated based on geometric averaging of the expression level of these reference genes and was used to quantify the expression levels of the target genes.

Gene	Forward	Reverse
ZO-1	TCACGCAGTTACGAGCAAGT	TGAAGGTATCAGCGGAGGGA
ZO-3	CCATCGAGCGCCTCAACTAT	CTGCTGTGTTTTCGCAGCTT
Claudin-5	GCGTGCTCTACCTGTTTTGC	CAGCTCGTACTTCTGCGACA
Ve-cadherin	GCCAGTTCTTCCGAGTCACA	AACTCCGGGGCATTGTCATT
CX3CL1	GTGTCTCCTGGCTTTGCTG	TGGTGGTGATGGCTCTGTAC

Table 2: Oligonucleotide primers used in this study.

3.19 Stereotaxis intervention

Before the surgery, the rat was anesthetized, and artificial tears were applied to the eyes for protection. The hair of the dorsal region of the skull between the two eyes was shorn and the surgical area was disinfected with 3 alternating washes of surgical betadine and 70% alcohol, and an ointment of 20 mg/ml lidocaine and epinephrine was applied (1: 200,000) on the skin intervention area before the scalpel incision. The animal was placed on a bed and the head was introduced into the stereotaxic apparatus. Electrodes were placed to monitor heart rate and oxygen saturation. Using forceps and scalpels, the skin was incised at the sagittal suture (≈ 2 cm) to remove the periosteum and expose the skull. Once the incision has been made and the skull exposed, it is necessary to identify the bregma, which is the anatomical point on the skull where the sagittal and coronal suture crosses. Once the bregma has been identified, two holes are made in the skull using the stereotaxic apparatus with coordinates of -0.8 mm along the anterior-posterior axis and +/- 1.4 mm along the lateral axis concerning the position of the bregma. The two holes will have a depth of ≈1mm and will allow the passage of the needle to reach the lateral ventricles. The microinjection of Streptozotocin (STZ) in citrate buffer or citrate buffer alone took place via a needle previously positioned in the arm of the stereotaxic device, which is connected to an automatic microinjection system. The needle dropped to a depth of -3.6 mm along the dorsal-ventral axis through the hole in the skull. Approximately 2-3 µl of STZ in citrate buffer or citrate buffer alone were injected into each lateral ventricle at a rate of 1 µl per minute. The amount of STZ injected depends on the bodyweight of each rat. At the end of the injection, it was necessary to wait 4 minutes before withdrawing the needle from the lateral ventricle of the brain to prevent reflux of the STZ solution. The same procedure was repeated on the other lateral ventricle of the brain. After the intracerebroventricular injections, the surgical incision was closed through sutures. In the following days, the rats were given antibiotics to prevent post-operative bacterial infections and an anti-inflammatory.

3.20 Extraction of Soluble Proteins from rats brain and Dot blot assay

The cerebral tissue was homogenized with a pestle resuspending it in an appropriate volume of RIPA Buffer 1× (50 mM Tris-HCl pH 7.5; 0.5% sodium deoxycholate; 150 mM NaCl; 1% Triton X-100) supplemented of proteases inhibitors (1 mM of phenylmethylsulfonyl fluoride (PMSF); 1 μM of Pepstatin A; 100 μM Leupeptin; 10 mM Ethylenediaminetetraacetic acid (EDTA). Therefore, samples were incubated in ice for 15 min and constantly subject to micro vortex mixer treatments and then centrifuged at 10,000 rpm for 20 min. The amount of proteins extracted presented into the supernatant were calculated by the Bradford assay (Bradford Reagent, Sigma Aldrich), using different concentrations of bovine serum albumin (BSA) as Standard Assay. Twenty micrograms of proteins are spotted on nitrocellulose membrane (Hybond, Amersham). Blocking of non-specific binding was achieved by placing the membrane in a solution of non-fat dry milk (3%) for 2 hours at room temperature. Therefore, Beta-Amyloid 1-42 antibody (1:1000, Abcam) was incubated overnight at 4 °C; after washing with TBS-T solution (0.6% Trizma base; 0.87% NaCl; 0.05% Tween 20), the peroxidase-linked anti-rabbit secondary antibody (0.04 μg/mL, Sigma Aldrich) was incubated for 2 h at room temperature. After other TBS-T washes, the presence of Beta-Amyloid 1-42 protein was identify using "SuperSignal West Femto Maximum Sensitivity Substrate" (Thermo Scientific) and the chemiluminescence signal was reveal using the ChemiDoc XRS (Biorad, Hercules, CA, USA). β-actin (antibody anti-β-actin 0.4 μg/mL, Sigma Aldrich) was used to normalize each sample.

3.21 Extraction of Soluble Proteins from rats brain and Western Blot Analysis

The cerebral tissue was homogenized with a pestle resuspending it in an appropriate volume of RIPA Buffer 1× (50 mM Tris-HCl pH 7.5; 0.5% sodium deoxycholate; 150 mM NaCl; 1% Triton X-100) supplemented of proteases inhibitors (1 mM of phenylmethylsulfonyl fluoride (PMSF); 1 μM of Pepstatin A; 100 μM Leupeptin; 10 mM Ethylenediaminetetraacetic acid (EDTA). Therefore, samples were incubated in ice for 15 min and constantly subject to micro vortex mixer treatments and then centrifuged at 10,000 rpm for 20 min. The amount of proteins extracted presented into the supernatant were calculated by the Bradford assay (Bradford Reagent, Sigma Aldrich), using different concentrations of bovine serum albumin (BSA) as Standard Assay. Twenty micrograms of proteins were mixed with sample buffer 1× (62.5 mM Tris-HCl pH 6.8; 2.5% SDS; 0.002% Bromophenol Blue; 0.7135 M (5%) β-mercaptoethanol; 10% glycerol) and incubated at 100 °C for 5 min and immediately situated in ice. The proteins were separate by 10% sodium dodecyl sulfate Polyacrylamide gel electrophoresis (SDS-PAGE). The proteins were transferred from the gel to a nitrocellulose membrane (Hybond, Amersham) through electroblotting at 100 V and 300 mA for 90

min at low temperature, in transfer buffer (20% methanol; 10% Running buffer 1×: Tris base 3 g/L-Glycine 14.4 g/L). Blocking of non-specific binding was achieved by placing the membrane in a solution of non-fat dry milk (3%) for 2 hours at room temperature. Therefore, Tau (phospho T181) antibody (1:1000, Abcam) was incubated overnight at 4 °C; after washing with TBS-T solution (0.6% Trizma base; 0.87% NaCl; 0.05% Tween 20), the peroxidase-linked anti-rabbit secondary antibody (0.04 µg/mL, Sigma Aldrich) was incubated for 2 h at room temperature. After other TBS-T washes, the presence of Tau (phospho T181) protein was identify using "SuperSignal West Femto Maximum Sensitivity Substrate" (Thermo Scientific) and the chemiluminescence signal was reveal using the ChemiDoc XRS (Biorad, Hercules, CA, USA). β-actin (antibody anti-β-actin 0.4 µg/mL, Sigma Aldrich) was used to normalize each sample.

3.22 RNA Isolation and cDNA Synthesis of experimental *in vivo*

Total RNA was extracted from NAM co-cultures using Trizol reagent (Invitrogen, CA, USA). RNA concentrations and quality were verified by spectrophotometry (optical density (OD) at 260 nm), whereas the RNA integrity was checked using a 1.5 % agarose gel. The RNA was stored at −80 °C for future use. The extracted RNA (500 ng) was treated with RNA qualified 1 (RQ1) RNase-Free DNase (Promega, Madison, WI, USA) to remove any residual genomic DNA contamination, and the DNase was inactivated by adding 25 mM EDTA. First-strand cDNA was synthesized from 250 ng DNase-treated total RNA samples using random primers and High Capacity cDNA Reverse Transcription Kit (Life Technologies Corporation, Carlsbad, CA, USA), following the manufacturer's instructions. The cDNA mixture was stored at −20 °C.

3.23 RT-qPCR of NAM of experimental *in vivo*

RT-qPCR was performed using the BIO-RAD CFX96 System with Power Sybr Green as the chemical detection method (Applied Biosystems, Forster City, CA, USA). Real-time PCRs were carried out in 96-well plates in a 20 µL mixture containing 1 µL of a 1:20 dilution of the cDNA preparations, using the following PCR parameters: 95 °C for 10 min, followed by 40 cycles of 95 °C for 10 s, and 60 °C for 60 s. The sequences of the specific primer pairs used for qPCR are shown in table 1. Samples were run in duplicate. The GAPDH was chosen as reference gene. A normalization factor was calculated based on geometric averaging of the expression level of these reference genes and was used to quantify the expression levels of the target genes.

4. RESULTS

4.1 Analyses of CSF samples

The patients were divided into two groups based on the AT (N) biomarker classification: "Alzheimer's continuum"(Group A) and "non-AD pathological changes" (Group B). Group A includes twenty-eight Alzheimer patients; Group B includes seven patients with vascular dementia (38.8%), two patients with Lewy bodies (11.1%), four patients with frontotemporal dementia (22.2%), one patient with Parkinson's disease (5.5%), one patient with subjective cognitive decline (5.5%), two patients with corticobasal degeneration (11.1%), and one patient with paraneoplastic syndrome (5.5%).

The cerebrospinal fluid (CFS) obtained from AD and not AD patients were analyzed for the presence of the soluble form of CX3CL1 by ELISA test, together with the canonical markers A42, A40, ratio A40/A42, t-tau, and p-tau by CLEIA test.
The result of CLEIA test divided group A (AD group) into two groups A' and A''. The expression of Aβ 1–42 and Aβ 1–40, and the Aβ 42/40 ratio in the CSF both subpopulations A' and A" had Aβ values canonically attributable to AD patients (figure 10) [93].

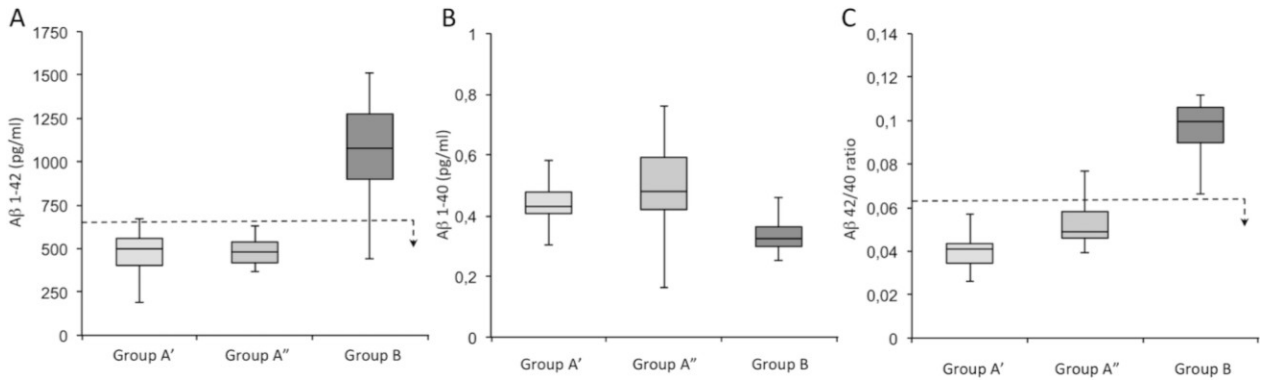

Figure 10: Classification of patients into three groups regarding the expression of Aβ 1–42 (A) and Aβ 1–40 (B), and the Aβ 42/40 ratio (C). The dotted line represents the threshold for a subject to be considered AD or non-AD; the arrow indicates the direction of values for which the subjects are affected by AD. Group A' is depicted in light gray, Group A" is depicted in medium gray, and Group B is depicted in dark gray [93].

The difference between the group A' and A'' is based on the expression of Tau-total and Tau-

phosphorylated. The population of Group A' showed values ascribable to AD for Tau-total, and Tau-phosphorylated markers; on the other hand, in Group A", the values of Tau-total and Tau-phosphorylated were within normal limits, like patients of Group B, the non-AD subjects (Figure 11).

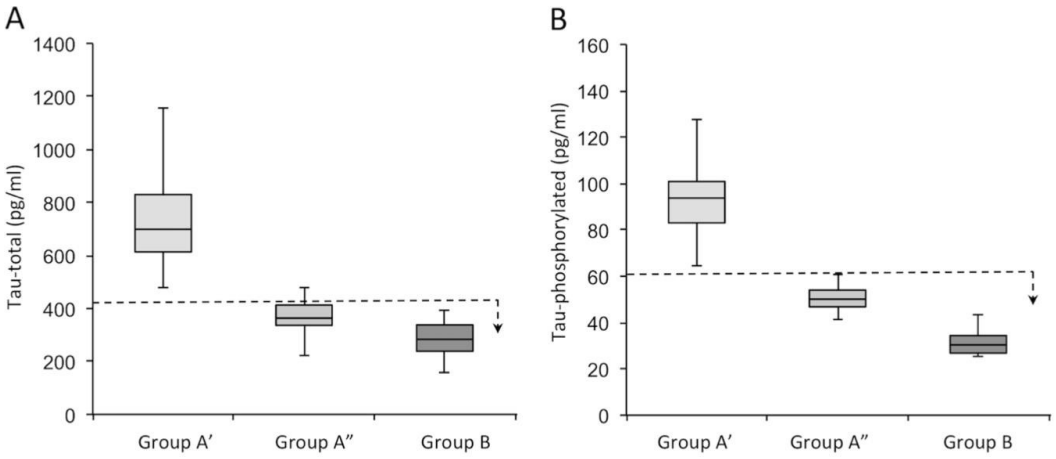

Figure 11: Classification of patients into Groups A', A", and B according to the expression of Total Tau (A) and Tau-phosphorylated (B). The dotted line represents the threshold for a subject to be considered AD or normal; the arrow indicates the direction of values for which the subjects are not affected by AD. Group A' is depicted in light gray, Group A" is depicted in medium gray, and Group B is depicted in dark gray [93].

The CSF of patients belonging to Groups A', A", and B was compared using ELISA test for the presence of sCX3CL1. The results obtained highlighted the level of sCX3CL1 differed quantitatively, with Group A' and Group A" having 33% and 40% greater levels of sCX3CL1, respectively, compared to Group B (figure 12). This suggests that sCX3CL1 could be considered a possible new marker for Alzheimer's in the disease.

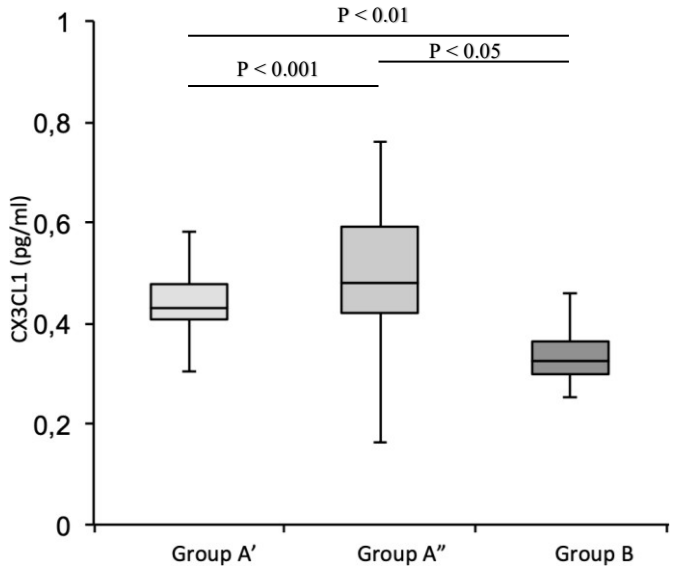

Figure 12: Expression of CX3CL1 in the CSF of subjects belonging to Groups A', A", and B. Group A' is depicted in light gray, Group A" is depicted in medium gray, and Group B is depicted in dark gray [93].

4.2 Morphologic analyses of NAM co-cultures

CFS samples from AD patients and non AD patients were used as evaluation elements on morphological effects in neuron-astrocyte-microglia (NAM) co-culture system.

The NAM co-cultures were treated with CSF from 8 AD patients (4 patients belonging to the group "A'" and 4 patients to the group "A''") and 4 non-AD patients (group "B"), while the control wells have been treated with the same volume of CSF used in complete sterile PBS. After 24h and 48h of incubation time with CSF or PBS, the morphology of the co-cultures were observed by optical microscopy.

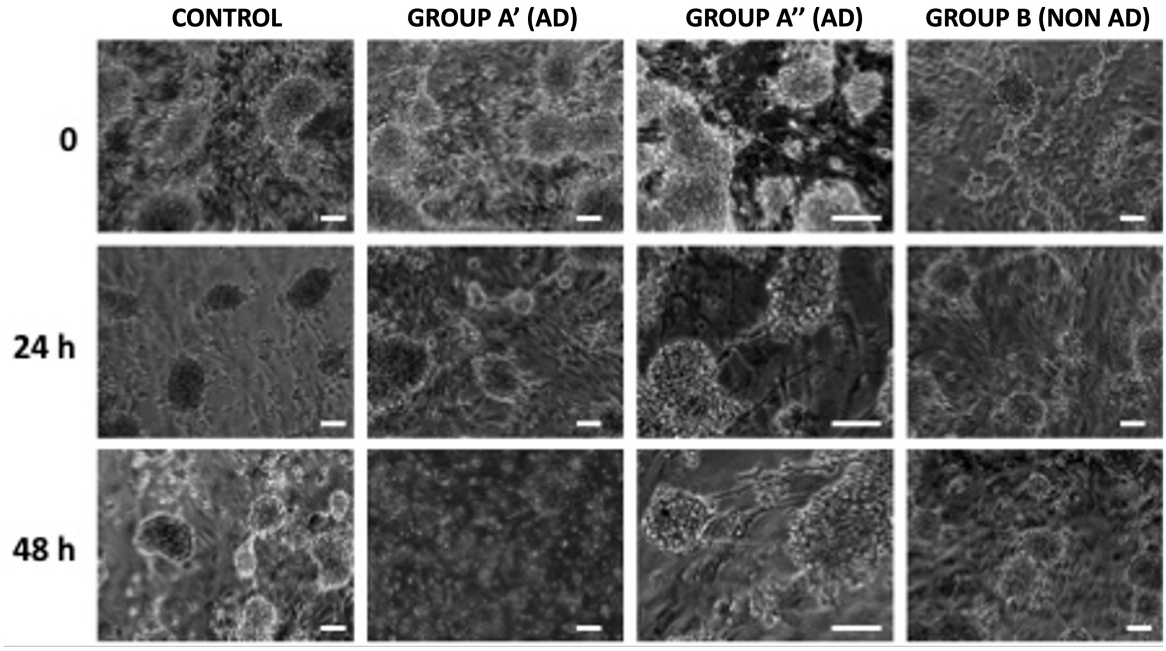

Figure 13: Morphology of the co-cultures observed by optical microscopy. The imagine represents the NAM co-cultures at time 0 before the treatment e the NAM co-coltures at time 24 and 48 hours after the treatment with CSF from AD patients (Group "A' " and Group "A'' ") and non-AD patients (group "B"), while the control wells treated with complete sterile PBS.

As show in Figure 13, at time 0 the astrocytes had a starry morphology with different extensions and had formed a support network for the overlying neurons, the neuronal cells aggregated forming multiple neurospheres. After 24h of incubation, no notable differences were observed between the co-cultures treated with CSF from AD patients (group A' and A'') compared to that of non AD patients (group B) and co-cultures not treated with CSF, used as a check. While at 48h of incubation, the same morphology appeared for the co-cultures treated with the liquor of patients of groups "A'' " and "B" and for the control co-cultures, while the neural network of the co-cultures treated with the liquor of patients in group "A' " had missing completely the neurofilaments and spheroid and many cells were in suspension. This suggest that in the CSF of AD patients of group "A' " there are elements that destabilize neurofilaments, cellular adhesion processes, and intercellular contacts.

4.3 Proteolytic assay of NAM co-cultures

An analysis of the expression of proteolytic enzymes was also carried out.
In vitro evaluation in NAM co-culture models of the proteolytic cascade was carried out following the CSF treatment of AD subjects and normal subjects, through zymography experiments (Zy) to

identify enzymes belonging to the MMP family. The zymography results, although preliminary, indicated the activation of the cascade of MMPs by elements present in the CSF in AD subjects but not in non-AD subjects in the protein extracts. The results also showed a difference in MMPs expression based on CSF incubation time (24 and 48 hours). Only in Group A' (with the same number of proteins loaded) there is a decrease in the presence of the pro- and active forms MMP2 and MMP9 in the conditioned medium; an effect that is not evident in the samples of Group A'' and B. As a control, a zymographic analysis with CSF alone of AD and non-AD patients was performed to evaluate the baseline expression of MMPs present in the CSF (figure 14). The results of this zymographic analysis did not show any activation of the pro- and active forms of MMP2 and MMP9.

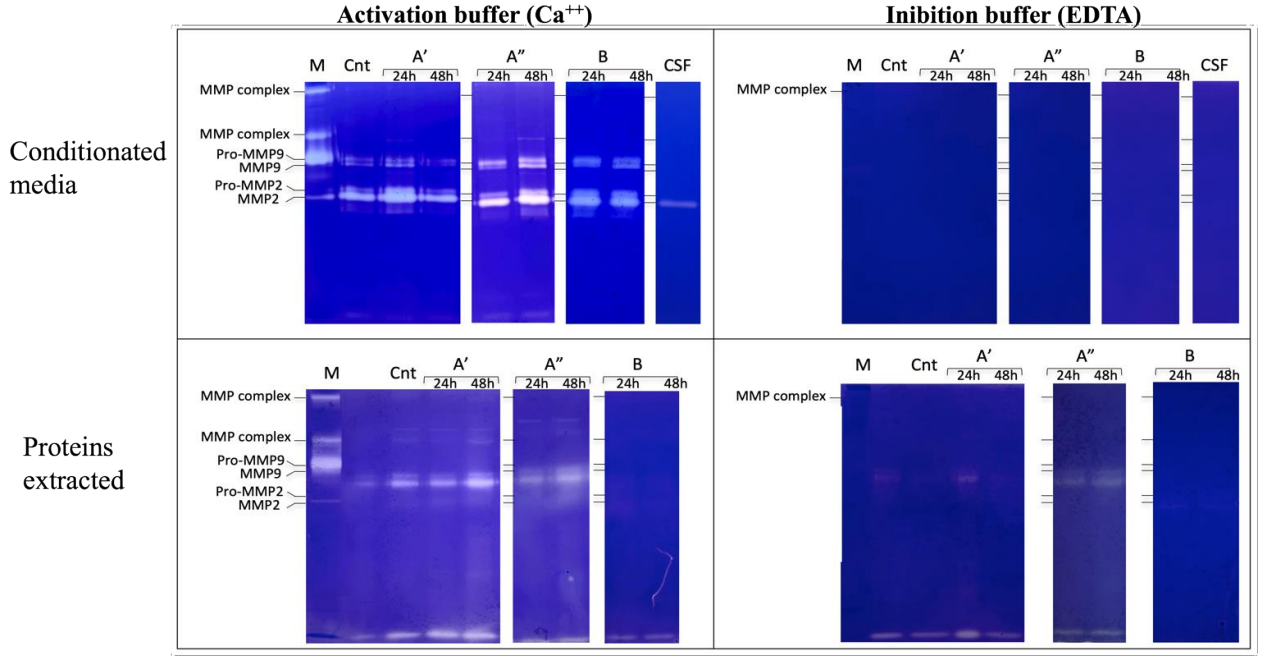

Figure 14: Zymography assay of protein extracts and conditioned media of the NAM co-cultures treated with CSF of AD patients (Group A' and Group A'') and non AD patients (Group B). The control are the NAM co-cultures treated with complete sterile PBS.

Was performed a densitometry evaluation of the gelatinolytic activities quantifies with respect to the negative control (PBS) present in the conditioned medium of the NAM co-cultures treated with CSF from AD and non AD subjects, in the presence of Ca^{2+}(figure 15). This analyses showed the activation of MMP2 and MMP9 pro and active form and the activation of other two proteases with unidentified activity. One of this should be MMP8 for the molecular weight about 80 kDa and the second one should be MMP10 or MM1 Mt1MMP for the molecular weight about 57,5 kDa.

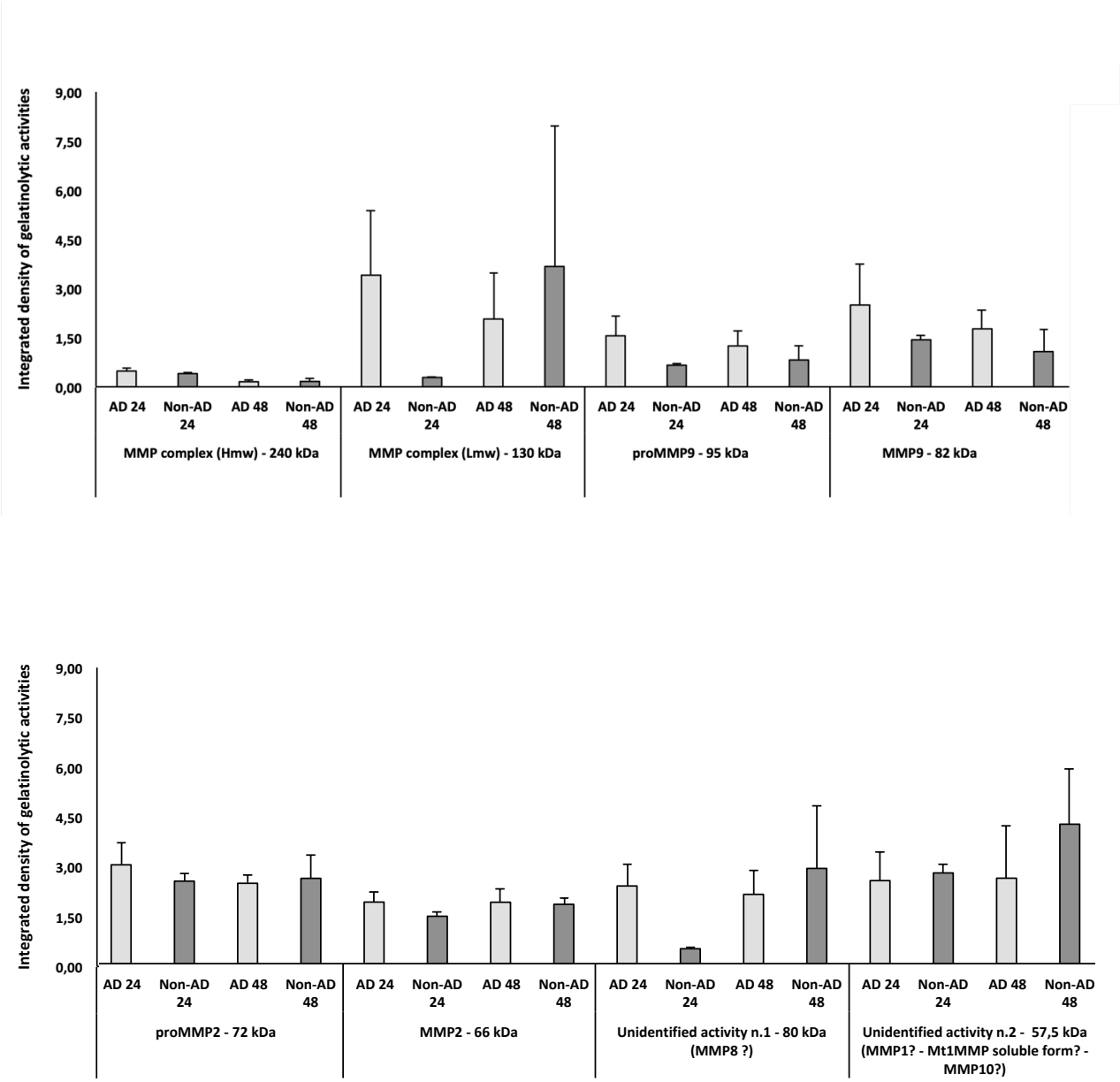

Figure 15: Densitometry evaluation of the gelatinolytic activities quantifies with respect to the negative control (PBS) present in the conditioned medium of the NAM co-cultures treated with CSF from AD and non AD subjects, in the presence of Ca^{2+}.

Moreover, was performed a densitometry evaluation of the gelatinolytic activities quantified with respect to the negative control (PBS) present in the cell extract of the NAM co-cultures treated with CSF from AD and non-AD subjects, in the presence of Ca^{2+} and in the presence of EDTA (figure 16). These analyses in the presence of Ca^{2+} showed the activation of proteases with unidentified activity only in the protein extract from co-cultures treated with the liquor of AD subject compared to the protein extract from co-cultures treated with the liquor of non-AD subject.

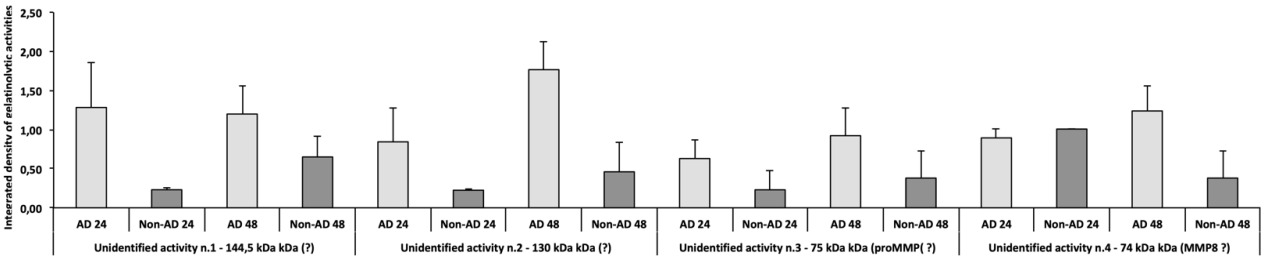

Figure 16: Densitometry evaluation of the gelatinolytic activities quantified with respect to the negative control (PBS) present in the cell extract of the NAM co-cultures treated with CSF from AD and non-AD subjects, in the presence of Ca^2.

Also in presence of EDTA these analyses showed the activation of proteases with unidentified activity after 48h of treatment in all protein extract (figure 17).

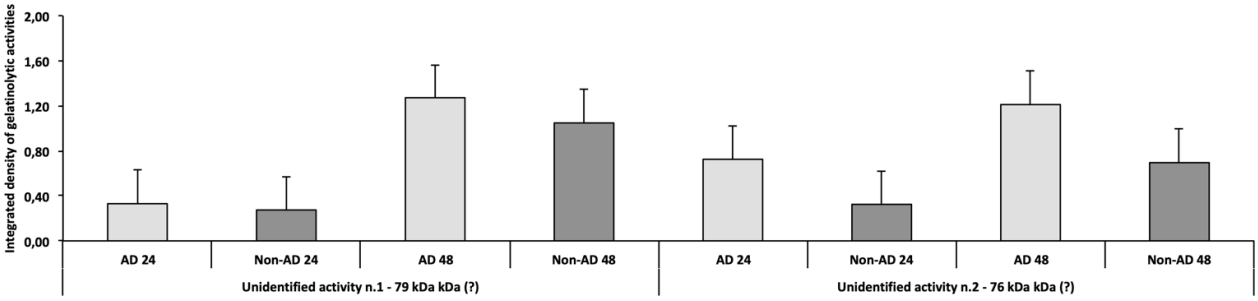

Figure 17: Densitometry evaluation of the gelatinolytic activities quantified with respect to the negative control (PBS) present in the cell extract of the NAM co-cultures treated with CSF from AD and non-AD subjects, in the presence of EDTA.

4.4 Immunofluorescence assay of NAM co-cultures

Part of the co-cultures was analyzed by immunofluorescence (IF) assays using primary antibodies such as anti CX3CL1, anti CX3CR1, anti p38, anti β-catenin, and anti PECAM. The immunofluorescence results showed that group A'' has a high expression of p38 compared to groups A' and B and the control group; the expression of CX3CL1 was evident in all groups, because is the membrane form of CX3CL1. Furthermore, the astrocytes and microglia, were identified by antibodies against specific antigens: anti-glial and anti CD11b fibrillar acid protein, respectively (figure 18).

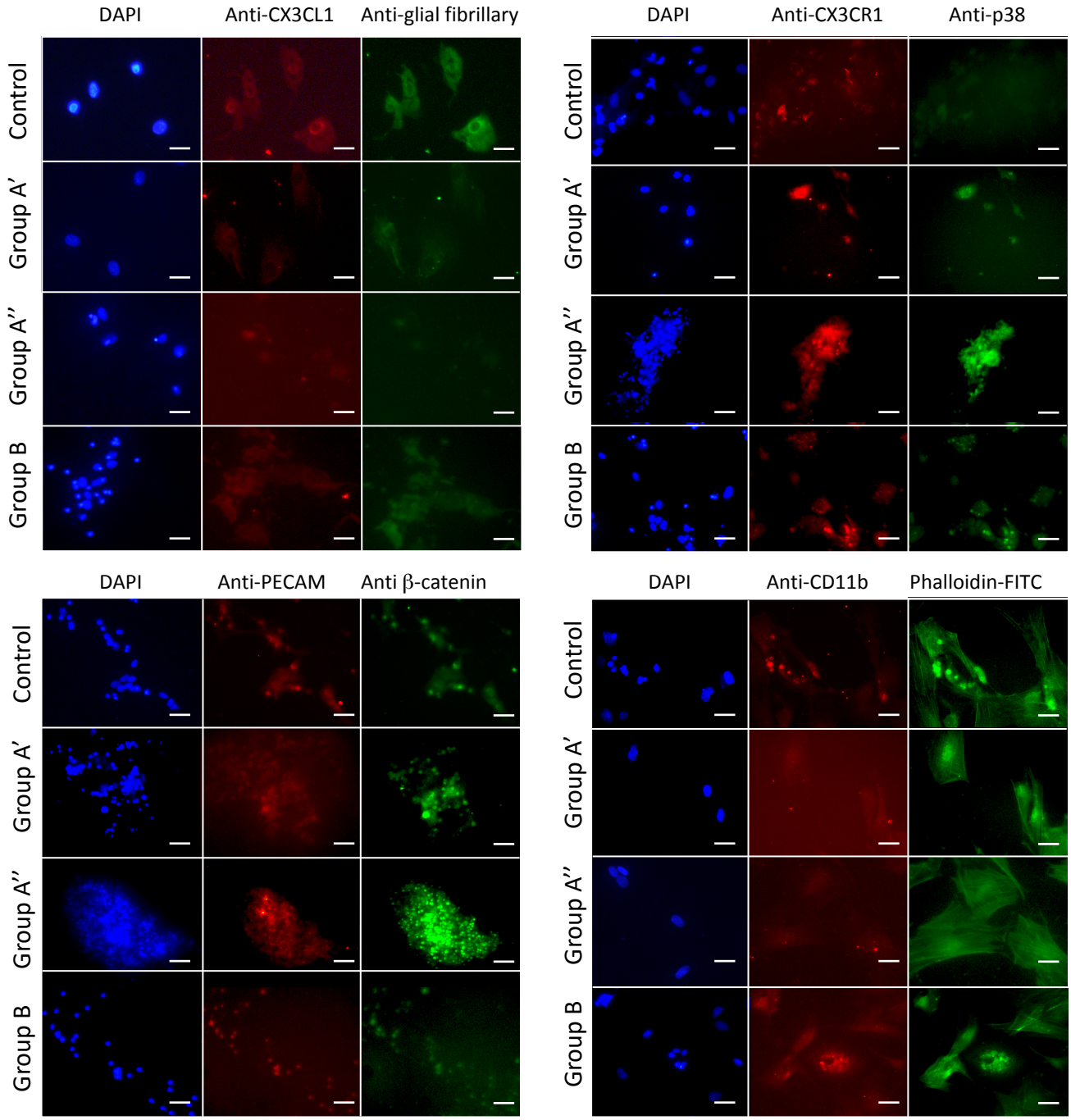

Figure 18: Immunostaining of NAM co-cultures after treatment with CSF from AD (A' - A"), Non-AD (B) patients, and with similar volume of PBS (Control) for 24 hrs. In the figure the blue stanning represent the cells' nuclei stained with DAPI, in green (FITC) and red (Texas Red) are shown different antigens as indicated. The bar = 5 m.

4.5 Real Time PCR assay of NAM co-cultures

Was performed a Real Time PCR analysis about RNA extract from the NAM co-cultures treated with

the cerebrospinal fluid samples of AD and non-AD patients. Were analyzed 39 gene involved in the process that characterize Alzheimer's disease. First group of genes are involved in inflammation pathways (*Il1a, Il1b, Il6, Il10, tnf, nfkb, tgfb, p38, akt, CX3CL1*), second group of genes are involved in the hyperphosphorylation of tau (*beta-catenin, cdk5, gsk3b*) and in the formation of tangle of tau (*prkca, gnaz, gnao*), third group of genes are involved in the amyloid genesis (*app, psen1, psen2, bace1, bace2, apoE, fmrp, abca, apbb1, apbb2, a2m, aplp2, aph1a, hnrpc*) and the last group of genes are some metalloproteases (*MMP2, MMP3, MMP7, MMP8, MMP9, MMP10, MMP11*). In the figure 19 there is a schematic representation about the role and the influence of these 39 genes on Alzheimer's disease.

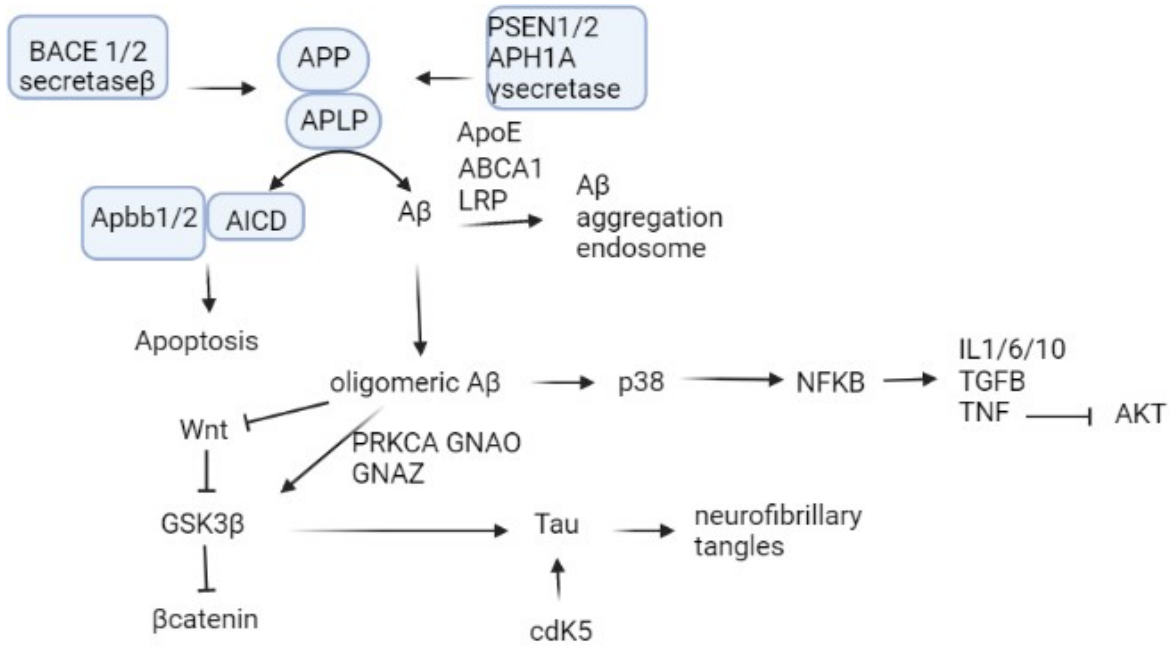

Figure 19: Schematic representation of the genes of Real Time PCR analyses and their influence in the process of Alzheimer's disease.

The results obtained from Real Time PCR analyses of the co-cultures of group A' and A'' are more similar, so for this reason are regrouped in only one group called group A. Real Time PCR analyzes on mRNAs extracted from NAM co-cultures of AD and non-AD subjects were conducted using the *gapdh* coding gene as housekeeping and normalizing the values respect the genes expression in NAM

co-cultures treated with PBS (negative control).

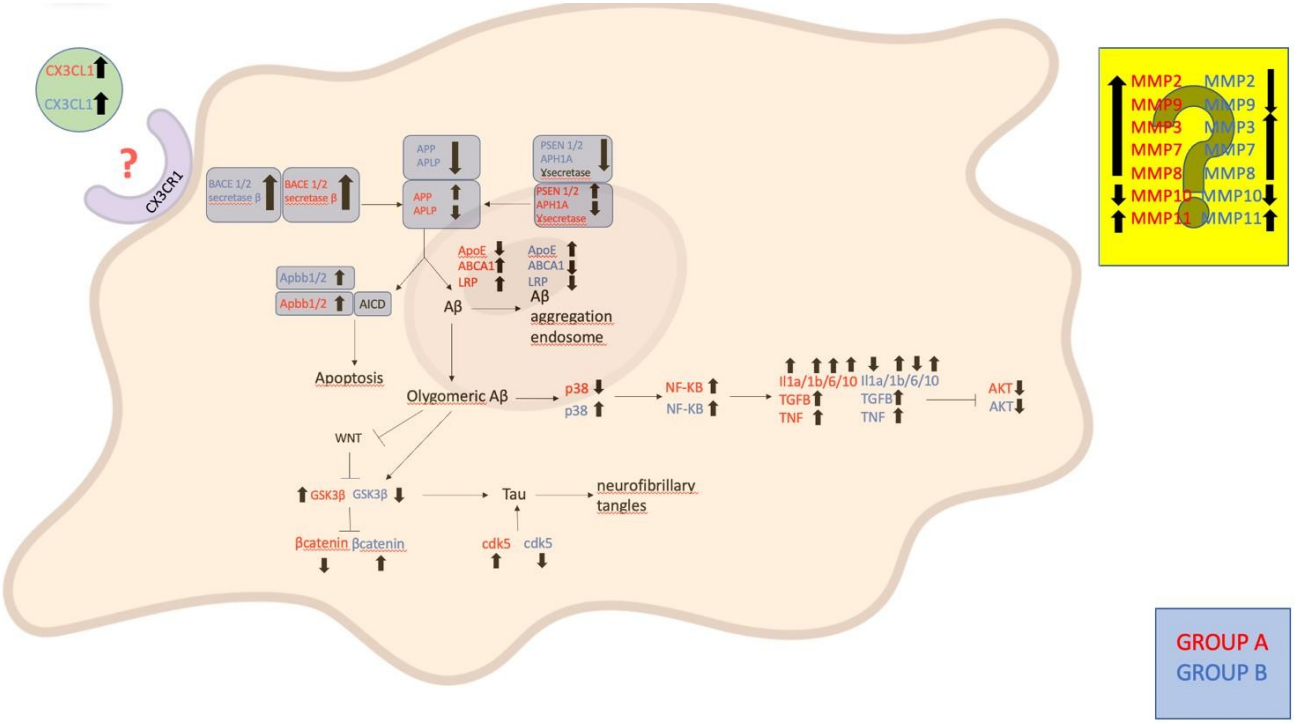

Figure 20: Schematic representation of Real Time PCR of extract RNA from NAM co-cultures.

The results of Real Time PCR analyses are represented in a Heat map (figure 21). The results showed an up regulation in genes involved in inflammation pathways both in group A and in group B regardless of treatment time. While the gene involved in the hyperphosphorylation of tau showed an opposite expression in Group A compared group B. *Cdk5* and *gsk3b* are upregulated in group A and downregulated in group B and *beta-catenin* is downregulated in group A and upregulated in group B. Also the genes involved in the formation of tangle of tau showed and opposite pathway: *Gnao, Gnaz and Prkca* are upregulated in group A and downregulated in group B. The group of genes involved in amyloidogenesis showed a contrasting results. There are some genes that showed the same up or downregulation in group A both in group B, and other genes that showed an opposite pathway. Regarding the genes of metalloproteases, the Real Time PCR analyses confirm the results obtained thank to zymography assay. In general, there is an upregulation of the genes *MMP3, MMP7, MMP8, MMP10, MMP11* in group A both in group B. While there is a different expression into the two group about the genes *MMP2* and *MMP9*: there is an upregulation of *MMP2* and *MMP9* in group A compared a downregulation in group B.

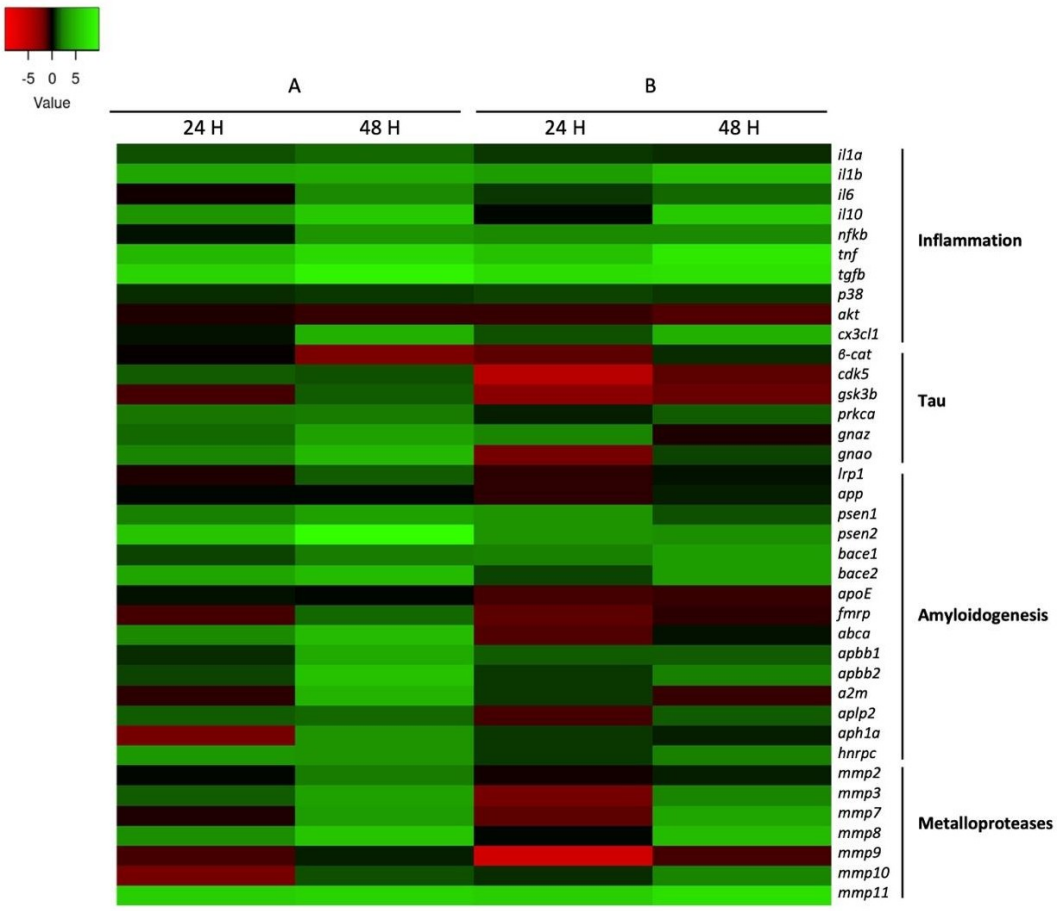

Figure 21: Heat Map Real Time PCR of RNA extract from NAM co-cultures.

4.6 Influence of sCX3CL1 and liquor AD and non-AD on a BBB

Since CX3CL1 appears to be important and influential cytokine in the process of neurodegeneration in Alzheimer's disease was tested its influence on a blood brain barrier (BBB). Was used *in vitro* model an organ-on chip that mimic the BBB. The design of the BBB-oC was inspired by the model developed by Farahat and collaborators. The organ-on chip was composed of a central chamber enclosed by trapezoidal posts with 100 µm between them, and by two lateral channels to the central chamber. The posts can confine a hydrogel matrix in the central chamber without leaks due to the high hydrophobicity of the PDMS surface in relation to the hydrogel. The two lateral channels can be used for as cell medium suppliers, or like my case for endothelial culture, and the reservoirs avoid media evaporation. The design was then engraved on a silicon wafer and replicated in PDMS. Finally, the bonding between PDMS replicas and the glass slides was done. For the construction of the BBB, human astrocytes and pericytes cells were included in a fibrin hydro- gel as ECM scaffold in the central chamber of the chip and human endothelial cells in one of the lateral channels. To mimic the

extracellular matrix was chosen to use the fibrin because is a natural hydrogel formed by the action of the protease thrombin, which cleavages the protein fibrinogen leading to fibrinogen monomers that self-associate into a stable fibrin mesh by the action of disulfide bridges with no need for radiation or additional crosslinking reagents. Thanks to use the fibrin was formed in the central channels of the organ-on chip a low stiff sup- porting extracellular matrix that is suitable for hosting vascular networks (figure 22).

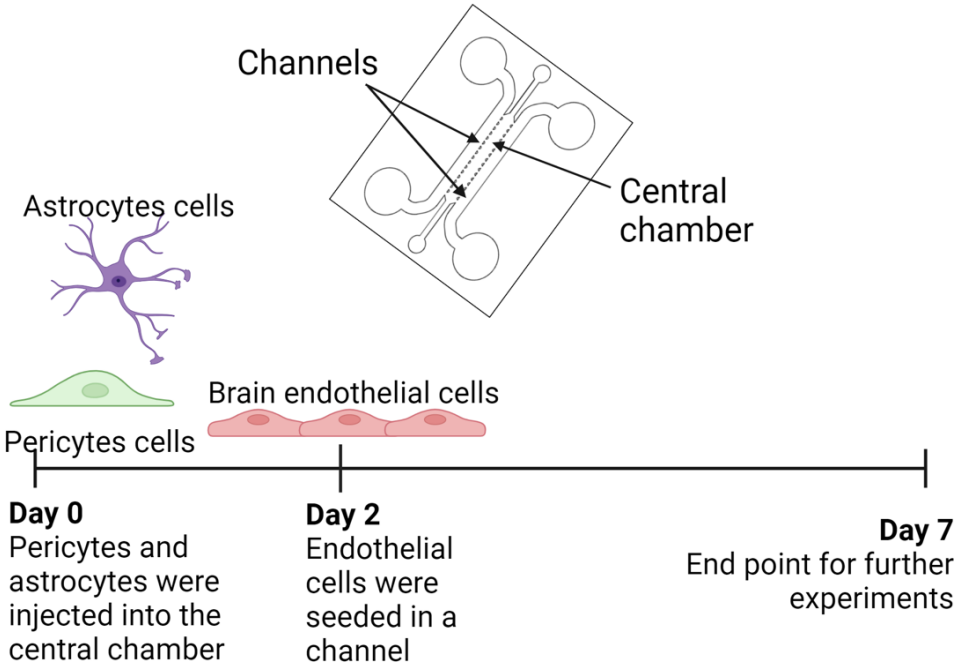

Figure 22: BBB-oC's structure and timeline of cell seeding [91].

After the cell seeding of the human astrocytes, pericytes and endothelial cells, on day 7 the organ-on chip was observed by optical microscopy. The endothelial cells are accumulated on the hydrogel-channel interface of the device allowing close contact with the pericytes and astrocytes, as the natural BBB, which are embedded in the 3D scaffold in the central chamber (figure 23).

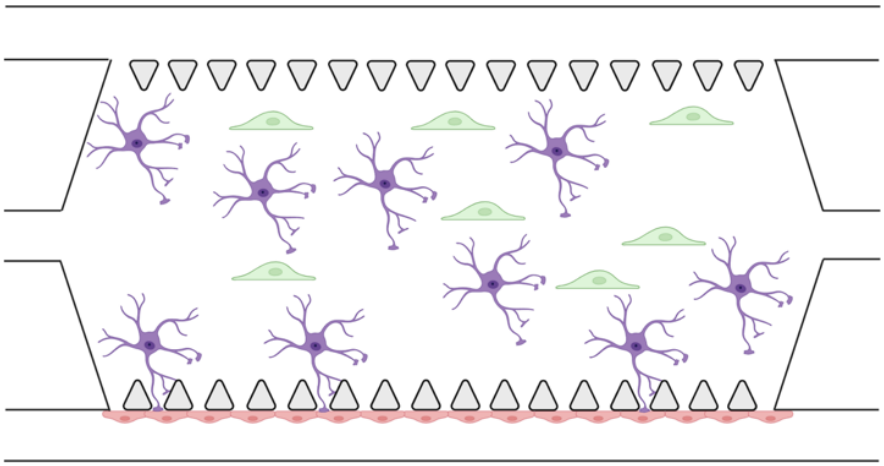

Figure 23: Schematic representation of neurovascular cells arrangement into the BBB-oC [91].

On day 7, was added in the part of the brain of the BBB-oC sCX3CL1 (purify protein), in particular 0,6 pg/ml of concentration of purify protein (the same concentration of protein that we analyzed in the liquor of AD patients) for 24 hours. After 24h of treatment, at day 8, optical bright field images were taken at the endothelial and neuronal zone of the BBB-oC. to evaluate the the effect of sCX3CL1 on the BBB. In the untreated BBB-oC the endothelial cells are accumulated on the hydrogel-channel interface of the device allowing close contact with the pericytes and astrocytes. While in the BBB-oC treated with sCX3CL1 the BBB is damaged, the close contacts between endothelial cells and astrocytes and pericytes are lost (figure 24).

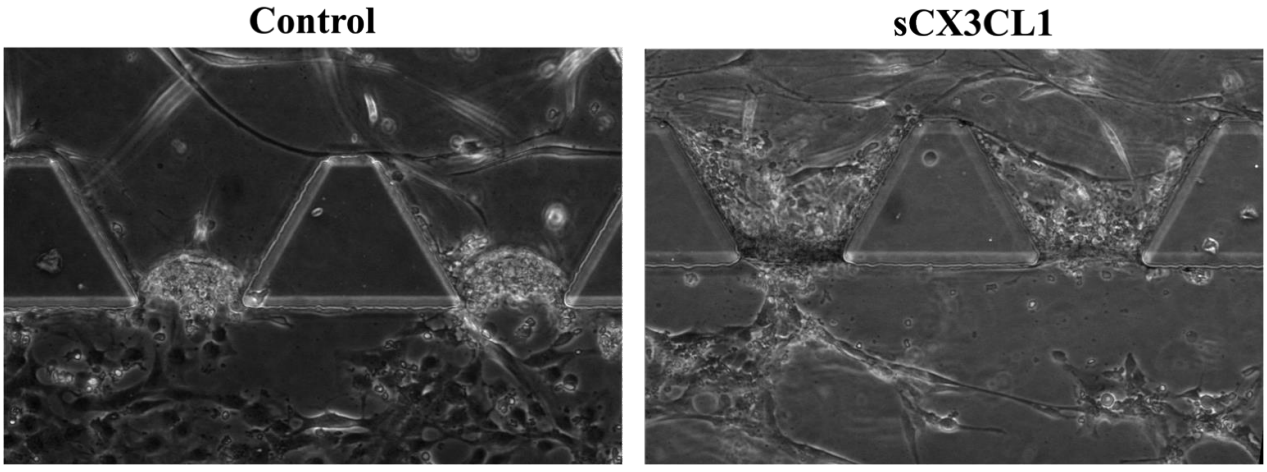

Figure 24: Morphology of the BBB observed by optical microscopy after 24h from the treatment with sCX3CL1.

At the same way, on day 7, on other organ-on chip was added in the part of the brain of the BBB-oC

the liquor of AD patients and on other organ-on chip the liquor of non-AD patients. The treatment was for 24 hours. After 24h of treatment, at day 8, optical bright field images were taken at the endothelial and neuronal zone of the BBB-oC. to evaluate the effect of Alzheimer and non-Alzheimer liquor on the BBB. In the BBB-oC treated with non-AD liquor, the endothelial cells are accumulated on the hydrogel-channel interface of the device allowing close contact with the pericytes and astrocytes. While in the BBB-oC treated with AD liquor the BBB is damaged, also here the close contacts between endothelial cells and astrocytes and pericytes are lost (figure 25).

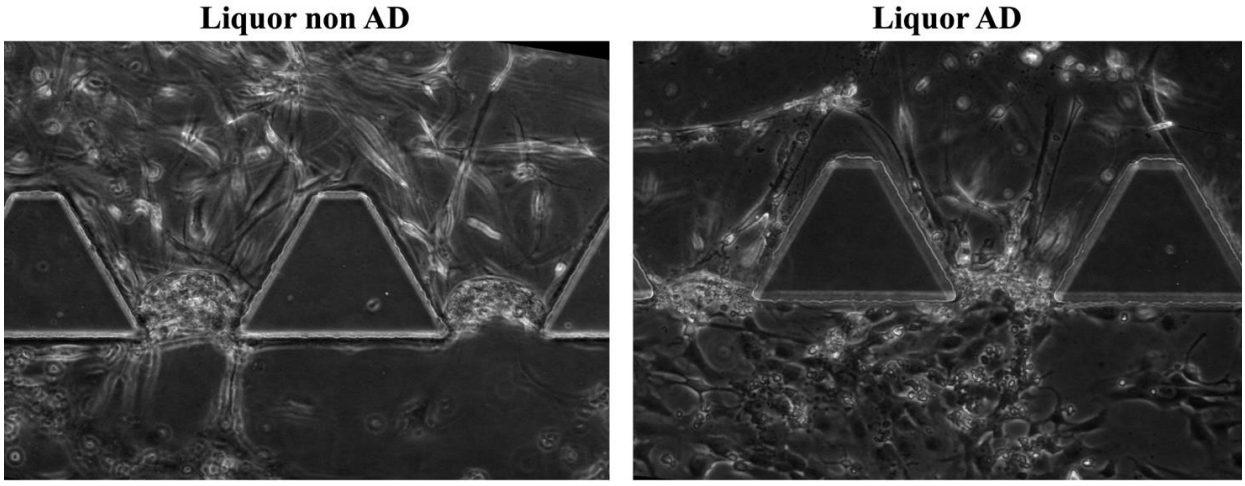

Figure 25: Morphology of the BBB observed by optical microscopy after 24h from the treatment with AD and non-AD liquor.

4.7 Confocal microscopy of BBB-oC treated

TJs structures linking the ECs were formed inside the chip. For this reason, to evaluate the BBB development and the appropriate formation of the TJs between the endothelial cells, ZO-1 and VE-cadherin were immunostained and observed under a confocal microscope at the BBB zone. Zonula occludens 1 (ZO-1) is a scaffolding protein that connects the TJs proteins between actin from the cytoskeleton structure in cell-to-cell interactions. On the other hand, VE-cadherin is a strictly endothelial-specific adhesion molecule located at junctions between endothelial cells. In the BBB-oC untreated is markedly evidenced the presence of ZO-1 stained in green and VE-cadherin in red between adjacent endothelial as well as the merged, at the same way also in the BBB-oC treated with non-Alzheimer liquor. On the contrary, in the BBB-oC treated with sCX3CL1 and with AD liquor there is a decrease in the expression of the TJs connecting the ECs, this confirms the damage to the BBB after 24 hours of treatment. Furthermore, the merger between ZO-1 and VE-cadherin, which normally indicates correct development of the BBB within the chip, is also clearly lost (figures 26-27).

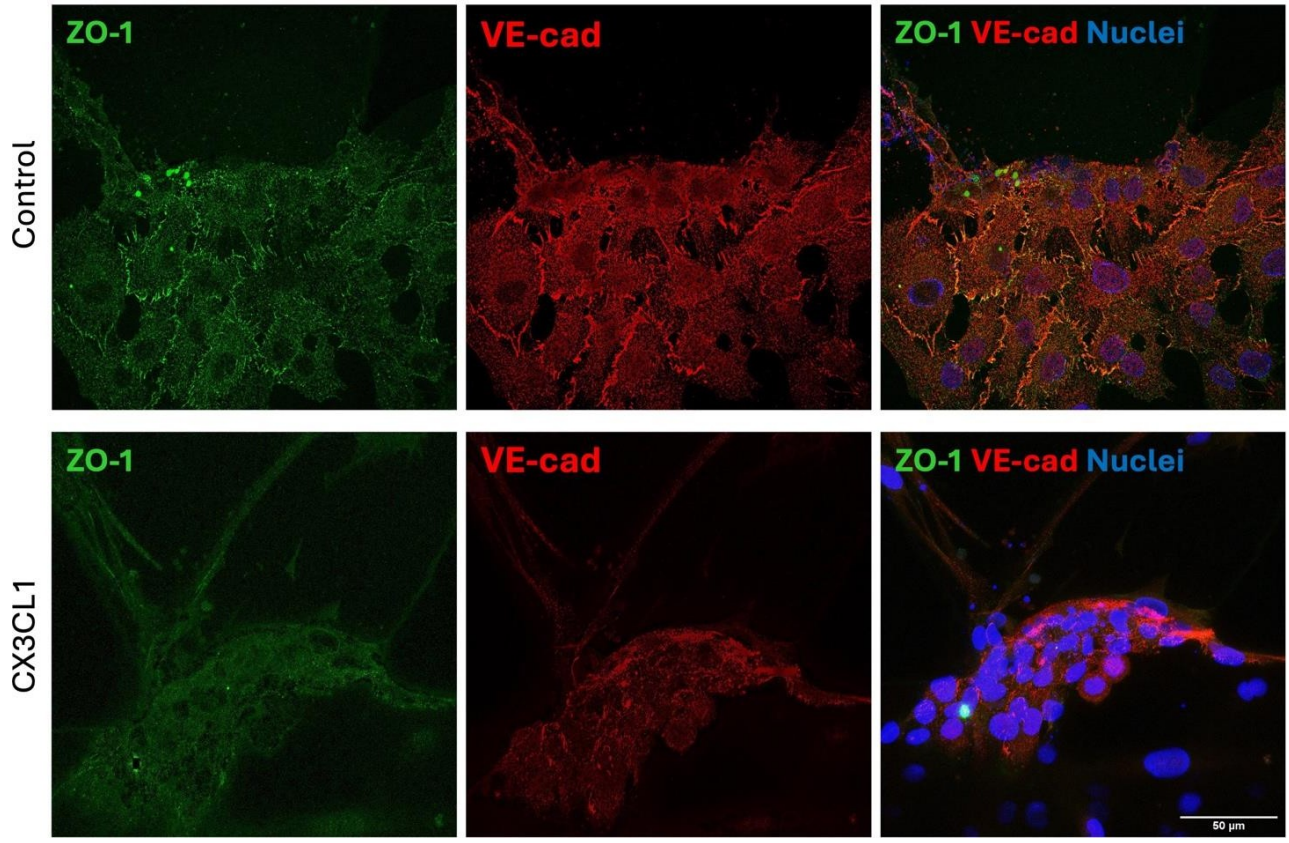

Figure 26: Immunofluorescence assay of TJs protein expression on BBB-oC treated with sCX3CL1 for 24h.

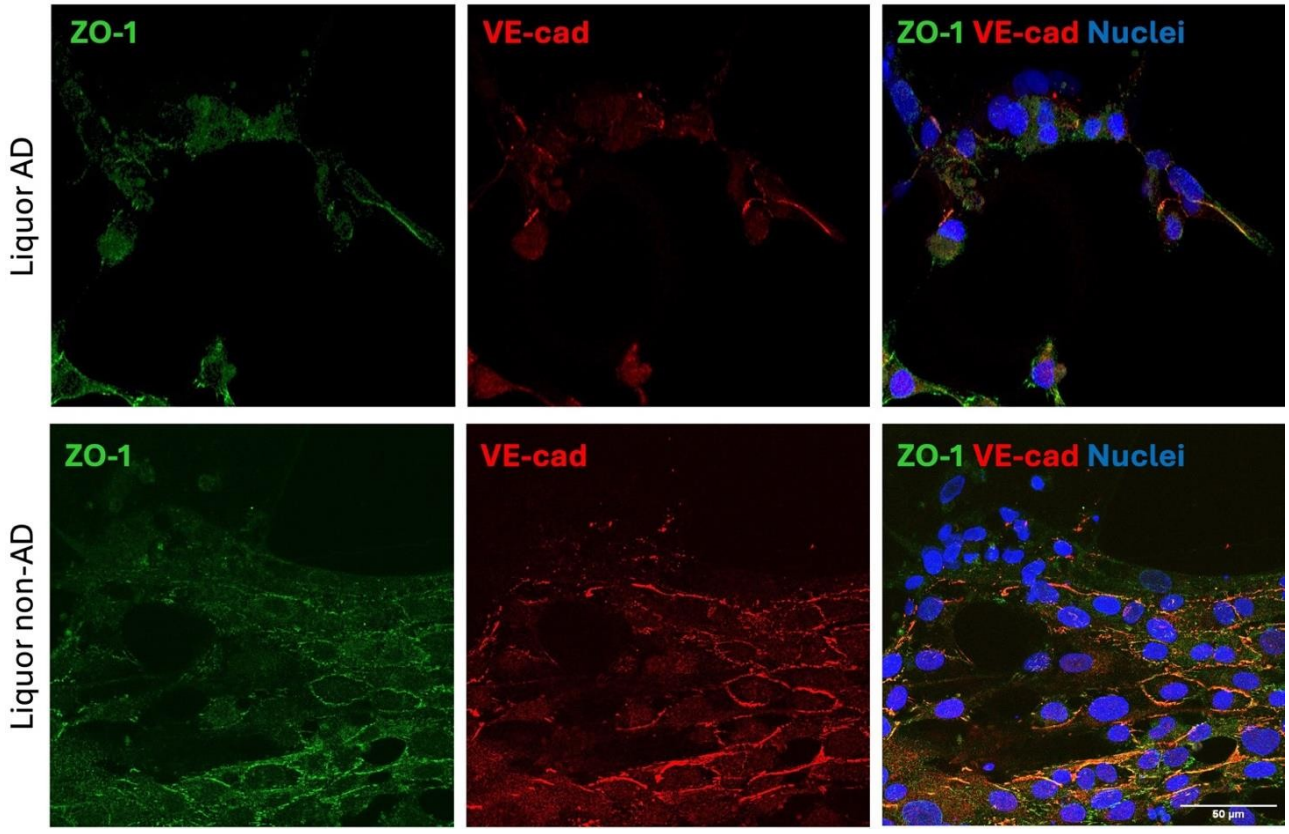

Figure 27: Immunofluorescence assay of TJs protein expression on BBB-oC treated with AD and non-AD liquor for 24h.

To evaluate the effect of the treatment also on the morphology of BBB astrocytes, GFAP was immunostained and observed under a confocal microscope in the BBB area. Furthermore, CX3CL1 was also immunostained and observed under a confocal microscope. The images showed very little or almost no fluorescence for CX3CL1 in the untreated BBB-oC and in that treated with non-AD CSF. On the contrary, in BBB-oCs treated with sCX3CL1 and AD CSF there is a marked expression of the cytokine. Regarding GFAP it showed two different morphologies of astrocytes. BBB-oC astrocytes untreated or treated with non-AD CSF appear with a regular elongated morphology and various prolongations. BBB-oC astrocytes treated with sCX3CL1 and AD liquor showed an increase in nuclear volume and a change in morphology, appearing more enlarged (figures 28-29). Most likely this is the phenomenon of astrogliosis, typical in Alzheimer's disease and which also occurs following a harmful insult.

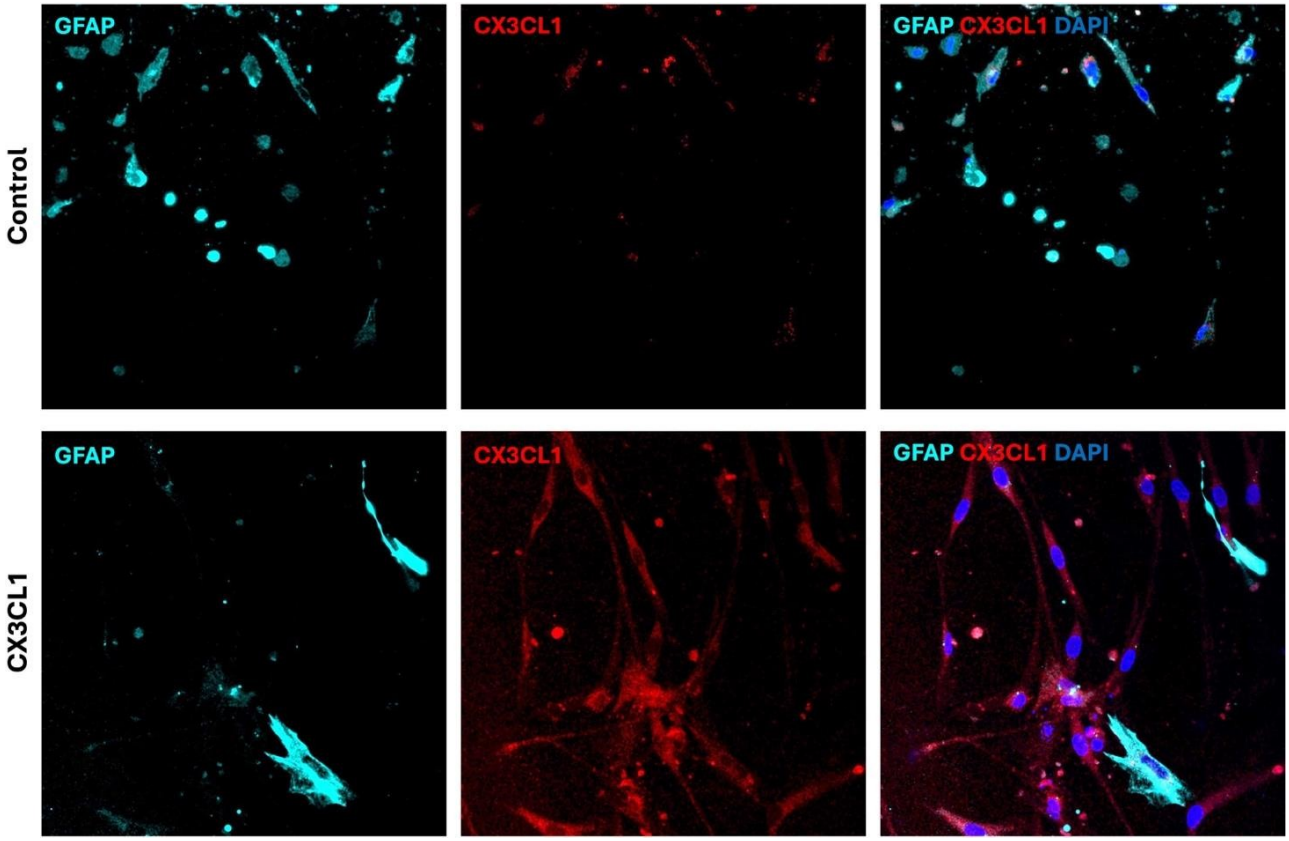

Figure 28: Immunofluorescence assay of CX3CL1 protein expression and GFAP on BBB-oC treated with sCX3CL1 for 24h.

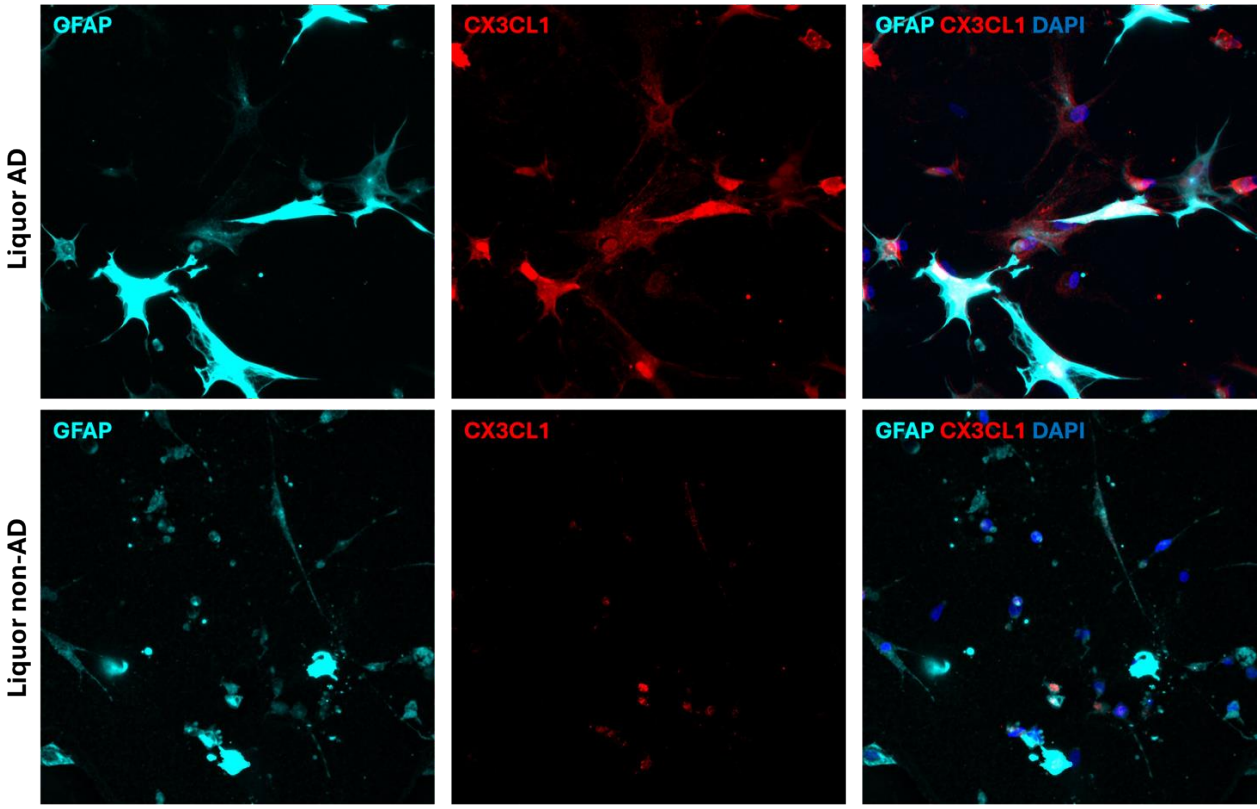

Figure 29: Immunofluorescence assay of CX3CL1 protein expression and GFAP on BBB-oC treated with AD and non-AD liquor for 24h.

4.8 Real Time PCR analyses of RNA extract from BBB-oC

Was performed a Real Time PCR analysis about RNA extract from the BBB-oC untreated and the BBB-oC treated with the purify protein sCX3CL1, liquor AD and liquor non-AD. Were analyzed the expression of 4 genes involved in the correct process of BBB's structure formation, the TJs (*ZO-1, Claudin-5, ZO-3 and VE-cadherin*). Moreover, was analyzed the expression of gene *CX3CL1* to analyze the change of expression of this cytokine involved in Alzheimer's disease. Q-PCR analyzes on mRNAs extracted from BBB-oC untreated and from BBB-oC treated with sCX3CL1, liquor AD and non-AD were conducted using the β-*actine* coding gene as housekeeping and normalizing the values respect the genes expression in BBB-oC untreated (negative control).

As can be seen from the graph in figure 30, the results showed a notable increase in CX3CL1 gene expression in the mRNAs extracted from the BBB-oC treated with sCX3CL1. As regards the mRNAs extracted from the BBB-OCs treated with the patient's liquor, the results showed a notable increase in CX3CL1 gene expression in the BBB-OCs treated with the AD CSF, although always smaller than the increase had in the BBB-oCs treated with sCX3CL1. An almost non-existent increase in CX3CL1 gene expression in BBB-oC treated with non-AD CSF.

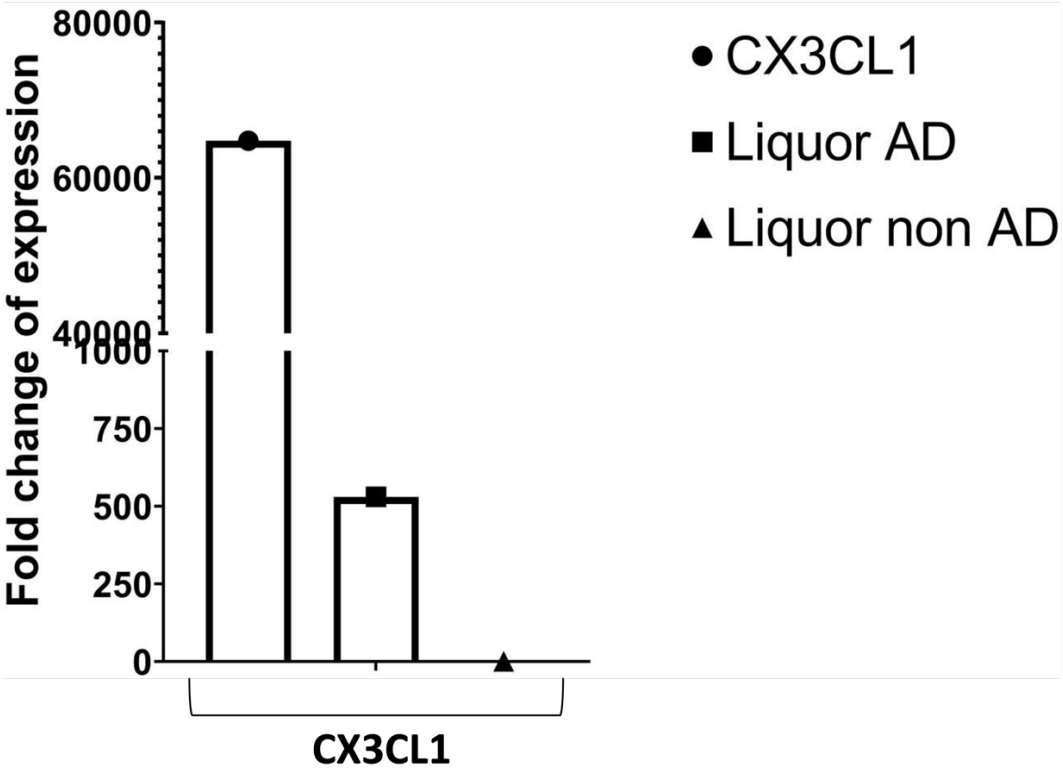

Figure 30: Genic expression of *CX3CL1* in the BBB-oC treated with the purify protein sCX3CL1, liquor AD and liquor non-AD. As reported in the figure, the histogram on the left is related to sCX3CL1 treatment, the histogram in the middle to liquor AD treatment and the histogram on the right to the liquor non AD treatment, respectively.

As can be seen from the graph in figure 31, the results showed a notable increase in *ZO-1, Claudin-5, ZO-3 and VE-cadherin* genes expression in the mRNAs extracted from the BBB-oC treated with sCX3CL1. Also in the mRNAs extracted from the BBB-OCs treated with the AD liquor there is an increase of *ZO-1, Claudin-5, ZO-3 and VE-cadherin* genes expression, although always smaller than the increase had in the BBB-oCs treated with sCX3CL1. An almost non-existent increase in *ZO-1, Claudin-5, ZO-3 and VE-cadherin* genes expression in BBB-oC treated with non-AD CSF. This increase in expression of the TJs genes represents a cellular response to the damage suffered by the BBB after the treatment, as if the cell was trying to repair the damage to the BBB by increasing the expression of the TJs.

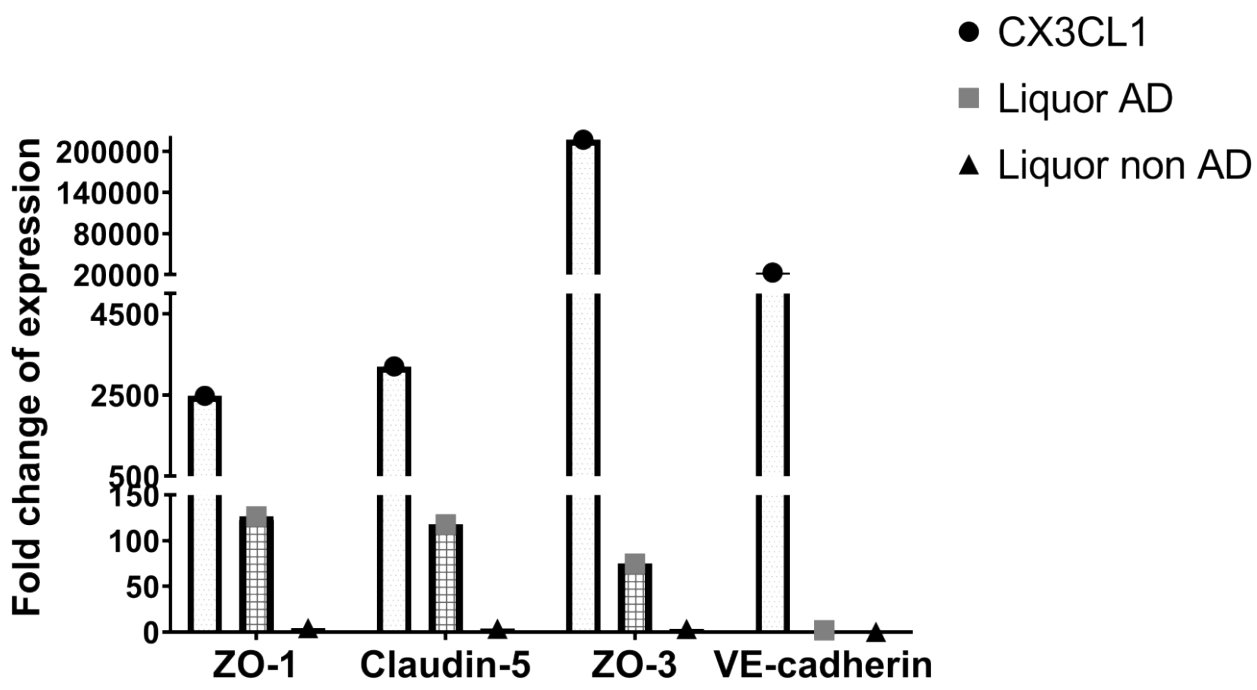

Figure 31: Genic expression of *ZO-1, Claudin-5, ZO-3 and VE-cadherin* in the BBB-oC treated with the purify protein sCX3CL1, liquor AD and liquor non-AD. For each gene expression the first histogram on the left is related to sCX3CL1 treatment, the second histogram in the middle to liquor AD treatment and the last histogram on the right to the liquor non AD treatment, respectively.

4.9 Analyses of Alzheimer disease and CX3CL1 in rat model

After carrying out the preliminary *in vitro* studies, we moved on to the *in vivo* study. The animals used for the *in vivo* study conducted so far are 25 male 11-month-old Wistar rats (figure 32). The objective of this study is to induce Alzheimer's in rats through the intracerebroventricular stereotaxis microinjection of Streptozotocin (STZ) dissolved in 0.1M citrate buffer at a concentration of 2mg/Kg animal weight. The choice of the use of inducing Alzheimer's in rats by brain injection of STZ is closely related to what is now called type 3 diabetes and to the fact that it seems that compared to mutant rats, the disease, in this case, has a course (at least from a behavioral point of view) more like the typical evolution of patients with AD (figure 32).

Figure 32: Stereotaxis surgery in rat model.

Streptozotocin (STZ) is a glucosamine-nitrosourea compound originally identified as an antibiotic. It is toxic to pancreatic beta cells and is usually transported via glucose transporter 2 and is commonly used to induce experimental diabetes in animals. Administration of STZ via intracerebroventricular injection produces impaired cognition and an increase in β-amyloid fragments, total tau protein, and Aβ plaque deposits. These changes were accompanied by a decrease in the alpha/beta ratio of glycogen synthase kinase (GSK-3) (phosphorylated/total) in the brain. Therefore, at sub-diabetic doses, the intracerebral injection of STZ induces an insulin-resistant brain state in the rodent which is associated with memory impairment, glucose hypometabolism, oxidative stress, and neurodegeneration, elements present in AD (figure 33). Insulin also negatively regulates the metabolism of Aβ plaque deposits and tau proteins which are key building blocks of amyloid plaques and neurofibrillary tangles and are well-documented neuropathological hallmarks of AD [49].

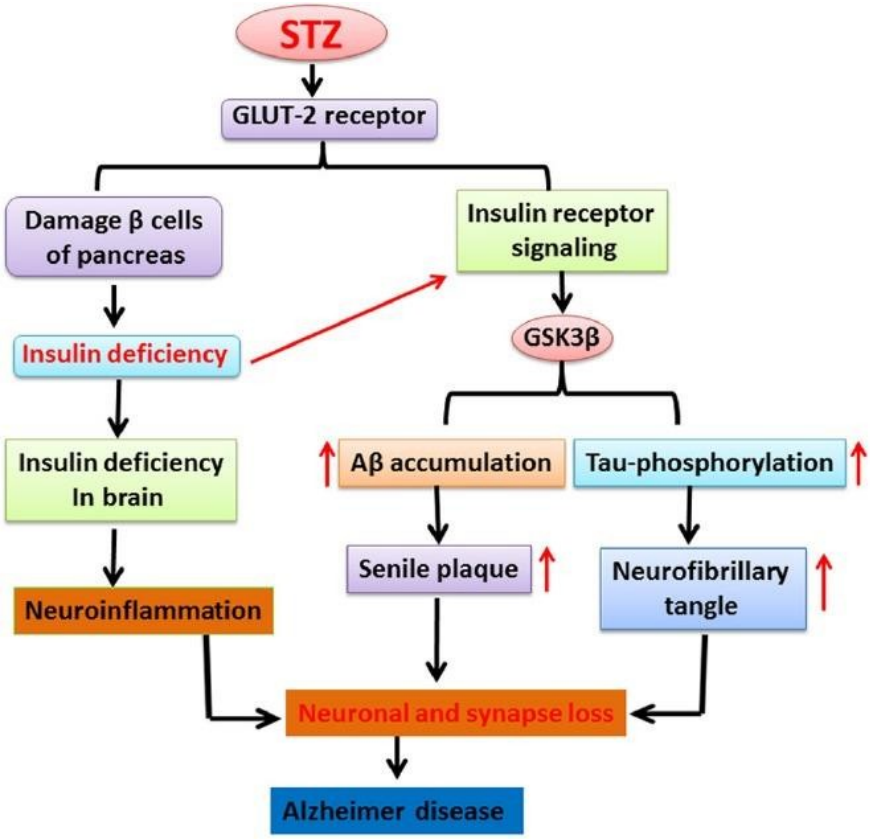

Figure 33: Schematic representation of the role of Streptozotocin in the brain.

The 25 rats were divided into three groups: Alzheimer's group (AD), Sham group, Health group. The AD group rats were treated with STZ dissolved in 0.1M citrate buffer, the Sham group rats were treated with 0.1M citrate buffer only, the Health group rats were not treated. This procedure is called stereotaxis intervention. Following the stereotaxis surgery, the animals were sacrificed by cervical dislocation after sedation with isofluorane. The sacrifice took place at different times, group "A" after 10 days, group "B" after 20 days, group "C" after 30 days. In each of these group's A, B, and C there were 3 rats from the AD group, 3 rats from the Sham group, 2 rats from the Health group. From there, the brain divided into the two hemispheres (right and left) together the cerebellum and blood were taken. The blood of the rats was partly stored whole in 2mM EDTA, complete blood components, partly in the form of serum. Also, different organs (liver, spleen, lung, intestine, stomach, heart, kidney) were explanted and all storage at -80 °C.

From the two hemispheres (right and left) of rats of each groups protein extraction in RIPA buffer was performed. To confirm the induction of Alzheimer disease in rats the proteins extract were analyzed through Dot Blot and Western Blot analyses.

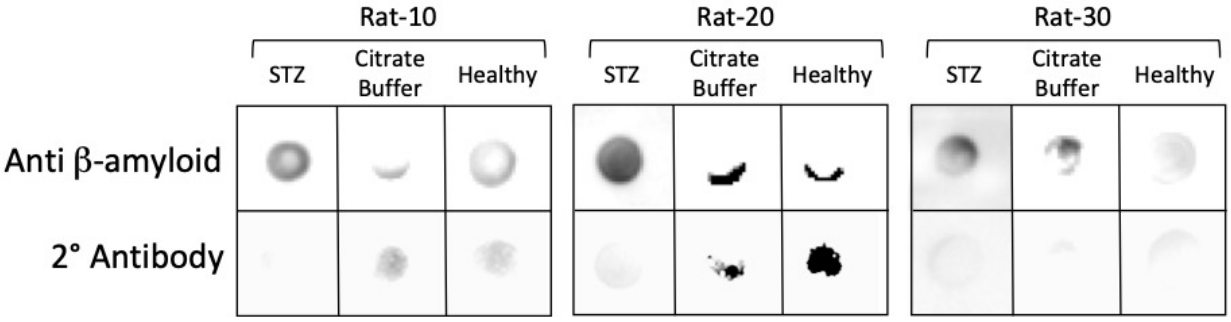

Figure 34: Dot blot analyses of protein extract from cerebral hemispheres treated with STZ (2mg/Kg), treated with citrate buffer and untreated and sacrifices at ten, twenty and thirty days after the induction.

Dot blot analyses showed the expression of β amyloid fragment β1-42 in the protein extract from hemisphere of treated rats with Streptozotocin (2mg/Kg) compared to untreated rats and treated rats with only citrate buffer. Moreover, it shows a different expression of β amyloid fragment β1-42 based on different times of sacrifices. β amyloid fragment β1-42 expression was higher at 20 days than at 10 days, but there was a decrease at 30 days (figure 34). For this reason, we re-performed the stereotaxis intervention in 3 other rats by changing the concentration of STZ (3mg/Kg) and the sacrifice took place at 30 days. The dot blot of the protein extract from these rats showed an increase of β amyloid fragment β1-42 expression (figure 35).

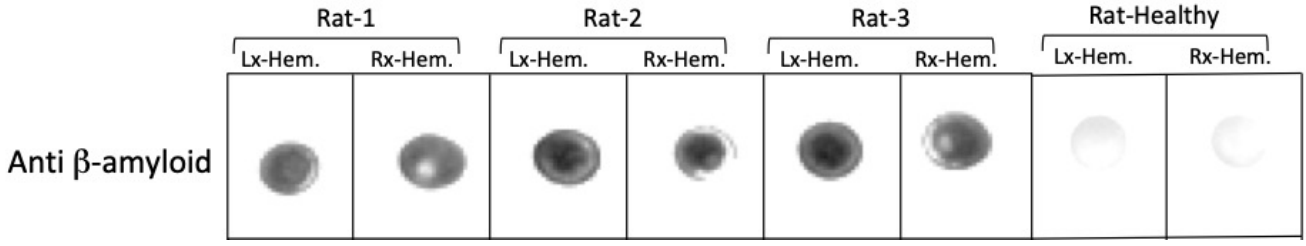

Figure 35: Dot blot analyses of protein extract from left and right cerebral hemispheres (Lx-Hem and Rx-Hem) of rats treated and untreated with Streptozotocin (3mg/Kg) and sacrifices at thirty days after the induction.

Western Blot analyses showed the expression of phosphorylated tau in the protein extract from

hemisphere of treated rats with Streptozotocin (3mg/Kg) (figure 36).

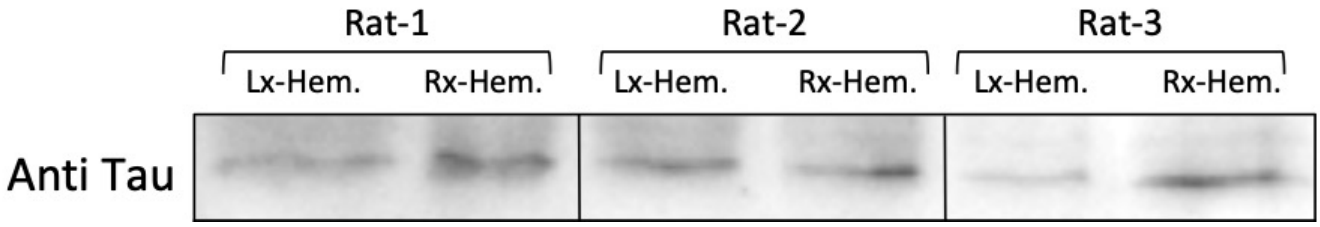

Figure 36: Western Blot analyses of protein extract from left and right cerebral hemispheres (Lx-Hem and Rx-Hem) of treated rats with Streptozotocin (3mg/Kg).

Once we have confirmed the induction of Alzheimer's disease in rat model through stereotaxis intervention with streptozotocin (figure 37), we have repeat other surgery in other rats. Stereotaxis intervention was performed in fourteen rats, these were classified in four different group A, B, C and D based ondifferent time of sacrifices after the induction of Alzheimer's disease. The group A includes three ratssacrificed after four weeks from the induction. The group B includes three rats treated with Streptozotocin and sacrificed after three weeks from the induction. The group C includes three rats treated with Streptozotocin and one rats treated with only citrate buffer sacrificed after two weeks from the induction. The group D includes three rats treated with Streptozotocin and sacrificed after one week from the induction.

Figure 37: Stereotaxis intervention in rat model through intracerebroventricular microinjection of Streptozotocin.

After the sacrifices the brains of the rats were taken to do extraction of protein analyzed by Western blot analyses (figure 38).

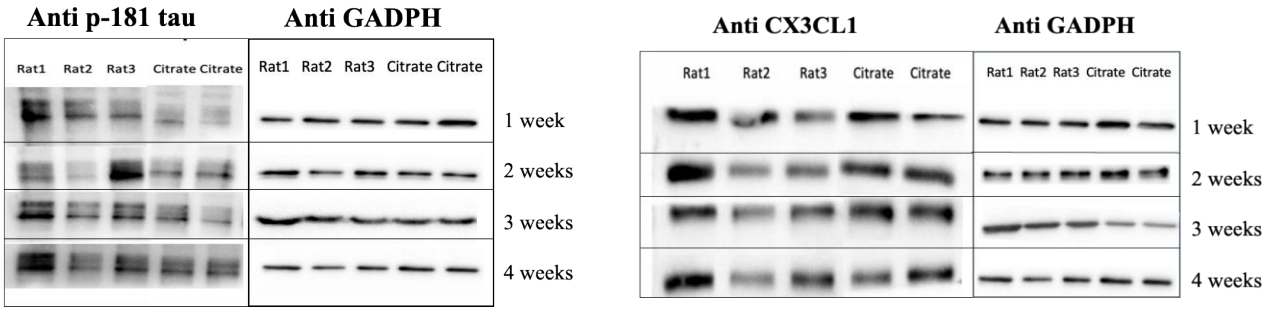

Figure 38: Western blot analyses of protein extract from hemisphere of treated rats with Streptozotocin (3mg/Kg).

The results showed an increase of expression of p-181 tau and sCX3CL1 after one, two, three and four weeks from the induction of Alzheimer's disease in the samples of the rats treated with Streptozotocin (3mg/Kg) compared to the samples of rats treated with citrate buffer, the control (figure 39).

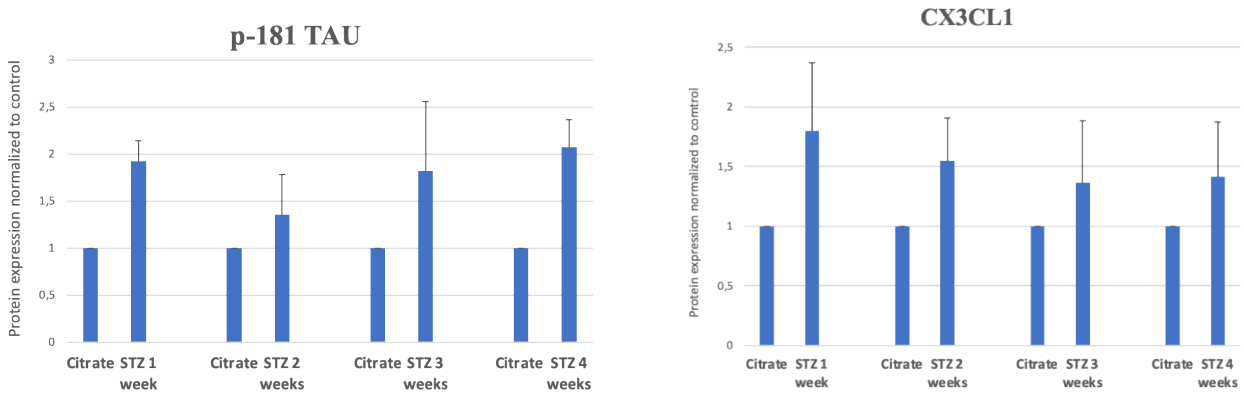

Figure 39: Graphic representation of changing of expression of p-181 Tau and CX3CL1 in rats treated with Streptozotocin (3mg/Kg) compared to rat treated with citrate buffer (the control).

4.10 Real Time PCR analyses of experimental "*in vivo*"

Real Time PCR analysis about RNA extract from the brain of rats treated with Streptozotocin and rats treated with citrate buffer were performed. 39 genes involved in the process that characterize Alzheimer's disease, the same genes analyzed for the NAM co-cultures were analyzed. Real Time PCR analyzes, on mRNAs extracted from brains of rats treated with STZ, were conducted using the *gapdh* coding gene as housekeeping and normalizing the values respect the genes expression in rats treated with citrate buffer (negative control).

The results of Real Time PCR analyses are represented in a Heat map (figure 40). Three different times were analyzed: one week, two week and four weeks. The inflammatory pathway genes are summarily up-regulated at the 3 different times analyzed, except *il10* which is clearly down-regulated, such as *nfkb* after two e four weeks. The genes involved in the hyperphosphorylation of Tau and in the formation of tangle of tau are upregulated, including β-*catenin*. The upregulation of β-*catenin* could be a response to contrast the increase of *gsk3*β. The genes involved in amyloidogenic pathways are all upregulated except *bace2* for the three times and *a2m* for two and four weeks. Also, the genes of the metalloproteases are all upregulated, with the exception of MMP10; and partially of MMP11.

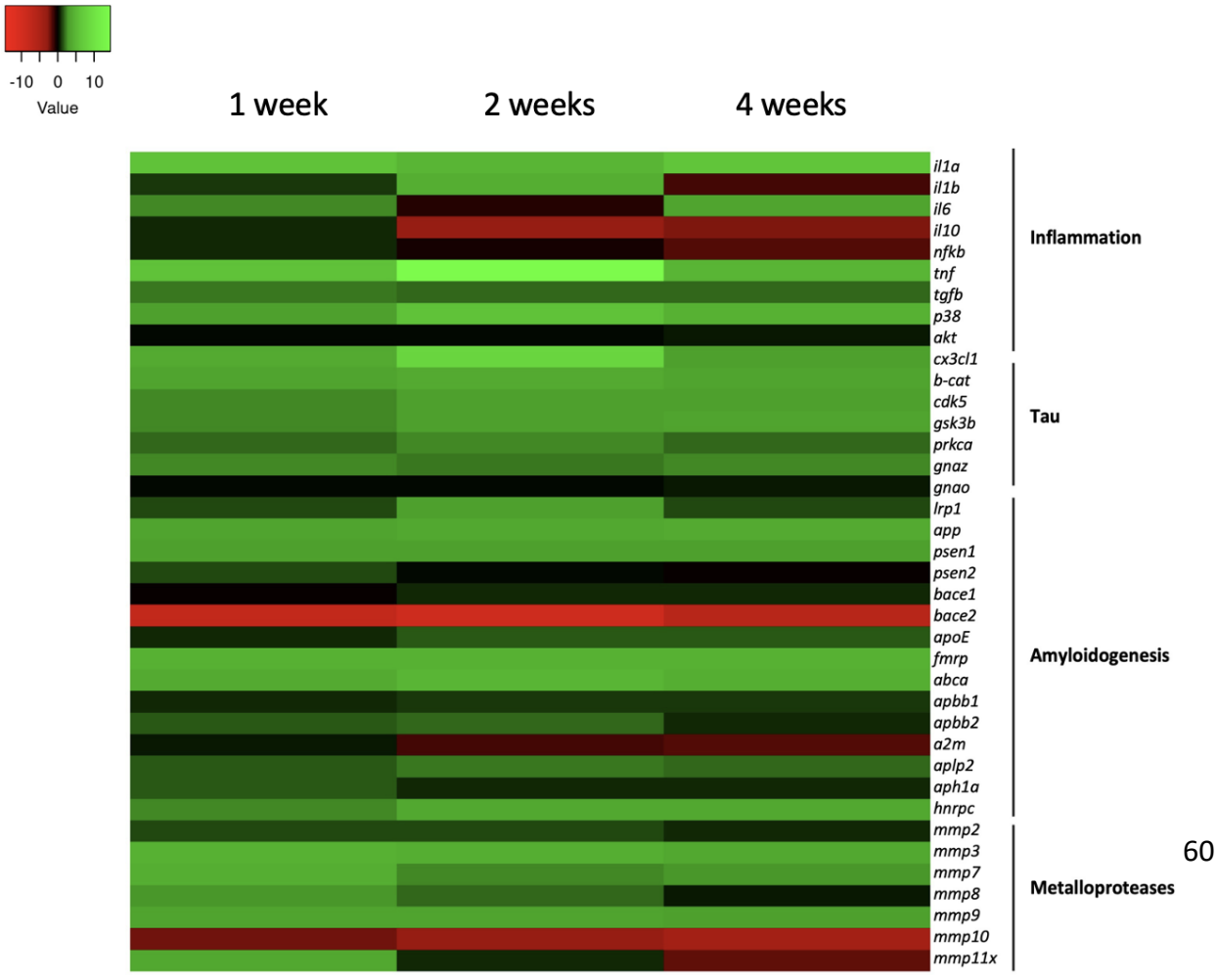

Figure 40: Heat Map Real Time PCR of RNA extract from brain of rats treated with STZ and scarifies after one week, two weeks and three weeks from the induction of AD.

5. DISCUSSION

In this work, the combination of the cytokine CX3CL1 and its signaling axis CX3CL1/CX3CR1 with Alzheimer's pathology was studied. The change in the expression of transcriptional factors involved in its signaling cascade *in vivo* and *in vitro* such as *p38*, *β-catenin* and others was also evaluated. For the *in vitro* part, cerebrospinal fluid samples from Alzheimer's patients and non-Alzheimer's patients were used. The cerebrospinal fluid samples were analyzed by Elisa test and CLEIA test for the presence of canonical AD markers such as total tau, hyperphosphorylated tau,
β 1-40, β 1-42, ratio β 1-42/ β 1-40 and for the presence of sCX3CL1. The results classified the CSF samples into 3 different groups: group A' and A" which include CSFs from AD patients and group B which include CSFs from non-AD patients. The CSFs of group A' differ from the CSFs of group A" by the high level of total tau and hyperphosphorylated tau which in the CSFs of group A" is around normal values. Regarding the expression of sCX3CL1, high concentrations of sCX3CL1 were found in the CSFs of patients with AD compared to the CSFs of non-AD patients. Similar results were obtained from other previous studies, this shows us how sCX3CL1 could be considered as a possible new marker for AD pathology. Subsequently, the effects induced by cerebrospinal fluid from AD and non-AD subjects on NAM co-cultures were evaluated. From a morphological point of view, the loss of a canonical morphology in NAM co-cultures was seen, referring to the formation of neurospheres, when these were treated with liquor from AD subjects of group A'; while in the Control, Group A" and Group B no morphological changes were observed. This suggests that inflammatory elements are present in the CSF of group A' AD patients, including the high level of sCX3CL1, which interfere in the structural organization of neurons, neurofilaments, cell adhesion processes and intercellular contacts.
Through zymographic analysis, both the conditioned medium and the protein extracts of NAM co-cultures treated with CSF from AD subjects (Groups A' and A") and non-AD patients (Group B) were analyzed to evaluate the presence of gelatinolytic activities. The zymographic analysis was carried out both in the presence of $CaCl^2$ (activator of MMPs and other Ca^{2+}-dependent proteolytic enzymes) and with EDTA. The amount of proteolytic activities was determined by densitometric analysis (Image J64 program) and showed greater digestive activity and therefore activation of the metalloprotease cascade by the elements present both in the conditioned media and in the protein extracts from the NAM co-cultures developed in presence of $CaCl_2$, in AD subjects compared to non-AD subjects. Furthermore, even in the presence of EDTA, the protein extracts of NAM co-cultured cells treated with CSF from subjects with AD showed Ca^{2+}-independent gelatinolytic activities compared to almost no gelatinolytic activity in the extracts obtained after treatment with CSF from non-AD subjects.

Immunofluorescence analysis highlighted increased expression of CX3CL1 in NAM co-cultures

treated with CSF from AD subjects compared to control and those treated with CSF from non-AD subjects.

Further support was obtained thanks to the results obtained from the Real Time PCR analysis. The results in fact showed a different expression of the messengers extracted from co-cultures treated or not with cerebrospinal fluid from patients with AD and non-AD, and compared to their basal expression in co-cultures treated with PBS alone. As expected, following this analysis, in fact, there was an increase in the expression of mRNAs involved in inflammatory processes, as it is well known that inflammation is a fundamental mechanism in Alzheimer's disease. Furthermore, there was also an increase in the expression of *Il10* and tgfb which probably represents a cellular response to try to counteract the overexpression of other elements of the inflammatory pathway.

Gene expression analyzes focused on the *tau* pathway reflected the conditions that these genes manifest in AD pathology. In fact, the results showed a concordant up-regulation of gsk3β and cdk5 and a down-regulation of *β-catenin* (negative regulator of gsk3β) especially at 48 hours, thus suggesting the onset of mechanisms that lead to the suppression of *Wnt/β-catenin* signaling in NAM co-cultures treated with AD CSF. qRT-PCR analyzes also showed the up-regulation of *gnaz*, *gano* and *prkca* mRNA, which are involved in the pathogenesis of Alzheimer's disease through tau phosphorylation and tangle formation. A completely opposite pattern is shown instead in the expression of NAM mRNAs co-cultured with non-AD CSF.

Furthermore, the overexpression of genes belonging to the amyloidogenic pathway is also evident, which clearly leads to neuronal degeneration.

The qRT-PCR analyzes confirmed the gelatinolytic activity obtained from the zymographic analysis, showing an increase in expression of MMP mRNAs, MMPs strictly involved in inflammatory processes and AD.

The effect of CX3CL1 and CSF from AD and non-AD patients was also evaluated in another *in vitro* model. The BBB-oC, an organ-on-chip that mimics the blood-brain barrier, was used to evaluate whether sCX3CL1 and also the CSF AD itself cause damage to the blood-brain barrier in the brain. Following treatment of the BBB-oC with sCX3CL1 (purify protein) and AD CSF, damage to the BBB level was morphologically detected. Especially endothelial cells that usually accumulate on the hydrogel channel interface of the device allowing close contact with pericytes and astrocytes (untreated BBB-oC and non-AD CSF-treated BBB) in the sCX3CL1-treated BBB-oC and with CSF AD, close contacts between endothelial cells and astrocytes and pericytes are lost, demonstrating damage to the BBB.

Thanks to immunofluorescent analysis under the confocal microscope, ZO-1 and VE-cadherin were visualized, TJs which indicate correct formation of the BBB. In untreated BBB-oC and in those

treated with non-AD CSF, ZO-1 and VE-cadherin are clearly visualized both between adjacent and fused endothelia. On the contrary, in the BBB-oC treated with sCX3CL1 and AD liquor, a decrease in the expression of the TJs connecting the ECs is observed and their fusion is also missing, which confirms the damage to the BBB.

Fluorescence images also showed notable CX3CL1 expression in sCX3CL1- and AD-treated BBB-oCs, as opposed to untreated and non-AD CSF-treated BBB-oCs. GFAP immunofluorescence showed an increase in nuclear volume and a change in the morphology of BBB-oC astrocytes treated with sCX3CL1 and AD liquor. Most likely it is the phenomenon of astrogliosis, typical of Alzheimer's disease and which also occurs following a harmful insult.

These data were supported by Real Time PCR analysis showing up-regulation in the expression of *cx3cl1*, *zo-1*, *claudin-5*, *zo-3* and *ve-cadherin* mRNAs extracted from BBB-oC treated with sCX3CL1 and CSF AD compared to their basal expression in untreated BBB-oC. An almost non-existent increase in the expression of *cx3cl1*, *zo-1*, *claudin-5*, *zo-3* and *ve-cadherin* mRNAs in BBB-oC treated with non-AD cerebrospinal fluid. This increase in the expression of TJ genes represents a cellular response to the damage suffered by the BBB after treatment, as if the cell was trying to repair the damage to the BBB by increasing the expression of TJs.

These results make us understand the negative effect that sCX3CL1 has on the brain level when it is at high concentrations and how this negative effect is specific to this cytokine perhaps assisted by other elements present in the AD liquor.

Having obtained encouraging results from the *in vitro* experiments, the animal model of Alzheimer's disease was reproduced in the laboratory by inducing microinjections at the level of the cerebral ventricles using the SZT. Dot blot and Western blot analyzes confirmed the induction of Alzheimer's disease in rats through the expression of amyloid β 1-42 fragment and phosphorylated tau in the protein extract of the hemisphere of streptozotocin-treated rats. On this type of animal model, the expression of both CX3CL1, but also of related elements, was evaluated in the very early developmental stages of induced AD. Western blot analyses showed an increase of expression of CX3CL1 and hyperphosphorylated tau. The results of real time PCR analyses are comply with the Alzheimer's path. The genes involved in the amyloidogenic pathways, in the metalloproteases are upregulated. The genes involved in inflammation pathways are upregulated, including *CX3CL1*.

In conclusion, therefore, it can be stated that CX3CL1 has an influence in the pathology of Alzheimer's. Various pieces of evidence underline its fundamental role in the neuroinflammatory process that occurs in AD. The increased expression of CX3CL1 in the cerebrospinal fluid of AD

patients, the increased expression and up-regulation of its mRNA both *in vitro* and *in vivo* experiments, as well as the morphological change that induces the cytokine itself at the brain level leads us to think its influence in neurotoxicity. Therefore, it is natural to ask: can CX3CL1 represent an early-stage marker for the diagnosis of AD and consequently, a therapeutic target?

6. BIBLIOGRAPHY

[1] "2015 Alzheimer's disease facts and figures," *Alzheimer's and Dementia*, vol. 11, no. 3, pp. 332–384, Mar. 2015, doi: 10.1016/J.JALZ.2015.02.003.

[2] S. Tiwari, V. Atluri, A. Kaushik, A. Yndart, and M. Nair, "Alzheimer's disease: pathogenesis, diagnostics, and therapeutics," *Int J Nanomedicine*, vol. 14, pp. 5541–5554, 2019, doi: 10.2147/IJN.S200490.

[3] A. Atri, "The Alzheimer's Disease Clinical Spectrum: Diagnosis and Management," *Medical Clinics of North America*, vol. 103, no. 2, pp. 263–293, Mar. 2019, doi: 10.1016/J.MCNA.2018.10.009.

[4] P. Scheltens *et al.*, "Alzheimer's disease," *Lancet*, vol. 397, no. 10284, p. 1577, Apr. 2021, doi: 10.1016/S0140-6736(20)32205-4.

[5] C. T. Loy, P. R. Schofield, A. M. Turner, and J. B. J. Kwok, "Genetics of dementia," *The Lancet*, vol. 383, no. 9919, pp. 828–840, Mar. 2014, doi: 10.1016/S0140-6736(13)60630-3.

[6] C. A. Lane, J. Hardy, and J. M. Schott, "Alzheimer's disease," *Eur J Neurol*, vol. 25, no. 1, pp. 59–70, Jan. 2018, doi: 10.1111/ENE.13439.

[7] E. H. Corder *et al.*, "Gene Dose of Apolipoprotein E Type 4 Allele and the Risk of Alzheimer's Disease in Late Onset Families," *Science (1979)*, vol. 261, no. 5123, pp. 921–923, Aug. 1993, doi: 10.1126/SCIENCE.8346443.

[8] H. Holstege *et al.*, "Characterization of pathogenic SORL1 genetic variants for association with Alzheimer's disease: a clinical interpretation strategy," *European Journal of Human Genetics*, vol. 25, no. 8, p. 973, Aug. 2017, doi: 10.1038/EJHG.2017.87.

[9] E. Cuyvers *et al.*, "Mutations in ABCA7 in a Belgian cohort of Alzheimer's disease patients: a targeted resequencing study," *Lancet Neurol*, vol. 14, no. 8, pp. 814–822, Aug. 2015, doi: 10.1016/S1474-4422(15)00133-7.

[10] R. Guerreiro *et al.*, "TREM2 Variants in Alzheimer's Disease ," *New England Journal of Medicine*, vol. 368, no. 2, pp. 117–127, Jan. 2013, doi: 10.1056/NEJMOA1211851/SUPPL_FILE/NEJMOA1211851_DISCLOSURES.PDF.

[11] G. G. Ortiz *et al.*, "Genetic, Biochemical and Histopathological Aspects of Familiar Alzheimer's Disease," *Alzheimer's Disease - Challenges for the Future*, Jul. 2015, doi: 10.5772/59809.

[12] P. H. Reddy, "A Critical Assessment of Research on Neurotransmitters in Alzheimer's Disease," *Journal of Alzheimer's Disease*, vol. 57, no. 4, pp. 969–974, 2017, doi: 10.3233/JAD-170256.

[13] S. H. Barage and K. D. Sonawane, "Amyloid cascade hypothesis: Pathogenesis and therapeutic strategies in Alzheimer's disease," *Neuropeptides*, vol. 52, pp. 1–18, Aug. 2015, doi: 10.1016/J.NPEP.2015.06.008.

[14] M. O. Grimm and T. Hartmann, "Recent Understanding of the Molecular Mechanisms of Alzheimer's Disease," *Journal of Addiction Research & Therapy 2013 0:0*, vol. s5, pp. 1–15, Jan. 2012, doi: 10.4172/2155-6105.S5-004.

[15] S. Khan, K. H. Barve, and M. S. Kumar, "Recent Advancements in Pathogenesis, Diagnostics and Treatment of Alzheimer's Disease," *Curr Neuropharmacol*, vol. 18, no. 11, p. 1106, May 2020, doi: 10.2174/1570159X18666200528142429.

[16] L. Crews and E. Masliah, "Molecular mechanisms of neurodegeneration in Alzheimer's disease," *Hum Mol Genet*, vol. 19, no. R1, p. R12, Apr. 2010, doi: 10.1093/HMG/DDQ160.

[17] F. Huang *et al.*, "CDT2-controlled cell cycle reentry regulates the pathogenesis of Alzheimer's disease," *Alzheimers Dement*, vol. 15, no. 2, p. 217, Feb. 2019, doi: 10.1016/J.JALZ.2018.08.013.

[18] P. I. Moreira, C. Carvalho, X. Zhu, M. A. Smith, and G. Perry, "Mitochondrial dysfunction is a trigger of Alzheimer's disease pathophysiology," *Biochimica et Biophysica Acta (BBA) - Molecular Basis of Disease*, vol. 1802, no. 1, pp. 2–10, Jan. 2010, doi: 10.1016/J.BBADIS.2009.10.006.

[19] Z. Liu, T. Zhou, A. C. Ziegler, P. Dimitrion, and L. Zuo, "Oxidative Stress in Neurodegenerative Diseases: From Molecular Mechanisms to Clinical Applications," *Oxid Med Cell Longev*, vol. 2017, 2017, doi: 10.1155/2017/2525967.

[20] T. T. Nguyen, Q. T. H. Ta, T. T. D. Nguyen, T. T. Le, and V. G. Vo, "Role of Insulin Resistance in the Alzheimer's Disease Progression," *Neurochem Res*, vol. 45, no. 7, pp. 1481–1491, Jul. 2020, doi: 10.1007/S11064-020-03031-0/TABLES/2.

[21] W. Farris *et al.*, "Insulin-degrading enzyme regulates the levels of insulin, amyloid β-protein, and the β-amyloid precursor protein intracellular domain in vivo," *Proc Natl Acad Sci U S A*, vol. 100, no. 7, pp. 4162–4167, Apr. 2003, doi: 10.1073/PNAS.0230450100/SUPPL_FILE/0450FIG4.PDF.

[22] L. Li and C. Hölscher, "Common pathological processes in Alzheimer disease and type 2 diabetes: A review," *Brain Res Rev*, vol. 56, no. 2, pp. 384–402, Dec. 2007, doi: 10.1016/J.BRAINRESREV.2007.09.001.

[23] W. Q. Zhao and M. Townsend, "Insulin resistance and amyloidogenesis as common molecular foundation for type 2 diabetes and Alzheimer's disease," *Biochimica et Biophysica Acta (BBA) - Molecular Basis of Disease*, vol. 1792, no. 5, pp. 482–496, May 2009, doi: 10.1016/J.BBADIS.2008.10.014.

[24] K. Talbot *et al.*, "Demonstrated brain insulin resistance in Alzheimer's disease patients is associated with IGF-1 resistance, IRS-1 dysregulation, and cognitive decline," *J Clin Invest*, vol. 122, no. 4, p. 1316, Apr. 2012, doi: 10.1172/JCI59903.

[25] R. Postina *et al.*, "A disintegrin-metalloproteinase prevents amyloid plaque formation and hippocampal defects in an Alzheimer disease mouse model," *J Clin Invest*, vol. 113, no. 10, pp. 1456–1464, May 2004, doi: 10.1172/JCI20864.

[26] A. M. Moloney, R. J. Griffin, S. Timmons, R. O'Connor, R. Ravid, and C. O'Neill, "Defects in IGF-1 receptor, insulin receptor and IRS-1/2 in Alzheimer's disease indicate possible resistance to IGF-1 and insulin signalling," *Neurobiol Aging*, vol. 31, no. 2, pp. 224–243, Feb. 2010, doi: 10.1016/J.NEUROBIOLAGING.2008.04.002.

[27] E. Grünblatt, M. Salkovic-Petrisic, J. Osmanovic, P. Riederer, and S. Hoyer, "Brain insulin system dysfunction in streptozotocin intracerebroventricularly treated rats generates hyperphosphorylated tau protein," *J Neurochem*, vol. 101, no. 3, pp. 757–770, May 2007, doi: 10.1111/J.1471-4159.2006.04368.X.

[28] C. Hölscher, "Diabetes as a risk factor for Alzheimer's disease: insulin signalling impairment in the brain as an alternative model of Alzheimer's disease," *Biochem Soc Trans*, vol. 39, no. 4, pp. 891–897, Aug. 2011, doi: 10.1042/BST0390891.

[29] C. M. Long-Smith *et al.*, "The diabetes drug liraglutide ameliorates aberrant insulin receptor localisation and signalling in parallel with decreasing both amyloid-β plaque and glial pathology in a mouse model of

alzheimer's disease," *Neuromolecular Med*, vol. 15, no. 1, pp. 102–114, Mar. 2013, doi: 10.1007/S12017-012-8199-5/FIGURES/5.

[30] O. Stöhr *et al.*, "Insulin receptor signaling mediates APP processing and β-amyloid accumulation without altering survival in a transgenic mouse model of Alzheimer's disease," *Age (Omaha)*, vol. 35, no. 1, p. 83, Feb. 2013, doi: 10.1007/S11357-011-9333-2.

[31] K. Talbot, L. Han, J. A. Schneider, R. S. Wilson, D. A. Bennett, and S. E. Arnold, "O3–02–02: Expression of pIRS–1 (S312 and S616) is elevated in MCI and AD and correlates with cognitive impairment and neurofibrillary pathology," *Alzheimer's & Dementia*, vol. 2, no. 3S_Part_2, Jul. 2006, doi: 10.1016/J.JALZ.2006.05.197.

[32] A. Y. Sim, S. Barua, J. Y. Kim, Y. H. Lee, and J. E. Lee, "Role of DPP-4 and SGLT2 Inhibitors Connected to Alzheimer Disease in Type 2 Diabetes Mellitus," *Front Neurosci*, vol. 15, p. 708547, Aug. 2021, doi: 10.3389/FNINS.2021.708547/BIBTEX.

[33] J. Hort *et al.*, "EFNS guidelines for the diagnosis and management of Alzheimer's disease," *Eur J Neurol*, vol. 17, no. 10, pp. 1236–1248, Oct. 2010, doi: 10.1111/J.1468-1331.2010.03040.X.

[34] G. B. Frisoni, N. C. Fox, C. R. Jack, P. Scheltens, and P. M. Thompson, "The clinical use of structural MRI in Alzheimer disease," *Nat Rev Neurol*, vol. 6, no. 2, p. 67, Feb. 2010, doi: 10.1038/NRNEUROL.2009.215.

[35] T. Kato, Y. Inui, A. Nakamura, and K. Ito, "Brain fluorodeoxyglucose (FDG) PET in dementia," *Ageing Res Rev*, vol. 30, pp. 73–84, Sep. 2016, doi: 10.1016/J.ARR.2016.02.003.

[36] C. M. Clark *et al.*, "Use of Florbetapir-PET for Imaging β-Amyloid Pathology," *JAMA*, vol. 305, no. 3, p. 275, Jan. 2011, doi: 10.1001/JAMA.2010.2008.

[37] M. D. Ikonomovic *et al.*, "Post-mortem histopathology underlying β-amyloid PET imaging following flutemetamol F 18 injection," *Acta Neuropathol Commun*, vol. 4, no. 1, p. 130, Dec. 2016, doi: 10.1186/S40478-016-0399-Z.

[38] C. R. Jack *et al.*, "NIA-AA Research Framework: Toward a biological definition of Alzheimer's disease," *Alzheimers Dement*, vol. 14, no. 4, p. 535, Apr. 2018, doi: 10.1016/J.JALZ.2018.02.018.

[39] K. Höglund *et al.*, "Cerebrospinal fluid neurogranin in an inducible mouse model of neurodegeneration: A translatable marker of synaptic degeneration," *Neurobiol Dis*, vol. 134, p. 104645, Feb. 2020, doi: 10.1016/J.NBD.2019.104645.

[40] D. Galasko *et al.*, "Synaptic biomarkers in CSF aid in diagnosis, correlate with cognition and predict progression in MCI and Alzheimer's disease," *Alzheimer's & Dementia : Translational Research & Clinical Interventions*, vol. 5, p. 871, Jan. 2019, doi: 10.1016/J.TRCI.2019.11.002.

[41] S. Janelidze *et al.*, "Cerebrospinal fluid neurogranin and YKL-40 as biomarkers of Alzheimer's disease," *Ann Clin Transl Neurol*, vol. 3, no. 1, p. 12, Jan. 2016, doi: 10.1002/ACN3.266.

[42] F. H. Duits *et al.*, "Synaptic proteins in CSF as potential novel biomarkers for prognosis in prodromal Alzheimer's disease," *Alzheimers Res Ther*, vol. 10, no. 1, Jan. 2018, doi: 10.1186/S13195-017-0335-X.

[43] V. Calsolaro and P. Edison, "Neuroinflammation in Alzheimer's disease: Current evidence and future directions," *Alzheimers Dement*, vol. 12, no. 6, pp. 719–732, Jun. 2016, doi: 10.1016/J.JALZ.2016.02.010.

[44] M. T. Heneka *et al.*, “Neuroinflammation in Alzheimer’s Disease,” *Lancet Neurol*, vol. 14, no. 4, p. 388, Apr. 2015, doi: 10.1016/S1474-4422(15)70016-5.

[45] J. W. Kinney, S. M. Bemiller, A. S. Murtishaw, A. M. Leisgang, A. M. Salazar, and B. T. Lamb, “Inflammation as a central mechanism in Alzheimer’s disease,” *Alzheimer’s & Dementia : Translational Research & Clinical Interventions*, vol. 4, p. 575, Jan. 2018, doi: 10.1016/J.TRCI.2018.06.014.

[46] Z. Cai, M. D. Hussain, and L. J. Yan, “Microglia, neuroinflammation, and beta-amyloid protein in Alzheimer’s disease,” *Int J Neurosci*, vol. 124, no. 5, pp. 307–321, 2014, doi: 10.3109/00207454.2013.833510.

[47] Y. Yu and R. D. Ye, “Microglial Aβ Receptors in Alzheimer’s Disease,” *Cell Mol Neurobiol*, vol. 35, no. 1, pp. 71–83, Jan. 2015, doi: 10.1007/S10571-014-0101-6/FIGURES/1.

[48] C. R. Stewart *et al.*, “CD36 ligands promote sterile inflammation through assembly of a Toll-like receptor 4 and 6 heterodimer Europe PMC Funders Group,” *Nat Immunol*, vol. 11, no. 2, pp. 155–161, 2010, doi: 10.1038/ni.1836.

[49] P. S. Sung, P. Y. Lin, C. H. Liu, H. C. Su, and K. J. Tsai, “Neuroinflammation and Neurogenesis in Alzheimer’s Disease and Potential Therapeutic Approaches,” *Int J Mol Sci*, vol. 21, no. 3, Feb. 2020, doi: 10.3390/IJMS21030701.

[50] M. Hosokawa, A. Klegeris, J. Maguire, and P. L. McGeer, “Expression of complement messenger RNAs and proteins by human oligodendroglial cells,” *Glia*, vol. 42, no. 4, pp. 417–423, Jun. 2003, doi: 10.1002/GLIA.10234.

[51] Y. F. Liaoi, B. J. Wang, H. T. Cheng, L. H. Kuo, and M. S. Wolfe, “Tumor necrosis factor-α, interleukin-1β, and interferon-γ stimulate γ-secretase-mediated cleavage of amyloid precursor protein through a JNK-dependent MAPK pathway,” *Journal of Biological Chemistry*, vol. 279, no. 47, pp. 49523–49532, Nov. 2004, doi: 10.1074/jbc.M402034200.

[52] Y. Li, L. Liu, S. W. Barger, and W. S. T. Griffin, “Interleukin-1 Mediates Pathological Effects of Microglia on Tau Phosphorylation and on Synaptophysin Synthesis in Cortical Neurons through a p38-MAPK Pathway,” *The Journal of Neuroscience*, vol. 23, no. 5, p. 1605, Mar. 2003, doi: 10.1523/JNEUROSCI.23-05-01605.2003.

[53] G. E. Ringheim, A. M. Szczepanik, W. Petko, K. L. Burgher, S. Z. Zhu, and C. C. Chao, “Enhancement of beta-amyloid precursor protein transcription and expression by the soluble interleukin-6 receptor/interleukin-6 complex,” *Molecular Brain Research*, vol. 55, no. 1, pp. 35–44, Mar. 1998, doi: 10.1016/S0169-328X(97)00356-2.

[54] J. K. Harrison *et al.*, “Role for neuronally derived fractalkine in mediating interactions between neurons and CX3CR1-expressing microglia,” *Proc Natl Acad Sci U S A*, vol. 95, no. 18, pp. 10896–10901, Sep. 1998, doi: 10.1073/PNAS.95.18.10896.

[55] P. Pawelec, M. Ziemka-Nalecz, J. Sypecka, and T. Zalewska, “The Impact of the CX3CL1/CX3CR1 Axis in Neurological Disorders,” *Cells*, vol. 9, no. 10, Oct. 2020, doi: 10.3390/CELLS9102277.

[56] H. Umehara, E. T. Bloom, T. Okazaki, Y. Nagano, O. Yoshie, and T. Imai, “Fractalkine in vascular biology: from basic research to clinical disease,” *Arterioscler Thromb Vasc Biol*, vol. 24, no. 1, pp. 34–40, Jan. 2004, doi: 10.1161/01.ATV.0000095360.62479.1F.

[57] C. Hundhausen *et al.*, “The disintegrin-like metalloproteinase ADAM10 is involved in constitutive cleavage of CX3CL1 (fractalkine) and regulates CX3CL1-mediated cell-cell adhesion,” 2003, doi: 10.1182/blood-2002-12-3775.

[58] K. J. Garton *et al.*, “Tumor Necrosis Factor-α-converting Enzyme (ADAM17) Mediates the Cleavage and Shedding of Fractalkine (CX3CL1),” *Journal of Biological Chemistry*, vol. 276, no. 41, pp. 37993–38001, Oct. 2001, doi: 10.1074/jbc.m106434200.

[59] S. A. O’Sullivan, F. Gasparini, A. K. Mir, and K. K. Dev, “Fractalkine shedding is mediated by p38 and the ADAM10 protease under pro-inflammatory conditions in human astrocytes,” *J Neuroinflammation*, vol. 13, no. 1, pp. 1–13, Aug. 2016, doi: 10.1186/S12974-016-0659-7/FIGURES/6.

[60] M. Satoh, M. Nakamura, H. Satoh, H. Saitoh, I. Segawa, and K. Hiramori, “Expression of tumor necrosis factor-alpha–converting enzyme and tumor necrosis factor-alpha in human myocarditis,” *J Am Coll Cardiol*, vol. 36, no. 4, pp. 1288–1294, Oct. 2000, doi: 10.1016/S0735-1097(00)00827-5.

[61] E. Jorissen *et al.*, “The Disintegrin/Metalloproteinase ADAM10 Is Essential for the Establishment of the Brain Cortex,” 2010, doi: 10.1523/JNEUROSCI.5221-09.2010.

[62] I. R. Patel *et al.*, “TNF-α Convertase Enzyme from Human Arthritis-Affected Cartilage: Isolation of cDNA by Differential Display, Expression of the Active Enzyme, and Regulation of TNF-α,” *The Journal of Immunology*, vol. 160, no. 9, pp. 4570–4579, May 1998, doi: 10.4049/JIMMUNOL.160.9.4570.

[63] Q. Fan *et al.*, “The intracellular domain of CX3CL1 regulates adult neurogenesis and Alzheimer’s amyloid pathology,” *J Exp Med*, vol. 216, no. 8, pp. 1891–1903, Aug. 2019, doi: 10.1084/JEM.20182238.

[64] A. Schulte *et al.*, “Sequential processing of the transmembrane chemokines CX3CL1 and CXCL16 by α- and γ-secretases,” *Biochem Biophys Res Commun*, vol. 358, no. 1, pp. 233–240, Jun. 2007, doi: 10.1016/J.BBRC.2007.04.100.

[65] B. De Strooper *et al.*, “A presenilin-1-dependent γ-secretase-like protease mediates release of Notch intracellular domain,” *Nature 1999 398:6727*, vol. 398, no. 6727, pp. 518–522, Apr. 1999, doi: 10.1038/19083.

[66] M. N. Manuel, D. Mi, J. O. Masonand, and D. J. Price, “Regulation of cerebral cortical neurogenesis by the Pax6 transcription factor,” *Front Cell Neurosci*, vol. 9, Mar. 2015, doi: 10.3389/FNCEL.2015.00070.

[67] J. Lu, Y. Wu, N. Sousa, and O. F. X. Almeida, “SMAD pathway mediation of BDNF and TGFβ2 regulation of proliferation and differentiation of hippocampal granule neurons,” *Development*, vol. 132, no. 14, pp. 3231–3242, Jul. 2005, doi: 10.1242/DEV.01893.

[68] J. Massagué and Q. Xi, “TGF-β control of stem cell differentiation genes,” *FEBS Lett*, vol. 586, no. 14, pp. 1953–1958, Jul. 2012, doi: 10.1016/J.FEBSLET.2012.03.023.

[69] A. N. Winter *et al.*, “Two forms of CX3CL1 display differential activity and rescue cognitive deficits in CX3CL1 knockout mice,” *J Neuroinflammation*, vol. 17, no. 1, pp. 1–14, May 2020, doi: 10.1186/S12974-020-01828-Y/FIGURES/6.

[70] G. Gunner *et al.*, “Sensory lesioning induces microglial synapse elimination via ADAM10 and fractalkine signaling,” *Nature Neuroscience 2019 22:7*, vol. 22, no. 7, pp. 1075–1088, Jun. 2019, doi: 10.1038/s41593-019-0419-y.

[71] M. Iemmolo, G. Ghersi, and G. Bivona, “The Cytokine CX3CL1 and ADAMs/MMPs in Concerted Cross-Talk Influencing Neurodegenerative Diseases,” *International Journal of Molecular Sciences 2023, Vol. 24, Page 8026*, vol. 24, no. 9, p. 8026, Apr. 2023, doi: 10.3390/IJMS24098026.

[72] K. Biber, J. Vinet, and H. W. G. M. Boddeke, “Neuron-microglia signaling: Chemokines as versatile messengers,” *J Neuroimmunol*, vol. 198, no. 1–2, pp. 69–74, Jul. 2008, doi: 10.1016/j.jneuroim.2008.04.012.

[73] D. P. Schafer *et al.*, “Microglia Sculpt Postnatal Neural Circuits in an Activity and Complement-Dependent Manner,” *Neuron*, vol. 74, no. 4, pp. 691–705, May 2012, doi: 10.1016/J.NEURON.2012.03.026/ATTACHMENT/29EF4910-1D22-44CF-B97A-3A9BFC0F0AB0/MMC3.MOV.

[74] “Related Content Characterization of Fractalkine in Rat Brain Cells: Migratory and Activation Signals for CX 3 CR-1-Expressing Microglia Combinatorial Model of Chemokine Involvement in Glomerular Monocyte Recruitment: Role of CXC Chemokine Receptor 2 in Innltration During Nephrotoxic Nephritis,” 2000, doi: 10.4049/jimmunol.165.1.397.

[75] “CHEMOKINE (C-X3-C MOTIF) LIGAND 1 (CX 3 CL1) AND CHEMOKINE (C-X3-C MOTIF) RECEPTOR 1 (CX 3 CR1),” 2018, doi: 10.4110/in.2018.18.e5.

[76] M. Lee, Y. Lee, J. Song, J. Lee, and S. Y. Chang, “Tissue-specific Role of CX3CR1 Expressing Immune Cells and Their Relationships with Human Disease,” *Immune Netw*, vol. 18, no. 1, Jan. 2018, doi: 10.4110/IN.2018.18.E5.

[77] A. Nimmerjahn, F. Kirchhoff, and F. Helmchen, “Neuroscience: Resting microglial cells are highly dynamic surveillants of brain parenchyma in vivo,” *Science (1979)*, vol. 308, no. 5726, pp. 1314–1318, May 2005, doi: 10.1126/SCIENCE.1110647/SUPPL_FILE/1110647S9.MOV.

[78] A. E. Cardona *et al.*, “Control of microglial neurotoxicity by the fractalkine receptor,” *Nature Neuroscience 2006 9:7*, vol. 9, no. 7, pp. 917–924, Jun. 2006, doi: 10.1038/nn1715.

[79] K. Bhaskar, M. Konerth, O. N. Kokiko-Cochran, A. Cardona, R. M. Ransohoff, and B. T. Lamb, “Regulation of tau pathology by the microglial fractalkine receptor,” *Neuron*, vol. 68, no. 1, pp. 19–31, Oct. 2010, doi: 10.1016/j.neuron.2010.08.023.

[80] M. Bolós *et al.*, “Absence of CX3CR1 impairs the internalization of Tau by microglia,” *Mol Neurodegener*, vol. 12, no. 1, Aug. 2017, doi: 10.1186/S13024-017-0200-1.

[81] J. R. Guedes, T. Lao, A. L. Cardoso, and J. El Khoury, “Roles of microglial and monocyte chemokines and their receptors in regulating Alzheimer’s disease-associated amyloid-β and tau pathologies,” *Front Neurol*, vol. 9, no. AUG, p. 549, Aug. 2018, doi: 10.3389/FNEUR.2018.00549/BIBTEX.

[82] L. Munoz and A. J. Ammit, “Targeting p38 MAPK pathway for the treatment of Alzheimer’s disease,” *Neuropharmacology*, vol. 58, no. 3, pp. 561–568, Mar. 2010, doi: 10.1016/J.NEUROPHARM.2009.11.010.

[83] G. Kheiri, M. Dolatshahi, F. Rahmani, and N. Rezaei, “Role of p38/MAPKs in Alzheimer’s disease: Implications for amyloid beta toxicity targeted therapy,” *Rev Neurosci*, vol. 30, no. 1, pp. 9–30, Jan. 2019, doi: 10.1515/REVNEURO-2018-0008/XML.

[84] C. Liu, F. Zhang, H. Liu, and F. Wei, “NF-kB mediated CX3CL1 activation in the dorsal root ganglion

contributes to the maintenance of neuropathic pain induced in adult male Sprague Dawley rats," *Acta Cir Bras*, vol. 33, no. 7, pp. 619–628, Jul. 2018, doi: 10.1590/S0102-865020180070000007.

[85] C. Ju Hwang, D.-Y. Choi, M. H. Park, and J. T. Hong, "NF-κB as a Key Mediator of Brain Inflammation in Alzheimer's Disease," *CNS Neurol Disord Drug Targets*, vol. 18, no. 1, pp. 3–10, Aug. 2017, doi: 10.2174/1871527316666170807130011.

[86] Z. M. Shi *et al.*, "Upstream regulators and downstream effectors of NF-κB in Alzheimer's disease," *J Neurol Sci*, vol. 366, pp. 127–134, Jul. 2016, doi: 10.1016/j.jns.2016.05.022.

[87] A. Kulczyńska-Przybik *et al.*, "Cerebrospinal Fluid and Blood CX3CL1 as a Potential Biomarker in Early Diagnosis and Prognosis of Dementia," *Curr Alzheimer Res*, vol. 17, no. 8, pp. 709–721, Nov. 2020, doi: 10.2174/1567205017666201109095657.

[88] L. Jia, J. Piña-Crespo, and Y. Li, "Restoring Wnt/β-catenin signaling is a promising therapeutic strategy for Alzheimer's disease," *Mol Brain*, vol. 12, no. 1, Dec. 2019, doi: 10.1186/S13041-019-0525-5.

[89] K. R. Nash *et al.*, "Fractalkine overexpression suppresses tau pathology in a mouse model of tauopathy HHS Public Access," *Neurobiol Aging*, vol. 34, no. 6, pp. 1540–1548, 2013, doi: 10.1016/j.neurobiolaging.2012.12.011.

[90] A. López-Canosa *et al.*, "A microphysiological system combining electrospun fibers and electrical stimulation for the maturation of highly anisotropic cardiac tissue," *Biofabrication*, vol. 13, no. 3, p. 035047, Jun. 2021, doi: 10.1088/1758-5090/ABFF12.

[91] S. Palma-Florez *et al.*, "BBB-on-a-chip with integrated micro-TEER for permeability evaluation of multi-functionalized gold nanorods against Alzheimer's disease," *J Nanobiotechnology*, vol. 21, no. 1, p. 115, Dec. 2023, doi: 10.1186/S12951-023-01798-2.

[92] M. Campisi, Y. Shin, T. Osaki, C. Hajal, V. Chiono, and R. D. Kamm, "3D Self-Organized Microvascular Model of the Human Blood-Brain Barrier with Endothelial Cells, Pericytes and Astrocytes," *Biomaterials*, vol. 180, p. 117, Oct. 2018, doi: 10.1016/J.BIOMATERIALS.2018.07.014.

[93] G. Bivona *et al.*, "High Cerebrospinal Fluid CX3CL1 Levels in Alzheimer's Disease Patients but Not in Non-Alzheimer's Disease Dementia," *J Clin Med*, vol. 11, no. 19, p. 5498, Oct. 2022, doi: 10.3390/JCM11195498/S1.